INTEGRATION OF VISIBLE LIGHT COMMUNICATIONS TRANSCEIVERS INTO SWITCHED-MODE POWER SUPPLIES

INTEGRATION OF VISIBLE LIGHT COMMUNICATIONS TRANSCEIVERS INTO SWITCHED-MODE POWER SUPPLIES

BY

ALIREZA BARMAKI, B.Sc., M.Sc.

A THESIS
SUBMITTED TO THE DEPARTMENT OF ELECTRICAL & COMPUTER ENGINEERING
AND SCHOOL OF GRADUATE STUDIES
OF MCMASTER UNIVERSTIY
IN PARTIAL FULFILMENT OF THE REQUIREMENTS
FOR THE DEGREE OF
DOCTOR OF PHILOSOPHY

Doctor of Philosophy (2024)	McMaster University
(Electrical & Computer Engineering)	Hamilton, Ontario, Canada

TITLE:	Integration of Visible Light Communications Transceivers into Switched-Mode Power Supplies
AUTHOR:	Alireza Barmaki M.Sc. (Electrical & Computer Engineering) Sharif University of Technology, Tehran, Iran B.Sc. (Electrical & Computer Engineering) Tehran University, Tehran, Iran
SUPERVISOR:	Dr. Steve Hranilovic
NUMBER OF PAGES:	xxiv, 194

Lay Abstract

Visible light communications (VLC) modulates the intensity of a light-emitting diode (LED) to transmit data, allowing for both communication and illumination to occur simultaneously. This technology leverages simple, inexpensive, and readily available LEDs used in lighting systems. For successful integration of VLC with existing lighting infrastructures, it is crucial to ensure that the implementation is simple and cost-effective and that the illumination quality and energy efficiency of LEDs are maintained. The VLC system should support high data rates and handle interference from other light sources. It must enable data transmission both ways: from the LEDs to nearby devices and from the devices back to the LEDs, termed downlink and uplink respectively. Additionally, the LEDs should be connected to a central data infrastructure, named backhauling, to enable efficient data transfer.

Firstly, this thesis introduces the concept of light-emitting commutating diodes (LECD) which simplifies the VLC transmitter design while enhancing illumination quality and efficiency. Next, it presents the joint switching and amplification application of a metal-oxide-semiconductor field-effect transistor (MOSFET), which supports orthogonal frequency division multiplexing (OFDM) to achieve high data rate and resilience to interference. Finally, an optical relay, integrated into a luminaire, is proposed which addresses the integration of uplink channel and backhauling in a VLC system in the infrared (IR) domain.

Abstract

The rise of IoT devices has increased RF spectrum demand, causing congestion and interference issues. As a solution, Optical Wireless Communications (OWC) uses unregulated IR, visible, and UV wavelengths. Visible Light Communication (VLC) is a practical OWC subset, benefiting from LEDs used in lighting due to their energy efficiency, affordability, long lifespan, and dimming capabilities. Integrating VLC into luminaires should not compromise these LED features and must meet optical communication wireless standards. An effective VLC system requires both downlink and uplink capabilities, compatibility with standards, and support for fronthauling and backhauling. Implementing this in LED luminaires while preserving light quality is challenging.

This thesis addresses this process by proposing a general approach to integrate VLC functionality into the LED drivers (power converters) present in all luminaires. Firstly, this work proposes the replacement of Schottky diodes conventionally found in a buck/boost converter with LEDs. These devices are referred to as light-emitting commutating diodes (LECD). The LECDs enable data transmission through simple modulation techniques such as pulse position modulation (PPM) or overlapping pulse position modulation (OPPM) while also contributing to the total light output of the luminaire. Importantly, since only the LECDs are modulated for data transmission,

the lifespan of the LEDs used for illumination is extended, and the risk of color shift is reduced. As a result, this approach successfully integrates a VLC transmitter into the LED driver while improving the efficacy of the boost converter up to 15% in comparison with a conventional boost converter.

Secondly, the integration of the VLC transmitter into LED drivers is further improved by utilizing the metal-oxide-semiconductor field-effect transistor (MOSFET) in a boost LED driver as both an amplifying and switching device. Specifically, the gate signal of the MOSFET is modified to bias it into saturation when the MOSFET is off, allowing it to function as an amplifier. Despite this modification, the MOSFET remains off from the perspective of the LED driver, ensuring that its operation is not disrupted. This approach eliminates the need for an inefficient linear power amplifier, allowing the data to be amplified and injected into the system directly through the MOSFET. This method supports advanced modulation schemes specified in current standards such as orthogonal frequency division multiplexing (OFDM) while maintaining simplicity and efficiency, thus outperforming current methods without requiring complex control schemes or additional components. The prototype of the proposed topology achieves a data rate of 3.84 Mbps using 64-QAM ACO-OFDM with 256 subcarriers, delivering an efficacy improvement of 6.25% compared to conventional VLC-enabled luminaires.

Finally, the thesis addresses the uplink channel and optical fronthauling and backhauling in VLC systems by developing an optical wireless repeater integrated into a luminaire. This is achieved by replacing the diodes of a multiphase boost converter with photodiodes which develops a power converter specifically for VLC applications. This system enables amplification and retransmission of received optical signals while

simultaneously addressing uplink and fronthauling and backhauling. A prototype featuring 7 LEDs and 1 photodiode in each phase of a 2-phase boost converter is implemented, demonstrating an optical amplification factor of 8.5 dB for infrared signals with a mean optical power of 1–10 mW. Unlike previous approaches which handle these functions separately, this configuration integrates them into a single system, thereby simplifying the overall design by consolidating multiple functions into one.

To my parents, my beloved spouse, and my dear Tommy,

Without your unwavering support and boundless love, none of this would have been possible.

Acknowledgements

First and foremost, I extend my heartfelt gratitude to my supervisor, Dr. Hranilovic. His unwavering support, both academically and emotionally, has been a cornerstone throughout the ups and downs of my Ph.D. journey. This thesis would not have reached its present form without his invaluable mentorship and insightful guidance. His encouragement and belief in my abilities have inspired me to push my boundaries and achieve more than I thought possible. I also wish to express my profound appreciation to my co-supervisor, Dr. Narimani, whose guidance has been instrumental in teaching me to take ownership of my work and navigate the challenges of my research. His constructive feedback and continuous support have significantly contributed to the depth and quality of this research.

I am profoundly grateful to my family, whose love and support have been a beacon of strength, even from thousands of miles away. As an only child, their companionship and encouragement have provided the true friendship I needed. Their countless sacrifices have paved the way for my success and personal growth. From the bottom of my heart, thank you for believing in me and for all the ways you have helped me flourish.

Tommy, my dear companion, imagining this journey without your loyal presence since day one feels unimaginable. Thank you, my sweet furry friend, for being by my side through it all. I am incredibly grateful that our lives intersected with that of my beloved, Ghazal. Together, you both fill my days with boundless joy and love. My heart overflows with gratitude for the profound impact you both have on my life.

I would like to extend my sincere gratitude to my supervisory committee members, Dr. Kumar, Dr. Nahid-Mobarakeh, and Dr. Zhang. Their invaluable insights and feedback consistently guided my research in the right direction. I am especially grateful for their encouragement and constructive criticism, which have been instrumental in shaping this thesis. Dr. Zhang, who has sadly passed away, will always be remembered for his contributions and the impact he had on my work. I also wish to express my deep appreciation for Dr. Davidson, whose guidance on how to best present our research underscored the significance of clear communication and has left a lasting impression on me.

I want to seize this moment to express my profound thanks to all my colleagues and friends, alongside the dedicated and warm-hearted staff at McMaster University. Their steadfast support and camaraderie have made McMaster feel like a second home to me. This is my chance to extend my sincere appreciation for their kindness and assistance throughout my time here.

Table of Contents

List of Figures

List of Tables

Notation, Definitions, and Abbreviations

Notation

$\phi_1, \ \phi_2$	Angle of irradiance (°)
$\psi_1, \ \psi_2$	Angle of incidence (°)
C	Capacitor (F)
F_{sw}/T_{sw}	Converter Switching Frequency/Period (Hz/s)
i_{ds}	Drain Source Voltage (V)
D	Duty Cycle (%)
K	Efficacy (lm/W)
η	Efficiency (%)
G_{e2e}	End to End Gain
$\Psi_1, \ \Psi_2$	Field of View (°)

E_V	Illuminance
L	Inductor (H)
i_L	Inductor Current (A)
ΔI_L	Inductor Current Ripple (A)
P_{in}	Input Electrical Power(W)
V_{in}	Input Voltage (V)
H_1	IR Channel Gain
d_1	IR transmitter distance from repeater (m)
θ_j	Junction Temperature (C°)
V_{LECD}	LECD Forward Voltage Drop (V)
ϕ	Luminous Flux (Lm)
V_{gs}	MOSFET Gate Source Control Signal (V)
K_o'	Normalized Efficacy
R_x	Optical Receiver
P_{out}	Output Electrical Power (W)
V_{out}	Output Voltage (V)
A_1	PD Detection Physical Area (mm^2)
i_{PD}	PD Generated Current (mA)

T	Period (s)
p_d	Photodiode Aperture
P_{loss}	Power Loss (W)
G	Repeater Gain
V_{sq}	Square waveform Voltage (V)
Δf	Subcarrier Frequency Spacing (Hz)
F_{sw}	Switching Frequency (Hz)
σ^2	Variance of the Voltage Signal (V^2)
H_2	VLC Channel Gain
A_2	VLC Detector Physical Area (mm^2)

Abbreviations

AC	Alternating Current
ACO-OFDM	Asymmetrically-Clipped OFDM
BER	Bit-Error Rate
DC	Direct Current
DCO-OFDM	DC-Biased Optical OFDM
EMI	Electromagnetic Interference
FFT	Fast Fourier Transformation
Gbps	Giga Bits per Second
IFFT	Inverse Fast Fourier Transformation
IM/DD	Intensity Modulation/Direct Detection
IoT	Internet of Things
LED	Light Emitting Diode
LECD	Light Emitting Commutating Diode
LPA	Linear Power Amplifier
MOSFET	Metal-Oxide-Semiconductor Field-Effect Transistor
OFDM	Orthogonal Frequency-Division Multiplexing
OOK	On-Off Keying

OPPM	Overlapping Pulse-Position Modulation
OWC	Optical Wireless Communication
PLC	Power Line Communications
PoE	Power over Ethernet
PPM	Pulse-Position Modulation
PWM	Pulse Width Modulation
QAM	Quadrature Amplitude Modulation
RF	Radio Frequency
SER	Symbol Error Rate
SNR	Signal to Noise Ratio
SMPC	Switching Mode Power Converter
SSL	Solid-State Lighting
UV	Ultra Violet
VLC	Visible Light Communication
V2V	Vehicle to Vehicle
WLAN	Wireless Local Area Network
WPAN	Wireless Personal Area Network

Declaration of Academic Achievement

I, Alireza Barmaki, hereby declare that I am the sole author of this thesis. This is a true copy of the thesis, including any required final revisions, as accepted by my examiners. I understand that my thesis may be made electronically available to the public.

Chapter 1

Introduction

The rapid expansion of smart home technologies, industrial automation, and connected consumer electronics has led to a surge in internet-of-things (IoT) devices. This increased demand for high-density, short-range wireless communications has put considerable strain on the already limited radio frequency (RF) spectrum. Additionally, the rise of high-bandwidth applications such as video streaming and online gaming, along with the growing use of AI-driven services that require significant data transmission, has further exacerbated spectrum congestion [1–8]. This situation has prompted an active search for alternative or complementary systems to RF to meet the growing demand. One promising solution is optical wireless communication (OWC), which utilizes the broad and unregulated spectrum of infrared (IR), visible, or ultraviolet (UV) bands to enable communication. Due to the widespread use of LEDs in lighting infrastructure, visible light communication (VLC), which is a subset of OWC that uses the visible light spectrum, has gained a particular advantage in realizing optical communication links, specifically in indoor applications such as IoT [3, 4].

1.1 Visible Light Communications

Visible light communications is a means of communication that employs visible light waves, with wavelengths ranging from 380 nm to 750 nm, to convey information. Data are encoded by modulating the intensity of LED light at a rate imperceptible by human eyes, thus enabling communication. Due to the non-coherent nature of LEDs, VLC systems are limited to intensity modulation/direct detection (IM/DD). In this context, only the power or intensity of the emitted light can be modulated, rather than the amplitude or phase of the underlying optical carrier. This imposes specific constraints on the signaling design in VLC systems. At the receiver, a photosensitive diode detects these changes in light intensity and converts them into corresponding electrical signals.

1.1.1 VLC Advantages

One of the primary advantages of VLC is the ability to leverage existing lighting infrastructure to enable data transmission [1, 5, 6]. Since VLC uses LED luminaires, which are already widely deployed for illumination [2, 7, 9], the system can be implemented with relatively less effort and at a lower cost compared to conventional RF wireless communications [8]. This allows VLC to provide communication services without the need for additional installations or substantial changes to current lighting systems. However, it is important to consider that the signal still needs to reach the LED luminaires, typically via a wired or wireless connection to a central data infrastructure [10]. Another significant benefit of VLC is the vast and unregulated available spectrum [1, 2, 11]. Unlike RF, which has a limited spectrum requiring regulation and authorization [7, 12], the visible light spectrum is much larger [13]. In many indoor illuminaiton scenarios, the SNR available for communications is also similarly high (often in excess of 40 dB) due to lighting requirements [14]. Security is another area where VLC excels due to its propagation properties. Visible light cannot penetrate walls, providing a natural confinement of the communication signal to a specific area [1, 15]. This containment reduces the risk of eavesdropping and unauthorized access, offering a significant security advantage over RF communication, which can easily pass through walls and be intercepted. Additionally, under standard lighting conditions [6, 16], there are no eye safety concerns with VLC, while RF signals can be harmful to humans if they contain a large amount of energy.

1.1.2 VLC Applications

Visible light communications have a wide array of applications, including indoor connectivity [5, 16, 23–31], vehicle-to-vehicle communication [32, 42–52], indoor positioning [60, 64–69], and underwater communications [70–74]. Among these, one of the significant applications of VLC is in indoor environments. Since the advent of the IoT [17–19] concept and the rise of smart homes [20–22], which connect nearly every household appliance to the internet, coupled with the growing reliance on the internet for daily activities such as media streaming, cloud storage, and online gaming, the demand for high-density, high data rate, and low-latency indoor connections has become more critical than ever [23–25]. The high data rate, high density, and low latency capability of VLC make this technology an ideal solution to support indoor IoT applications. [16, 26, 27]. The low latency characteristic of VLC is derived from the high SNR, which allows for straightforward encoding and signal processing, thereby minimizing computational delays relative to RF systems. This technology also proves valuable in hospitals, where electromagnetic interference (EMI) from RF signals can disrupt sensitive medical equipment. VLC offers a safe and reliable alternative for data transmission in these critical environments, ensuring seamless communication without compromising patient safety [16].

Research in the transportation sector has demonstrated that wireless data communications, both between vehicles (V2V) [32–34] and between vehicles and infrastructure (V2I) [35, 36], has the potential to prevent up to 81% of road accidents [37]. LEDs, due to their efficiency and longevity, are increasingly becoming the standard in transportation lighting, including streetlights [38], vehicle headlights and taillights [39], and traffic signals [40]. Given this trend, VLC, known for its low latency [24], is being considered as a viable option for implementing V2V and V2I communication systems. However, VLC in outdoor settings, particularly in vehicular applications, presents different challenges compared to indoor scenarios. Indoor VLC typically requires high data rates over short distances [41], while outdoor vehicular communication demands much longer ranges with a focus on minimizing latency [42, 43]. Current research on vehicular VLC primarily addresses challenges such as enhancing the system's robustness against noise [44–47], given the highly noisy environment of vehicular communication channel, which arises from sources like ambient sunlight, headlights, and streetlights [48–50], and extending communication range [45, 51, 52].

As the demand for location-based services (LBS), such as location tracking and navigation, continues to grow [53, 54], research on positioning technologies has received increased attention [55–57]. While outdoor positioning is provided by satellite-based systems like the global positioning system (GPS) [58], existing indoor positioning technologies, such as wireless fidelity (WiFi) and radio-frequency identification

(RFID), struggle to balance accuracy with implementation costs [59], all the while dealing with the issues of interference and security concerns. Due to its strong directionality and low susceptibility to multipath interference [1, 60], visible light positioning (VLP) is emerging as a promising candidate for delivering high-accuracy, low-cost indoor positioning services [61–66]. Additionally, VLP can be easily integrated into environments with existing VLC systems, contributing to both affordability and ease of deployment. VLP has been reported to offer accuracy down to the centimeter level [66, 67]. VLP can be classified into two primary approaches: active positioning and passive positioning, based on the involvement of the user in the localization process [59, 65, 68, 69]. In active positioning, the user typically carries a device, such as a mobile phone or sensor tag. In passive positioning, the user is not directly involved, and the location is determined by measuring the reflections of signals from the user.

Beyond these applications, VLC is also used in information display systems, serving as a medium for sign boards, identification tags, and even sound communication systems [75–77]. The diverse applications of VLC [5, 16, 23–30, 32, 42–52, 60, 64–77] underscore its versatility and potential to revolutionize communication infrastructure across various domains, from enhancing IoT connectivity in smart environments [78, 79] to ensuring safe and efficient communication in transport and sensitive medical settings.

1.2 VLC System Architecture

A visible light communication (VLC) link comprises a transmitter, a channel, and a receiver [80–82], as illustrated in Fig.1.1. The transmitter typically includes a signal modulator, an LED driver, an amplifier, and a series of LEDs. The LED driver, often

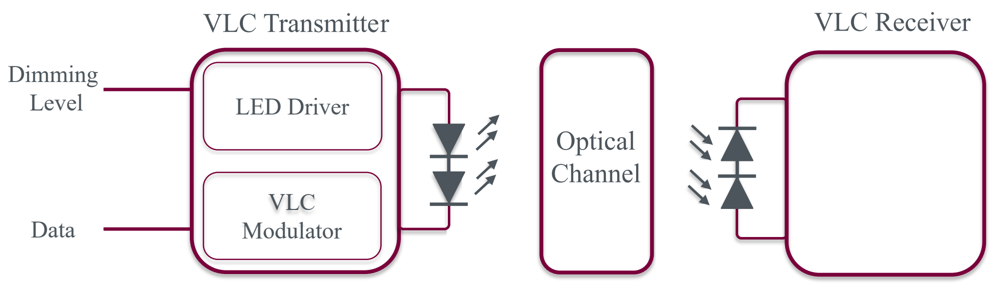

Figure 1.1: Generic structure of a VLC system

a DC/DC converter [83], supplies the LEDs with a stable DC current to maintain the desired brightness level. The data to be transmitted are modulated and amplified before being superimposed onto the DC current from the LED driver, resulting in intensity modulation of the emitted light. The optical signals then propagate through the optical channel to reach the receiver. At the receiver, a photosensitive diode detects the change in the intensity of the light signal and converts it into a corresponding electrical current. This signal is amplified and converted to a voltage signal through a transimpedance amplifier (TIA) [84]. After passing through the TIA, the signal undergoes filtering to remove noise and unwanted high-frequency components. It is then further amplified and conditioned to ensure sufficient signal strength and fidelity. Finally, the processed signal is demodulated to extract the transmitted data.

Since VLC adds a communication capability to luminaires, it is essential that the quality of illumination, the primary function of the luminaire, is not adversely impacted. Furthermore, integrating communication features into luminaires should be accomplished with minimal complexity and cost. Additionally, the communication performance must comply with standards [85–87] to be viable as a supplement to RF technology or as an alternative. Therefore, the implementation and commercialization of VLC, while balancing these three aspects presents a significant challenge.

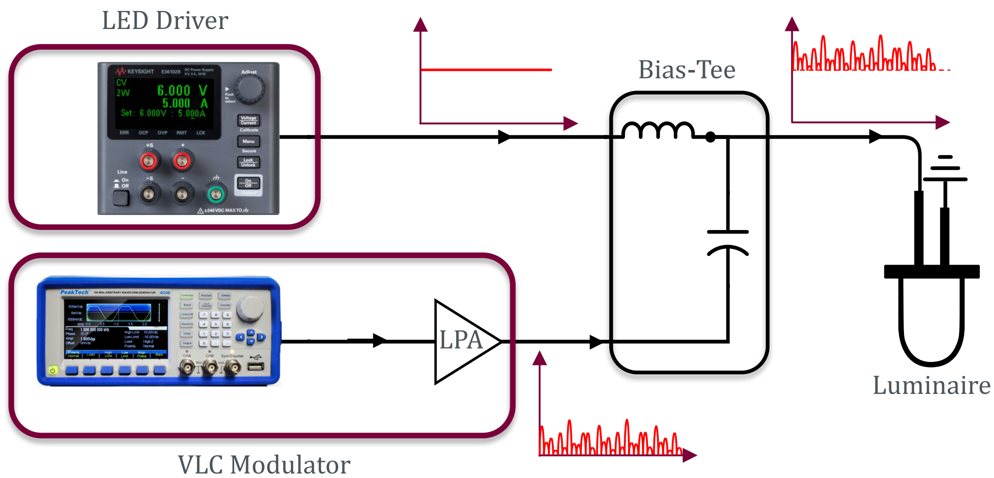

Figure 1.2: Conventional VLC transmitter

1.3 VLC Challenges

There are numerous challenges associated with the design and implementation of a VLC link, some of which are discussed in this section.

1.3.1 Maintaining Illumination Quality

One of the most important challenges is preserving illumination quality as a key consideration that can be analyzed from various aspects. One such aspect is efficacy [88–90], which refers to the total light output of the luminaire divided by the input power. This measures how efficiently a luminaire is converting electrical power (W) into illumination (lm). Another important aspect is dimming capability [91–93], a significant advantage introduced by LEDs, allowing the brightness of a luminaire to be adjusted to a fraction of its maximum output. Unwanted fluctuations in light intensity visible to the human eye, known as flicker, is another crucial aspect and should be minimized, as it can cause discomfort and health issues [93–95]. Although efficacy, dimming, and flicker are critical aspects of illumination quality, other factors—such as color shift [96] and aging pace [97]—also require attention. LEDs are valued for their efficiency, cost-effectiveness, dimming capability, and long lifespan [97, 88]. Therefore, when modulating LED luminaires to enable VLC, maintaining these features is of great importance. However, a typical VLC transmitter includes additional components such as RF linear amplifiers, which are known for their low electrical efficiency. For example for a class A, B, or AB electrical efficiency can be as low as 10% [98]. This significantly increases the losses in the system and consequently decreases the efficacy of the luminaire, and damages cost-effectiveness by increasing the number of required components. Moreover, the high-frequency modulation of LEDs in VLC systems can reduce their efficacy, shorten their lifespan, and cause color shifts [97, 88]. It should also be noted that enabling VLC can introduce flicker and constrain the dimming capability of an LED [91–94], issues that must be addressed.

1.3.2 Transmitter Design

Another key challenge in developing an effective VLC system is designing the transmitter to achieve a balance between efficient illumination and reliable, high-speed communication while minimizing complexity and component count [99–104]. In a conventional transmitter design, an off-the-shelf LED driver generates the DC current required to maintain the desired brightness, and a linear power amplifier (LPA) amplifies the modulated signal. Typically a bias-tee circuit is utilized to combine the two signals which are delivered to the LEDs [98–100], see Fig. 1.2. Although the design achieves high data rates, the significantly low efficiency of the LPAs and

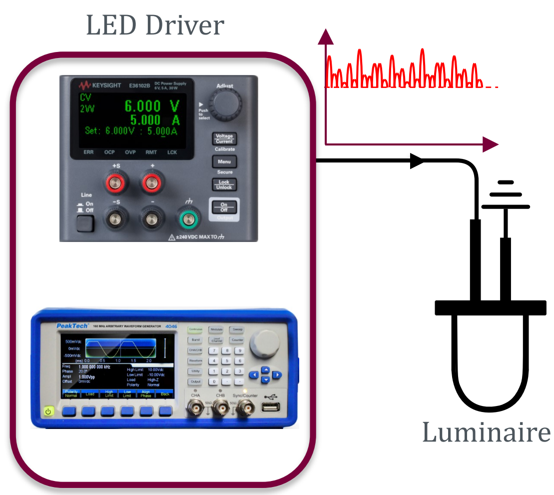

Figure 1.3: VLC transmitter integrated within an LED driver

additional components used reduce the efficacy and increase the complexity and cost of the VLC implementation [98]. In order to address the efficiency issue with the LPAs, using switched-mode power amplifiers (SMPAs) has been proposed in [101] which alleviates the efficacy loss but adds to the complexity of the circuit due to the natural complicated control scheme associated with SMPAs [90]. Another approach that has been studied regarding VLC transmitter design, focuses on embedding the modulator and amplifier within the LED driver, meaning that the modulation and amplification of the signal happens within the LED driver [102–104, 107–111]. As a result, the need for separate additional components such as LPA, and bias-tee circuit is eliminated, see Fig. 1.3. Although integrating modulators and amplifiers into LED drivers has been suggested in [102, 107–110] to enhance performance, there has been little consideration given to designing or adapting LED drivers specifically for VLC applications [104, 111].

1.3.3 Provision of Uplink Channel

An effective VLC system must facilitate both the transmission of data from LEDs to users (downlink) and the transmission of data from users back to the LEDs (uplink). While much of the existing research primarily addresses downlink communication and focuses on unidirectional data flow [98–115], a fully functional VLC system requires a well-established uplink channel [116–121]. Challenges associated with visible light uplink include potential interference with downlink data, user discomfort when handheld devices emit light to communicate with luminaires, and the limited power available from device batteries. As a result, VLC downlinks are often complemented by another technology for uplink channel implementation. In this regard, a hybrid solution was introduced in [121], where the uplink was realized through RF communications, or in another study, red-green-blue LEDs were utilized to deploy bi-directional VLC links where each colour of the LED carries a different signal [119]. Infrared spectrum is most often utilized to realize the optical uplink channel for VLC as they are imperceptible to human eyes, will avoid interference with visible light used for downlink, and comply with strict regulations on emitted power in generating uplink signals [116–118, 120].

1.3.4 Fronthauling and Backhauling

While establishing communication with users in the room is crucial, equally important is the connectivity of luminaires to a backbone internet infrastructure (backhauling) and among luminaires themselves (fronthauling) [122]. Various methods for this connectivity have been explored in the literature, including integrating VLC with power line communications (PLC) [123–125], power-over-ethernet (POE) that operates within the range of $44 - 47\ V$ [126], free-space optical (FSO) systems [127, 128], and radio frequency. While PLC and POE are wired backhaul solutions and suffer from infrastructure costs, FSO requires precise link alignment which also necessitates specialized implementation setups. In another study utilizing millimeter wave RF has been considered however, security and the special hardware required for implementation are the key disadvantages of this approach [129].

1.3.5 Establishing Standards

Visible light communications is considered a promising candidate for future communication systems. However, to fully realize its potential, challenges such as interference and the integration of VLC with existing technologies like WiFi must be addressed. To address these issues, various standards are being developed by organizations such as the Institute of Electrical and Electronics Engineers (IEEE), Japan Electronics and Information Technology Industries Association (JEITA), and International Telecommunication Union (ITU-T). The JEITA CP-1221 and JEITA CP-1222 standards [131] were developed to outline the fundamental concepts of visible light communication (VLC) and visible light identity detection systems, respectively. Later, IEEE 802.15.7 [132] was crafted to establish the guidelines for free-space optical communication using visible light, ensuring sufficient data rates for multimedia services and compatibility with illumination infrastructure for short-range applications. Following that the IEEE 802.15.7.13 task group [136, 87, 86] was formed to focus specifically on the PHY and MAC layers for Light Fidelity (LiFi) [133]. ITU-T G.9991 [85] defines home networking for visible light communications and introduces two physical layer approaches based on DC-biased OFDM (DCO-OFDM) and asymmetrically clipped OFDM (ACO-OFDM). The more recent IEEE 802.11.bb [134] reuses the existing physical and MAC layers of IEEE 802.11 [135]. It defines new channels over the light medium without significantly altering the rest of the standard.

Orthogonal frequency division multiplexing (OFDM) is a prevalent modulation technique extensively employed in both wired and wireless communication systems, including mobile communications [137], broadcasting [138], and wireline communications [139]. Its application has also expanded to wireless local area networks, fixed wireless systems [140], and television and radio broadcasting [141, 142], making it a global standard. This widespread adoption is primarily due to the resilience of OFDM to inter-symbol interference and its straightforward equalization processes. However, the direct application of OFDM, as used in RF systems, to optical channels is not feasible since visible light communication (VLC) systems rely on intensity modulation and direct detection (IM/DD), which necessitate real non-negative signals. Therefore, traditional OFDM requires adaptation for optical channel compatibility [143]. To meet this need, several variants, such as ACO-OFDM [144], DCO-OFDM [144], and layered ACO-OFDM (LACO-OFDM) [145, 146], have been developed, with ongoing research exploring further enhancements.

In addition to the challenges previously mentioned, VLC design also encounters issues such as inter-cell interference [147, 148], receiver design [149, 150], and transceiver [151, 152] implementation. However, this thesis primarily focuses on addressing transmitter design, provisioning an optical uplink channel, and briefly discussing fronthauling and backhauling in VLC, all while ensuring that the primary role of the luminaire, which is maintaining high-quality illumination, is upheld see Fig. 1.4

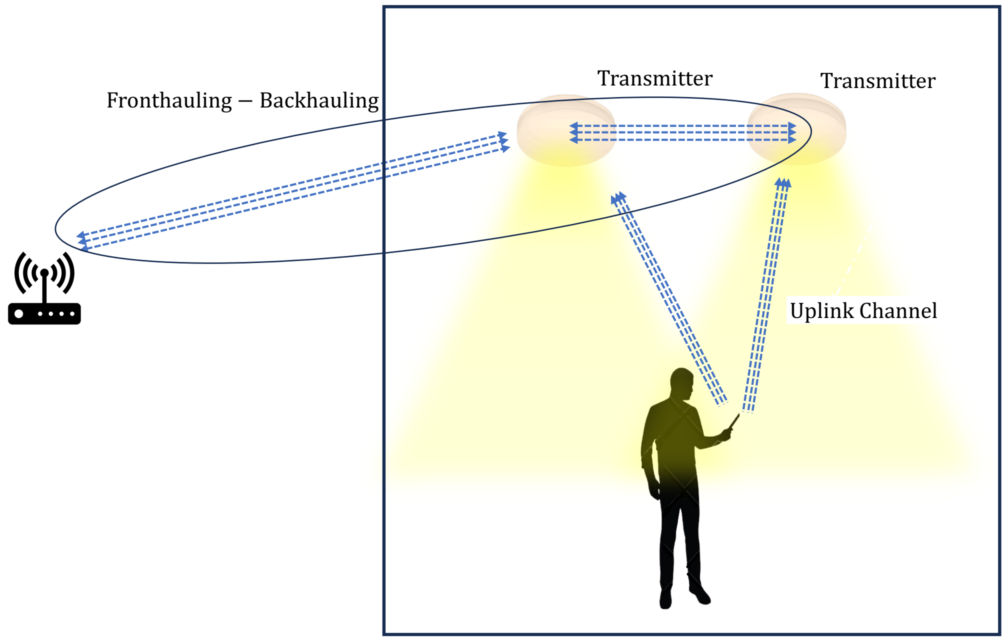

Figure 1.4: challenges in implementation of VLC

1.4 Thesis Layout

This thesis develops an approach to integrate VLC components directly into switched-mode power converters to address challenges in the deployment of a VLC system such as transmitter design, uplink provision, and backhauling solution, see Fig. 1.4. Unlike previous research in this field which predominantly incorporates off-the-shelf power converters and attempts to integrate VLC capabilities, this thesis explores the deliberate design of a power converter specifically tailored for VLC applications. By proposing new topologies or modifying existing ones to incorporate VLC equipment, this approach aims to simplify the design, enhance cost-effectiveness, and improve illumination quality. This thesis follows the guidelines for a 'sandwich' format as outlined in [153]. Fig. 1.5 illustrates the structure of the thesis. It consists of four distinct chapters, each containing abstracts, introductions, body sections, and

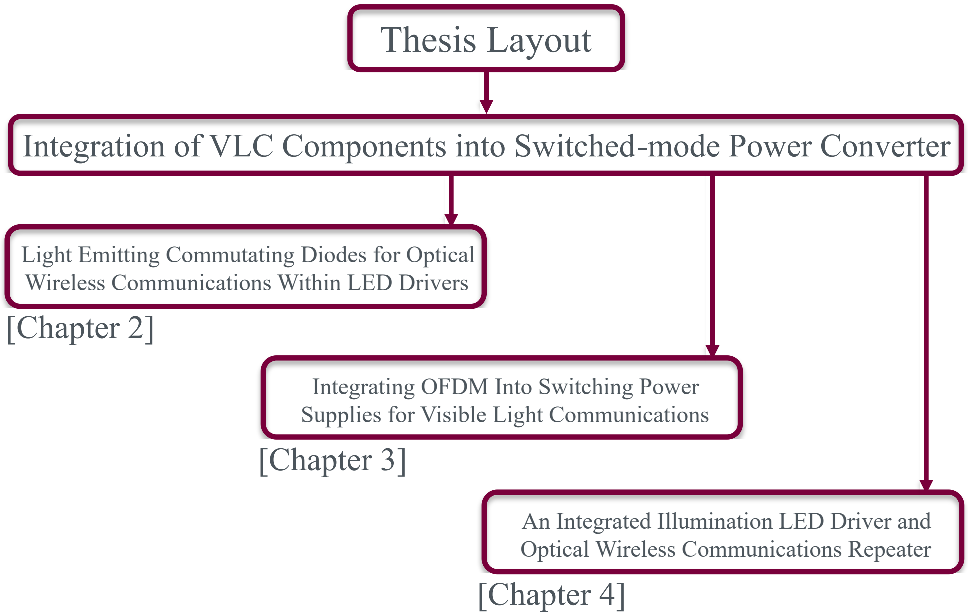

Figure 1.5: Thesis Layout

conclusions. Additionally, an appendix is included after the main body of the thesis, containing supplementary materials, detailed calculations, and additional data that support the findings presented in the chapters. Each chapter has references from the literature and citations are listed in the bibliography at the end of the document. The organization of this thesis is detailed as follows.

Chapter 2 introduces light-emitting commutating diodes (LECDs) as replacements for Schottky diodes in buck or boost converters [154]. By using pulse position modulation or overlapping pulse position modulation, data transmission through the LECDs is enabled, creating a VLC-capable LED driver without requiring additional equipment or components, and without using a linear amplifier. This integration embeds the VLC transmitter within the LED driver. The substitution of one or more LECDs enhances the overall efficacy of the luminaire, as the energy previously dissipated through the diodes is now harnessed for both data transmission and illumination in the LECDs. Consequently, enabling VLC not only maintains but also improves the efficacy of the luminaire. Additionally, since only the LECDs are modulated and not the entire illumination string, there is no color shift or reduction in the lifespan of LEDs. These findings are confirmed through both simulations and experimental demonstrations.

Chapter 3 further extends the performance of the LECD method introduced in **Chapter 2** by supporting advanced modulation schemes such as OFDM. **Chapter 3** introduces a novel technique where the switching MOSFET is used as an amplifier during its off intervals [155]. To the best of the author's knowledge, this approach has not been previously explored. The method described in Chapter 2, cannot perform advanced modulation schemes like OFDM, which is an effective solution for transmission with high spectral efficiency. This technique amplifies the transmission signal and injects it into the circuit through the gate pin of the MOSFET during its off periods, modulating the brightness of the LECDs. This method leverages the 'off' state of the MOSFET to function as an amplifier, effectively integrating the VLC transmitter and amplifier into the LED driver without additional complexity or components. This approach addresses the challenges of designing a comprehensive, efficient, and simple transmitter. The viability and performance of this topology are analyzed and verified through simulations and experiments using a boost converter and ACO-OFDM modulation.

While **Chapter 2** and **Chapter 3** focused on improving the performance of the downlink channel in a VLC system, **Chapter 4** introduces an optical repeater integrated into a luminaire to address the uplink channel in a VLC system. This design uses a multiphase boost converter where the diodes in each phase are replaced with photodiodes, and the capacitor at the final stage is removed. This topology can receive signals from users, amplify them, and transmit them omnidirectionally in the environment. The output can use different LED strings, such as visible light or infrared. This allows the IR LEDs to communicate with a central data source like an optical modem (backhauling) or connect to other luminaires in the room (fronthauling). Moreover, the amplification level can be adjusted by selecting the number of LEDs at the output. In this configuration, reception occurs in each phase of the converter when the MOSFET is on, while the off period of the MOSFET is used to amplify and inject a signal for transmission. The removal of the capacitor from the last stage ensures that the modulated signal reaches the output LEDs and is transmitted. This results in a transceiver that operates as a receiver and repeater when the MOSFET is on and as a transmitter when the MOSFET is off. Extensive simulations are used to support the design while the feasibility has been experimentally demonstrated on a two-phase boost converter.

Chapter 5 concludes the thesis and outlines potential directions for future research.

1.5 Description of Contributions to Publications

This thesis adheres to the "*sandwich thesis*" structure. Chapter 2 has been published in IEEE Photonics Journal [154], Chapter 3 has been published in IEEE Transactions on Circuits and Systems I [155], and Chapter 4 has been submitted to IEEE Transactions on Circuits and Systems I and is under peer review. The following section outlines the individual contributions of each co-author to the research.

Chapter 2: **Light-Emitting Commutating Diodes for Optical Wireless Communications within LED Drivers**

Authors: Warren Pawlikowski, Alireza Barmaki, Mehdi Narimani, and Steve Hranilovic

The original manuscript was drafted by the first author, Warren Pawlikowski, and revised by Alireza Barmaki. It was submitted to and published in the IEEE Photonics Journal, with Barmaki recognized as a co-author. According to IEEE authorship criteria, contributions of Barmaki encompassed intellectual input to the analysis and interpretation of data associated with the work, revising and rewriting the whole paper, and approving the final version of the paper. While the paper displayed innovation, its explanations for associated losses were not justified. Barmaki proposed a novel approach, suggesting the use of efficacy instead of efficiency to address perceived losses, highlighting the conversion of energy into lumens rather than Watts in illumination systems. Barmaki revised the paper and proactively sought alternative advantages for the proposed method, diligently scouring existing literature, and identified additional benefits, such as the prolonged LED lifespan due to the absence of modulation. Adapting the paper to this new perspective necessitated a comprehensive rewrite, including crafting a new introduction section titled “Commutating Diodes for Use in Optical Wireless Communications,” and contributing to the conclusion. Despite not conducting simulation or experimental research in this paper, Barmaki’s vision significantly reshaped the narrative and presentation of the paper, leading to its successful publication in IEEE Photonics Journal (Volume: 12, Issue: 5, pages: 1 - 11, October 2020). The majority of this work appears here, with minor adjustments to enhance the thesis clarity. The material within this chapter is under the copyright of IEEE, and it is allowed to be reused in the thesis.

Chapter 3: **Integrating OFDM into Switching Power Supplies for Visible Light Communications**

Authors: Alireza Barmaki, Mehdi Narimani, and Steve Hranilovic

The notion of employing a "switching MOSFET as an amplifier" originated from collaborative discussions between Alireza Barmaki and Dr. Steve Hranilovic. Barmaki subsequently conducted theoretical investigations and simulation analyses to assess the viability of this concept. He independently designed the printed circuit board required for experimental validation and carried out all experimental procedures. Throughout this endeavor, he received feedback from both Dr. Hranilovic and Dr. Narimani, pertaining to communication and power electronics aspects, respectively. Following the preparation of a draft manuscript, Dr. Hranilovic provided input, which Barmaki incorporated into the paper. Dr. Narimani also contributed additional insights during the final review stage, contributing to the completion of the paper. The contents of this chapter were published in IEEE Transactions on Circuits and Systems I [155] (Volume: 71, Number: 6, Pages: 2925 - 2937, June 2024), with the copyright held by the IEEE. Permission for the reuse of this material has been granted by the IEEE, as indicated in compliance with their request.

Chapter 4: **An Integrated Illumination LED Driver and Optical Wireless Communications Repeater**

Authors: Alireza Barmaki, Mehdi Narimani, and Steve Hranilovic

The concept of developing an optical wireless communications repeater occurred to Alireza Barmaki during his research on integrating a VLC receiver into an LED driver. When he discussed this idea with Dr. Hranilovic, he guided Barmaki towards additional applications, such as uplink channel provision, and fronthauling and backhauling. Barmaki pursued these research directions and developed the idea further. He then independently designed, simulated, and experimentally tested a prototype in the laboratory environment. Throughout the manuscript preparation, Dr. Hranilovic provided supervision, insights, and numerous invaluable comments, helping to finalize the draft. Dr. Narimani later reviewed the power electronics sections, ensuring the integrity of the paper. Part of this work has been submitted to IEEE Open Journal of the Communications Society and is currently under peer review.

Chapter 2

Light-Emitting Commutating Diodes for Optical Wireless Communications within LED Drivers

In this chapter, a novel approach is suggested to integrate a VLC transmitter within the led driver of a luminaire by substituting the Schottky diodes in a buck/boost converter with LEDs, addressing the transmitter design mentioned in Sec. 1.3.2. The added LEDs enhance illumination and improve efficacy, while the separation of illumination and communication LED strings reduces the risk of color shift and extends the lifespan of the LEDs—all of which align with the illumination quality considerations discussed in Sec. 1.3.1. Power-efficient PPM and OPPM modulation schemes are implemented for data transmission, and experimental measurements of

BER and efficacy are conducted to assess the performance of the topology.

2.1 Abstract

Although visible light communication (VLC) systems provide high-density links for use in Internet-of-Things (IoT) devices, the design of high rate VLC transmitters that maintain luminaire efficacy is an open problem. In this Chapter, a novel approach to the integration of VLC within light-emitting diode (LED) drivers is proposed through the replacement of freewheeling/blocking diodes with light-emitting devices termed a *light-emitting commutating diodes* (LECDs). In this manner, communications and illumination can be provided using a simple, cost effective design while employing no additional components. The subtle change of LED driver control signals facilitates the transmission of data from LECDs while simultaneously supporting illumination functions. Lighting controls such as dimming are maintained and combined with modulation through the use of overlapping pulse position modulation (OPPM) and performance is quantified. Prototype buck and boost converters with LECDs are implemented and their efficacy is measured. Though current commercial LEDs are not intended for such signalling applications, we experimentally demonstrate their feasibility in this application and suggest methods to make such

converters reliable. It is demonstrated that the addition of an LECD improves the efficacy of the luminaire as compared to conventional LED drivers while simultaneously enabling a VLC downlink.

2.2 Introduction

The use of high density, short range, wireless communication links is increasing with the rise of the IoT. The number of wireless connected devices is forecast to continue to increase to a staggering 15.7 billion devices by 2023 [156]. Currently, RF is used to establish these links, however, as the number of devices increases, so too does interference. Among the simplest solutions to this RF spectral crunch is the adoption of wireless physical layers that do not interact with RF directly, such as OWC.

In parallel, LED luminaires have become ubiquitous in modern lighting solutions due to their advantages in efficacy and lifetime. Solid-state lighting has allowed for VLC to develop and provide a method for RF-interference free, high density, communication links. The integration of VLC into LED luminaires is a compelling idea, however, without proper attention the inherent advantages of efficacy and lifetime of LED luminaires deteriorates with the integration of communication functionality.

Power-over-Ethernet (PoE) [157] is an obvious choice to provide both power and data to VLC luminaires [158]. Through the use of PoE, 44-57 V at powers from 15-100 W can be supplied in addition to Gbps data connectivity [159]. In a typical implementation, the DC power supplied over PoE is input to a step-down DC-DC converter such as a buck converter to ensure the proper current output to the illumination LEDs. It is important to note that while step-down converters may be among the most common converters used, many illumination applications require step-up converters as well. For example, boost converters are used for automotive headlights where many LEDs are used in series. VLC-enabled V2V communications using LED headlights/taillights has subsequently also become an active area of research [160] [161].

An important aspect of every power electronic device is the *efficiency* (η), which quantifies how well it is utilizing the input power (P_{in}) to convert it to useful output power (P_{out}). This directly depends on the inherent power losses (P_{loss}) in the system. In a luminaire, however, illumination is the primary function. Thus, in the design of a VLC modulator it is essential to quantify the impact on illumination performance, in particular, the *efficacy* of the luminaire measured in lumens/Watt. In other words, the measured useful output is not the electrical power but rather the illumination. As a result, in this work, rather than using efficiency as a metric, system performance is quantified by the luminous efficacy (K). That is, for a luminous flux output ϕ from the luminaire, define

$$\eta = \frac{P_{out}}{P_{out} + P_{loss}} \qquad \eta = \frac{P_{out}}{P_{in}} \tag{2.1a}$$

$$K_l = \frac{\phi}{P_{in}}. \tag{2.1b}$$

While both (2.1a) and (2.1b) measure the ability of a system to convert input electrical power into a useful output, definition (2.1b) is the most appropriate metric for a luminaire where the useful output is illumination. According to (2.1b), any increase in the total output lumen flux or reduction in power losses of the circuit while maintaining a constant input power will result in efficacy improvement.

Multiple methods have been proposed to integrate VLC into LED luminaires. Though inefficient, the bias-T is an example of an external modulation approach [162]. Direct modulation of LED outputs has also been proposed (e.g., [163]). While these techniques permit high rate communications, they suffer from reduced efficacy in addition to greater cost. The concept of replacing the commutating diodes in buck/boost converters by illuminating LEDs and short circuiting the output was presented in [164–166]. However, this approach maintains high efficacy at the cost of neglecting the capability of the LEDs to provide communication. Another recent approach to this problem is to integrate the VLC modulator within a DC-DC converter in order to preserve efficacy. One approach is to shunt the output LED current using an additional switch [167–169]. This design maintains high efficacy and is capable of high data rates, however, output brightness is proportional to the duty cycle of the shunting switch. A variation of this approach uses a switch in series with the illumination LEDs [103, 167, 98, 108] and has the same trade-offs as the previous case with design challenges caused by the open state of the switch. An additional solution to integrating VLC modulators into LED drivers is the use of pulse width modulation (PWM) to adjust the LED driver duty cycle, thereby slowly varying output brightness. While this approach maintains a desired brightness, is capable of high efficacy, and does not increase component count, its achievable data rates are approximately one tenth of the converter switching frequency [167–169]. Recently, in [107, 111] the use of interleaved converters is considered to allow for high efficiency

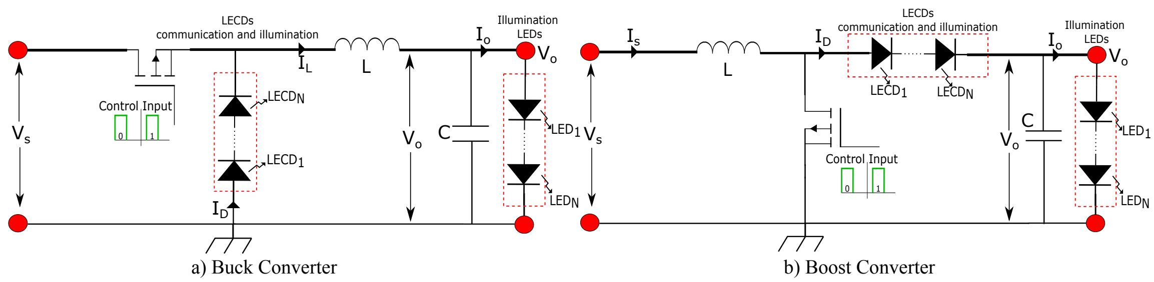

Figure 2.1: Simplified circuit diagrams of proposed LECD buck (a) and boost (b) converters

and high data rate communications. By changing the phase of switches within the interleaved converter, data may be transmitted through the ripple produced. The disadvantage of this approach is found in the increased amount of components and complexity.

In this chapter, a novel method of integrating VLC modulation into LED drivers is presented which achieves constant output brightness while allowing for modulation at the full rate of the LED driver switching frequency. As shown in Fig. 2.1, the freewheeling diode and blocking diode in the conventional buck and boost DC-DC converters respectively are replaced with an LED, termed a *light-emitting commutating diode* (LECD). The energy typically dissipated by the freewheeling/blocking diode found in LED driver topologies is now utilized to provide communications, leading to an improved efficacy. While replacing the freewheeling/blocking diodes by LECDs to provide data transmission, the illumination LEDs are kept at the output of the driver. This results in a system with *two* output ports of illumination, one of which provides data transmission. Since LECDs contribute to the overall illumination of the system, a desired brightness can be obtained with a lower required current compared to the traditional LED drivers. This yields lower junction temperatures in the illumination LEDs which slows degradation of LEDs, namely color shift and lumen depreciation which are major concerns in all LED drivers [170].

The underlying concept of the topology proposed in [164], where the Schottky diode of the driver is replaced with a white LED and the output is short circuited, is similar to that of our earlier conference paper [171] and both were developed simultaneously. However, the concept in [164] was presented for LED drivers solely being used for illumination purposes, aiming to reduce the complexity of the circuit and maintaining high efficacy. The focus here is to integrate VLC into LED drivers, meaning the LED driver is capable of data communication and illumination at the same time. Unlike [167–169, 103, 98, 108], the output brightness of the drivers in this work depends only on the duty cycle of the converter and is not limited by any other factor. In contrast to [167–169], no limit is imposed on the data rates of communication, since LECDs can be switched up to their nominal frequency. Dissimilar to [107], no increase in either the number of components or the complexity of the circuit is observed. Moreover, unlike earlier designs, driving illumination LEDs with a lower and unmodulated constant current for the same level of luminous intensity will also guarantee better colour quality and life span of LEDs [170]. Unlike [164–166] where the entire load current is being supplied by pulsed current, in this work the pulsed current flowing through the LECDs is just a small portion of the load leading to lower EMI and junction temperatures. This chapter extends our earlier conference paper [171] which considered only buck converters. Here, this concept of LECDs is extended to both buck and boost converters for use as VLC transmitters and further analysis of the systems presents design considerations for various operating conditions as well as communication performance results. It is apparent that many other topologies with such diodes can be altered to achieve VLC and some topologies require both freewheeling and blocking diodes such as forward or flyback DC-DC converters. These topologies may use LECDs in place of a freewheeling diode, blocking diode, or both to provide communications.

2.3 Commutating Diodes for Use in OWC

2.3.1 Concept

Buck and boost converter topologies were chosen for their simplicity as non-isolated LED drivers capable of constant current for use in indoor lighting applications and car headlights. By maintaining constant current through the inductor, illumination LEDs are able to be driven by constant DC.

Both freewheeling and blocking diodes are necessary for buck and boost converter operation respectively. These devices are typically a source of power loss within these circuits and many LED driver designs attempt to minimize this loss through the use of diodes with low forward bias (e.g., Schottky diodes) or replacing them with a switch (synchronous converter) [172]. In our approach, rather than minimizing loss, the lost power is harnessed to make it useful for enabling optical wireless communications and illumination. This is accomplished by replacing freewheeling and blocking diodes present in standard LED drivers with LECDs.

Energy typically dissipated within a freewheeling or blocking diode is used to provide modulated illumination for VLC. Wavelengths outside of the visible range can also be used, for example, LECDs that produce infrared light allow for OWC invisible to the human eye. The use of LEDs outside of the visible spectrum will not contribute to overall luminous flux of the proposed design and therefore will not benefit from increased efficacy demonstrated later in this chapter.

The proposed designs are able to modulate VLC signals at the full switching rate of the LED driver while retaining high efficacy. In addition to energy efficient modulation, the designs support a simple method of dimming through the use of PWM. By altering the duty cycle, D, the output power is scaled and the luminaire is dimmed. Finally, the proposed design remains simple and cost effective due to component count being kept the same when compared to a conventional luminaire.

Another advantage to this approach over earlier designs is that LEDs modulated for VLC are separated from illumination LEDs. A major concern for illumination is the degradation of LEDs which leads to colour shift and lumen depreciation [170]. Previously proposed VLC modulators use illumination LEDs to support modulation. Reductions in lifespan, quality of colour, and lumen output are potential disadvantages of these approaches. The separation of communication LEDs and illumination LEDs provides a solution to minimize the effects of supporting VLC on the quality of illumination provided by the luminaire.

By dividing the ratio of illumination LEDs to LECDs appropriately, it is possible to overcome the problem of low reverse bias voltage of a LED. The number of LECDs and illumination LEDs can be divided simply by choosing a different ratio of LEDs within a buck converter or changing the placement of the output capacitor in a boost converter. The number of illumination LEDs determines the required output voltage and also determines the reverse biasing of LECD(s) in boost converters.

2.3.2 Electrical Operation and Design Considerations

Replacement of freewheeling and blocking diodes with LECDs cannot be done without careful assessment of the consequences of replacing a conventional diode with an LED. Various elements of converter operation are affected and must be understood to produce a luminaire supporting VLC through use of an LECD.

LECDs in buck converters are reverse biased by V_s as shown in Fig. 2.1. Although reverse biasing may be problematic for LECDs as they are typically not designed to be driven in this manner (e.g., [173]), their capability to be reverse biased is already tested and verified in [164]. In cases where reverse breakdown of the LECD is low in comparison to desired V_s, $N > 1$ LECD can be used in series to combat relatively high reverse bias voltage. Similarly, boost converter operation relies on LECDs being reverse biased, however, they are reverse biased by V_o instead of V_s. In the case of buck converters, input voltage V_s is the larger than output voltage while V_o in boost converters is the largest voltage present in the circuit. This implies that LECDs must handle the largest potentials found in each topology in reverse bias.

Additionally, the forward voltage drop for LECDs is typically larger than conventional diodes. A conventional diode may have a forward voltage of approximately 0.7V, while a conventional high power white LED will be in the range of 3V [173]. To denote this difference, when referring to V_f of LECDs, V_f^{LECD} will be used. Increased forward voltage yields two major design considerations: the impact of forward voltage on efficacy and the maximum achievable output voltage.

Our proposed topology contributes to the efficacy of the driver in two aspects. First, the power delivered to the LECDs, unlike the power consumed by a switching diode, cannot be termed as a dissipating power, since it is being used for illumination and communications. As a result, the power loss in the circuit is reduced and the total luminous flux is increased simultaneously, both of which contribute to the efficacy according to (2.1b). In fact, the only remaining losses of the circuit will be switching losses of the MOSFET [174–176] and some conduction losses due to the small resistance of the inductor. Second, as a result of the compensation done by the LECDs in terms of illumination, the desired level of lighting can be obtained with a lower current flowing through the converter as compared to conventional topologies. This will reduce power loss in every element of the converter, indicating a better overall efficacy.

The use of N LECDs will also affect the output voltage control. Using N LECDs in series impacts the output voltage of a buck and boost converter respectively as,

$$V_o = V_s D - (1-D) N V_f^{\mathrm{LECD}}, \tag{2.2}$$

$$V_o = \frac{V_s}{(1-D)} - N V_f^{\mathrm{LECD}}. \tag{2.3}$$

To derive (2.2) and (2.3), a constant current through the inductor and a large output capacitor for constant V_o were assumed. These equations demonstrate that V_f^{LECD} reduces the achievable V_o, however, the existing LECDs will compensate for the illumination as long as the output voltage is high enough to forward bias all illumination LEDs in the case of using multiple illumination LEDs in series. This changes the selection of duty cycle D to yield a desired output illumination. To achieve the same V_o and I_o, as the base case buck or boost converters, higher values of D must be used in converters using LECDs. However, this is not an issue since

LECDs provide illumination in addition to communication signals. This results in an LED driver that can employ lower values of V_o and I_o to achieve the same illumination as the base case.

Use of multiple LECDs also results in higher losses and lower output range. Therefore, unless required, for the greatest efficacy and output range the number of LECDs used should be minimized. If dimming is not required and lower efficacy is acceptable, a greater number of LECDs may be used to improve communications performance by transmitting greater optical power.

2.3.3 Communicating with LECDs

Previous designs for VLC modulators introduce a modulated signal superimposed onto the constant (i.e., DC) driving signal required for illumination. By implementing a VLC modulator using LECD(s), the LEDs used for communications and those for illumination are separated.

For simplicity, the modulation schemes considered here are restricted to PPM and OPPM. These modulations work well to modulate LECDs because information can be sent for any combination of D and amplitude and avoid any flicker in the output light. However, PPM and OPPM encounter issues, including inefficient bandwidth utilization and the requirement for synchronization at both chip and symbol levels [44].

Define M as the modulation order and T as the symbol period. For $D > \frac{M-1}{M}$ the symbols are sent as PPM, while for smaller D the pulses must overlap, giving rise to OPPM.

Data are transmitted by varying the periodic nature of the current through the

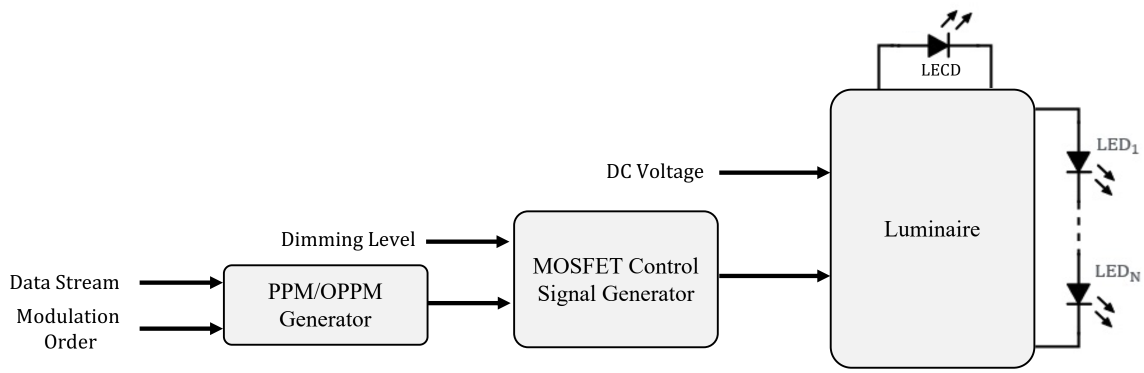

Figure 2.2: System block diagram of the LECD converter.

LECD, I_{LECD}, by changing the position of the on-time during each period of T seconds via PPM or OPPM Note that the freewheeling or blocking diode conducts during the non-conducting phase of the switch. Figure. 2.2 illustrates the system block associated with the VLC-enabled luminaire. Manipulating the control switch conduction interval to alter the position of the I_D current pulse in T using PPM or OPPM modulates the light emitted by the LECD thereby transmitting a VLC signal. The current flowing through the freewheeling diode I_D in its conducting periods is the same as the inductor current I_L. Figure 2.3.a and .b illustrate the control signal, V_{gs}, and the luminaire's output flux, ϕ_{tot}, as functions of time for 4OPPM and 4PPM, respectively. The labeling of the PPM pulses is done by Gray coding.

To enable dimming for LECD converters, D can be set to a lower value. This will yield lower V_{out} and I_{out}, resulting in I_{LECD} with a reduced peak amplitude flowing for a longer time in the diode. Once a desired dimming level is set, D should be kept constant to maintain a desired brightness. This will also maintain a constant state for receiving the signals from communicating LEDs. Changes in D of LECD converters will affect communications performance as a result of changing LECD pulse width

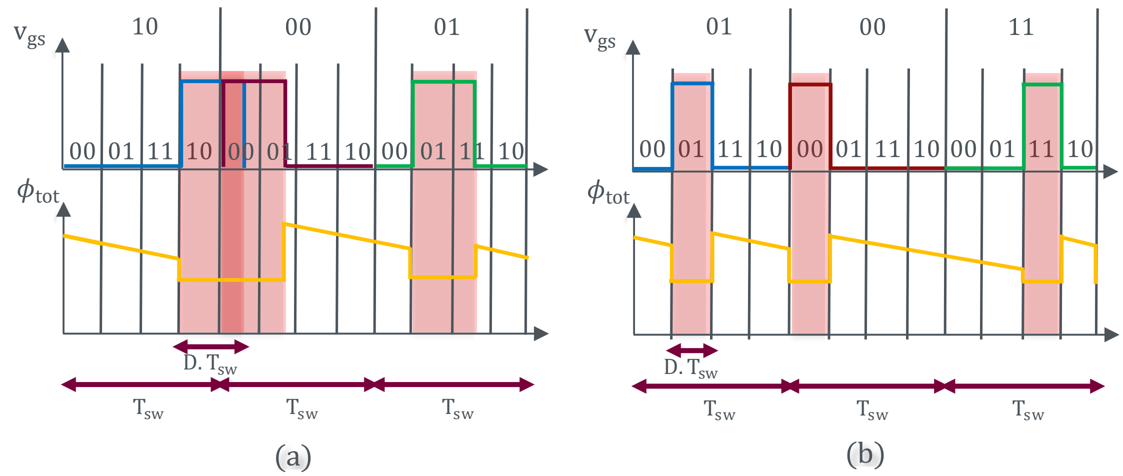

Figure 2.3: Time-domain control signal and output optical flux: a) 4OPPM b)4PPM

and amplitude. The highest communications performance will be achieved for high D and is due to resulting LECD pulses having less overlap with adjacent symbols in addition to greater amplitude. This will also determine the modulation order that is viable depending on required communications performance.

2.4 Experimental Results

2.4.1 Experimental Setup

The parameters and components used for the experimental setup are tabulated in Table 1. Component values were based on similar commercial designs used in practice for indoor lighting[177]. The LEDs used were white Philips Lumiled 3535L [179] or CREE XLamp XP-E2. Although these devices are not intended to be operated in reverse bias, our testing of 20 LEDs each illustrated a reverse breakdown of approximately 40 to 45 V (well above the given value on the data sheet and noted in

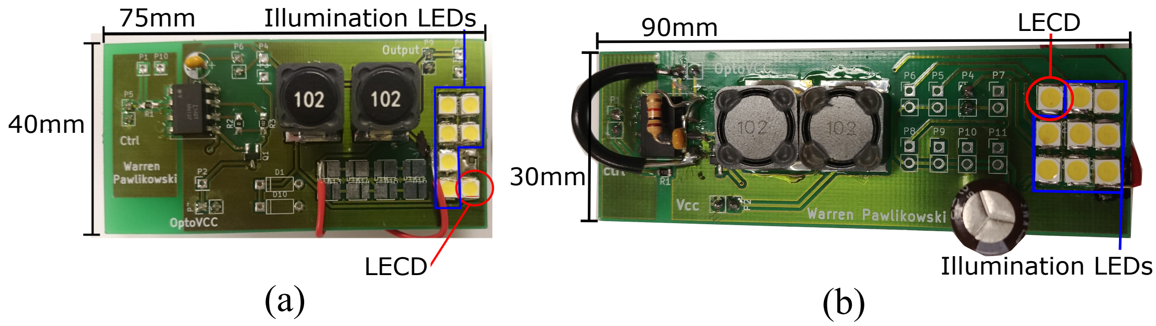

Figure 2.4: Experimental LECD buck (a) and boost (b) converter prototypes. Experimental setup is displayed in Fig. 2.6.

[180]). Due to reverse breakdown voltage, the source voltage used for experimental measurements was limited to 40 V.

Fig. 2.4 a) and b) display photographs of the LECD converter prototypes used to characterize and determine the performance of proposed buck and boost converter designs in terms of communication and illumination. The circuit diagram of both converters was earlier presented in Fig. 2.1.

Communicating and illumination LEDs are identified within the LED array. The modulated optical signal from the LECDs is summed spatially with the illumination LEDs causing an easily removed DC shift via high pass filter at the receiver.

Experimental buck and boost converter results were completed using a single LECD. The experimental luminaires were modulated to test communications in addition to quantifying efficacy. Random sets of data were created comprised of a binary BPPM/BOPPM, two bits per symbol 4-OPPM, and three bits per symbol 8-PPM, with the total size of the random sets sent amounting to 10^8 bits for each modulation order. BPPM was used for the case of tests that resulted in $D \geq 0.5$ and BOPPM was used when $D < 0.5$. Also, D was limited to 60% limiting the conduction losses in the converter [181]. For further tests of higher order, OPPM was used due to the larger

Table 2.1: Simulation and Experimental Parameters for the VLC OFDM Boost Converter (cf. Fig. 3.2)

Parameter	Symbol	Value
Inductor	L	2 mH
Capacitor	C	1 μF
Switching Frequency	F_{sw}	400 kHz
Light Emitting Diode	LED	Lumiled 3535L
Switching Device	Sw	IRLML0060TRPBF
Freewheeling Diode	D	1N4148
Input Voltage	V_{in}	40 $V(Buck)$12 $V(Boost)$
Max. Load Current,	I_{Lmax}	300 mA
Optical Receiver,	R_x	PDA36A
Photodiode Aperture,	d_p	1 in
Receiver Bandwidth,	BW	5.5 MHz
Receiver Gain Setting,	–	10 dB
Receiver Noise RMS,	n	280 μV

size of transmitted constellation. The data were saved into a ROM of a DE0-Nano FPGA [182] and converted into an appropriate control signal. This signal was applied to the switch of each converter through a 6N137 opto-isolator. The signal output from the opto-isolator was probed via a Teledyne Lecroy Wavesurfer 3024 to capture the sent sequence prior to being affected by the transmitter, channel, or receiver.

To test communications, light from the LECD was combined with illumination LEDs via the THORLABS DG20-1500 diffuser and captured by the THORLABS PDA36A photodiode with a 1 inch aperture and an adjustable gain initially set to 10dB as shown in Figure 2.6. The luminaire was placed 110 cm from the photodiode along the optical axis. After the waveforms were collected from the oscilloscope, they were saved and analyzed with MATLAB. Additionally, the signal persistance function within the oscilloscope was utilized to create eye diagrams for each modulation order. To improve received waveforms and reduce the effects of ambient light, eye diagrams and sample waveforms were collected using a THORLABS LB1761 bi-convex lens in front of the photodiode.

Experimental measurement of efficacy was accomplished by using a multimeter and integrating sphere. To monitor P_{IN}, voltage and current from the DC supply was monitored with a multimeter. In order to quantify the optical output, the illuminance, E_V, was measured using the Extech Instruments Model HD400 lux meter and normalized. Through the combination of the integrating sphere and the fixed area of the lux meter detector, a normalized measure of optical efficacy was made. The normalized optical efficacy used to contrast with simulated efficacy curves is defined as

$$K'_O = \frac{E_V/P_{in}}{E_V/P_{in}|_{\text{BCmax}}}. \tag{2.4}$$

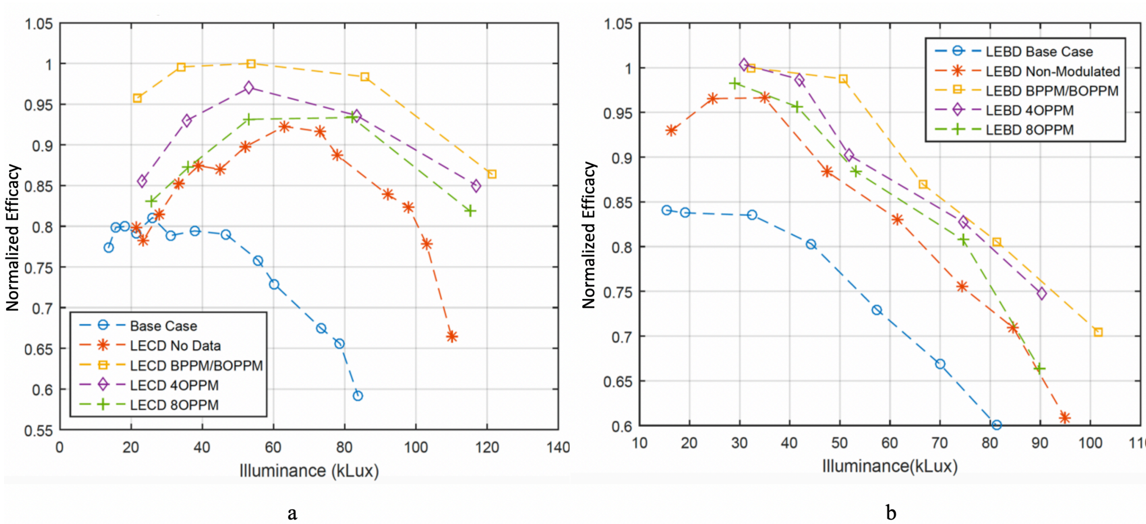

Figure 2.5: Experimental normalized optical efficacy of the Base Case, LECD (a)buck (b)boost design non-modulated, LECD design modulated by BPPM/BOPPM, 4-OPPM, and 8-OPPM.

where $E_V/P_{in}|_{\mathrm{BCmax}}$ is the maximum value of illuminance measured for the base case and the quantity used to normalize optical efficacy.

2.4.2 Experimental Efficacy

Efficacy using LECDs is shown to be improved over the base case of both LED driver topologies under all modulation orders as demonstrated by Fig. 2.5.

It is apparent that the LECD contributes a significant amount of illumination compared to power consumed. Additionally, both LECD converters produce more light for a given operating condition when compared to the base cases. Due to this, a luminaire can be designed to operate at lower current, with higher efficacy, and produce the same luminous flux, resulting in a lower junction temperature of the LED which leads to a longer life span. Additionally, LECD converters achieve maximum efficacy at higher duty cycles, which explains the rightward shift observed in the

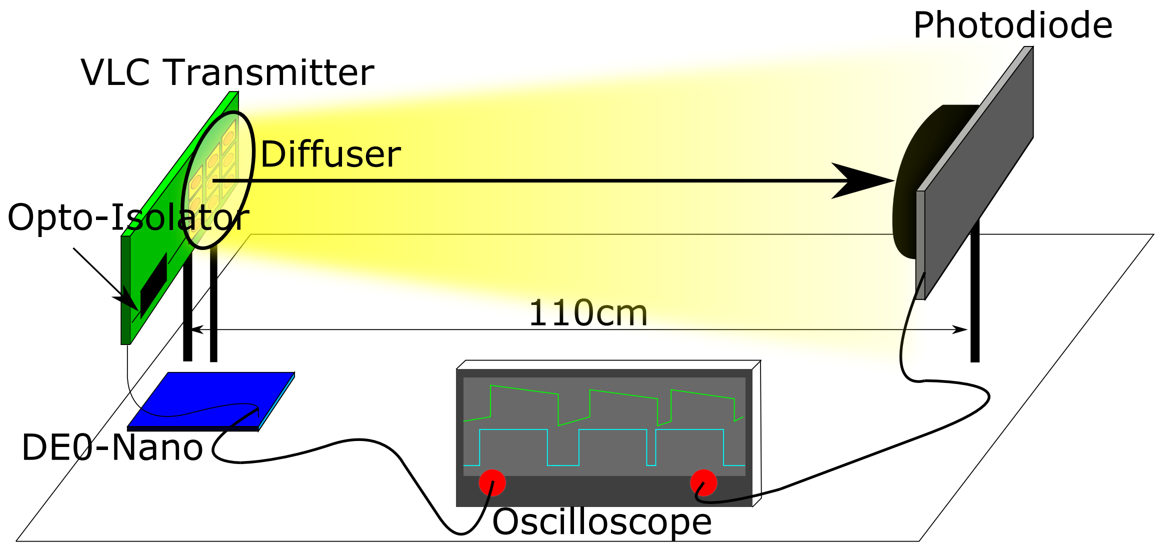

Figure 2.6: Diagram demonstrating the experimental setup to collect communication results.

efficacy peak in the figures.

In the cases where PPM or OPPM symbols are at either extreme of the period, two switching cycles are removed as illustrated in Fig. 2.7. Therefore, on average, for BPPM/BOPPM the amount of switching transitions is reduced by a half. Switching losses of the LECDs in addition to other switching losses are therefore reduced by half resulting in higher efficacy. As higher order modulation is used, the likelihood of removing switching transitions is reduced resulting in lower efficacy, up to 5% when comparing 8 OPPM and BOPPM. Therefore for a system capable of the greatest efficacy, BPPM/BOPPM should be used as this maximizes the amount of switching transitions saved. However, efficacy of the proposed design is still improved over by approximately 10% compared to the base case for higher orders of PPM and OPPM that make the elimination of switch transitions unlikely.

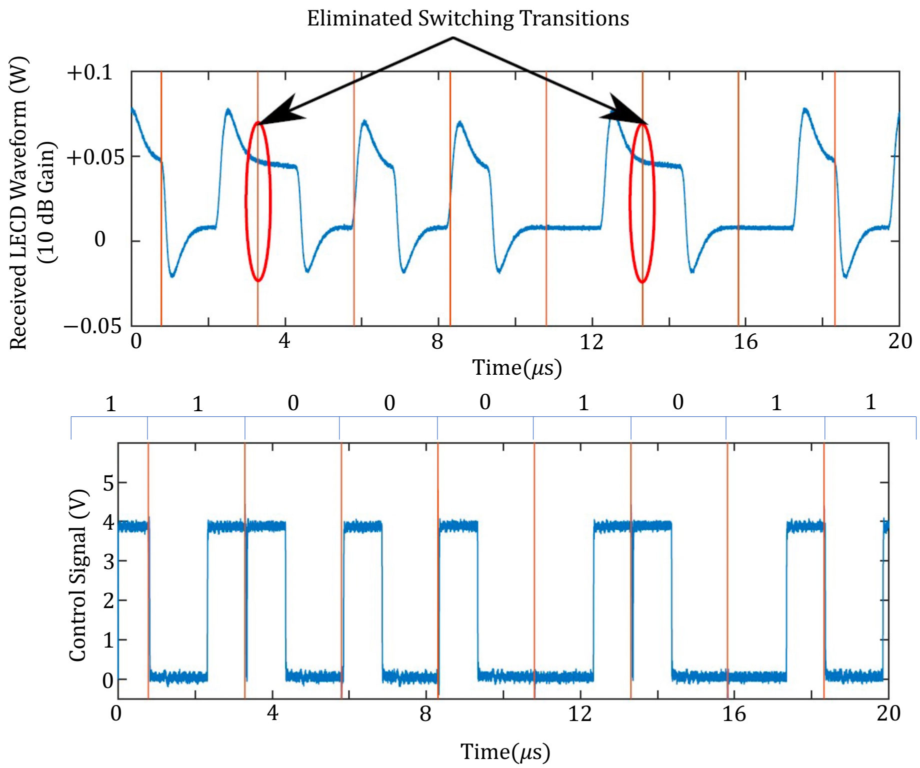

Figure 2.7: Experimental received and transmitted BPPM waveforms measured according to Fig. 2.6. The control signal was recorded at the MOSFET's gate-source, as illustrated in Fig. 2.1.

2.4.3 Experimental Communication Results

Initially, transmitted waveforms were visually inspected to verify that the control circuit generated appropriate waveforms that were sent and received (e.g., see Fig. 2.7). The received signals for the buck converter were heavily distorted by a resonant frequency above that of f_{sw}. This was determined to be caused by parasitic capacitance present in the PCB layout. Design of the boost converter was completed after tests of the buck converter and LECDs. Additionally, due to higher drive current, boost converter waveforms are received at greater amplitudes compared those of the buck. Received waveforms of LECD driver lag in time due to the presence of the inductor. Resultant lag quantities are based upon the size of the inductor.

Figure 2.8 presents a sample 8-OPPM eye diagram for the boost converter using an LECD and a $D = 0.5$. Although the data are overlapping, they are all distinct and the eye is open, indicating that the transmission can be done with a good SNR.

It can be seen that the amount of noise present is small relative to the amplitude of the signal. The eye diagram testing 8-OPPM is not impacted by jitter and timing issues. For lower D, eye diagrams will close as the amplitude is reduced and overlap of signals is increased.

As the order of PPM is increased and lighting is dimmed through a reduction in current, overlaps of OPPM symbols increases, and therefore eye diagrams deteriorate and symbol transitions become more difficult to differentiate. This results in more errors when demodulating for dimmed luminaires and an eye diagram that is closing and overlapping with other signals more.

One million symbols were sent at various duty cycles in order to produce symbol error (SER) and bit error rate (BER) curves. These curves are shown in Fig. 2.9 for 4-OPPM and 8-OPPM with a setup shown in Fig. 2.6.

(SNR) communication channel making this change less apparent. When SNRs are reduced by increasing range or using smaller receiver apertures (e.g., as in a mobile phone receiver), the change of system performance in M and D will be more notable though following the same trends. Notice also that if a specific minimum SER or BER is targeted, such as the typical 10^{-3} pre-FEC BER limit, as the luminaire is dimmed, it may be necessary to decrease the order of modulation used to maintain the desired error rate. As the luminaire is dimmed beyond a certain point, the achievable rate may necessarily be reduced. This is accomplished via a simple change of the control

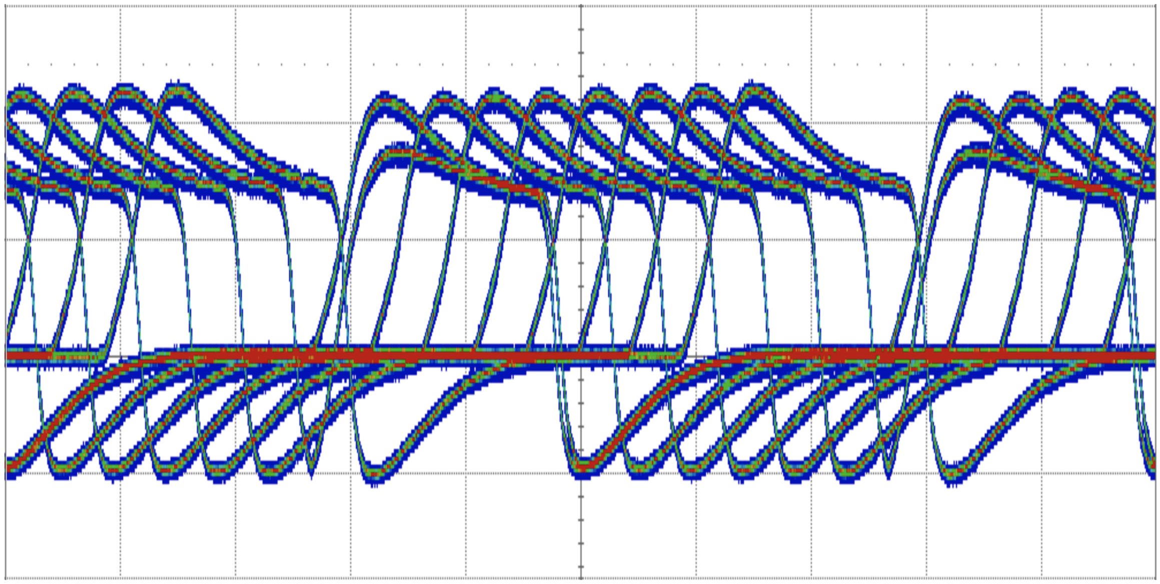

Figure 2.8: Example eye diagram of LECD boost topology modulated by 8-OPPM. Amplitude and time divisions set to 10mV / div and 500 ns / div respectively.

signal of the proposed design.

As previously stated, received symbols deteriorate for decreased D, resulting in higher SER and BER as illustrated in Fig. 2.9. The BER graph is presented as a function of the duty cycle, which represents the illuminance level (total luminous flux). This approach highlights the performance of the system under varying brightness conditions, an essential aspect of VLC systems where dimming plays a significant role. Furthermore, since the noise is modeled as white additive Gaussian noise, the corresponding SNR can be determined from the illuminance level [14]. Increasing modulation order will further deteriorate sent signals as symbols will overlap more and become more difficult to differentiate. Therefore, pulses of higher amplitude with less overlap (greater D) are required to achieve the same SER and BER as lower order modulation schemes. This is demonstrated by the comparison of 4-OPPM and 8-OPPM in Fig. 2.9 where 8-OPPM requires a D of the LECD boost converter

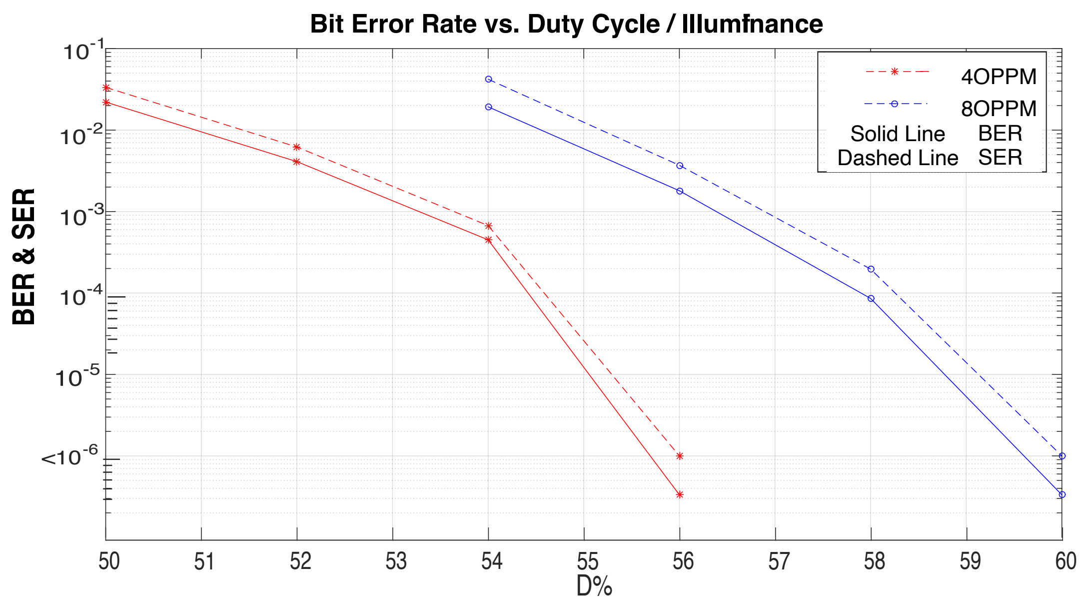

Figure 2.9: Symbol error rate (SER) and bit error rate (BER) curves for 4-OPPM and 8-OPPM at reduced intensity.

to be approximately 7% higher than necessary for the same error rate of 4-OPPM. However, the modulation order can be further increased, if sufficiently high SNR and bandwidth conditions exist, to increase data rate further [44]. Of course, this increase in rate will come at the expense of increased timing recovery requirements. It should be noted that in the particular experiment, small distances, large receiver apertures and sensitive receivers yield a high signal-to-noise ratio Data rates of 800 kbps and 1.2 Mbps were achieved by the experimental LECD buck and boost LED drivers using 4-OPPM and 8-OPPM respectively with a switching frequency of 400 kHz.

2.5 Conclusions

A VLC transmitter was designed and implemented to meet wireless communication standards without relying on complex control systems, increasing the number of elements, imposing limits on LED modulation speed, or using linear amplifiers that compromise efficiency. Furthermore, this topology increased efficacy and maintained illumination quality while preventing color shifting, a common issue in VLC systems.

By experimentally demonstrating the proposed changes in both buck and boost converter topologies, the use of LECD(s) was shown to be a viable solution to implementing VLC within LED drivers in a wide range of applications. The approach presented in this chapter demonstrates support for dimming and has the advantage of separating LEDs used for communications and illumination, hence preserving the life span of the illumination LEDs. This approach offers both an improved efficacy, up to 15% compared to the conventional boost converter, and communications up to 1.2 Mbps, without increasing component count for future IoT VLC transmitters.

This experimental research is a proof of the concept, while in practical and commercial VLC systems, pre- and post-equalization should be applied to overcome the data rate limits imposed either by the limited bandwidth of the LEDs or the modulation scheme. PPM was selected for its simplicity and flicker-free operation. With its current specification, the system can be implemented for low data rate VLC applications such as smart lighting control, indoor positioning, and IoT device communication.

While LEDs have a bandwidth limited to several MHz, in this approach, the MOSFET switching frequency, 400 kHz, becomes the primary bottleneck to data rate. Future work can explore high-frequency Gallium Nitride (GaN) MOSFET devices [108] to enhance switching frequency and system data rates. If the switching frequency increases to the point where the LECD bandwidth becomes the limiting factor, adopting Micro LEDs could overcome the constraints of phosphor-coated LEDs and further boost data rates. This would enable VLC transmitters with buck/boost converter topologies to achieve data rates in the tens of Mbps.

Chapter 3

Integrating OFDM into Switching Power Supplies for VLC

As highlighted in Sec. 1.3.5, VLC systems must comply with the latest standards, including the ability to perform advanced modulation schemes such as OFDM. Since indoor VLC channels often operate at high SNR and are bandwidth limited [14], the use of multi-level OFDM modulation is convenient to achieve high data rates. This chapter introduces the dual application of the MOSFET in the LED driver of a luminaire, functioning both as a switching and amplifying element. Consequently, the need for an additional linear amplifier is eliminated, and the modulated signal is injected directly into the transmitter via the MOSFET. The elimination of the linear amplifier reduces losses, thereby enhancing efficacy, while also providing simplicity and cost-effectiveness compared to traditional methods, as verified by experimental measurements in a lab environment. In contrast with the approach in Chapter 2, the data rate in this OFDM modulator is limited by the bandwidth of the LECD device and not the MOSFET switching frequency.

3.1 Abstract

VLC is a promising technology that combines the ubiquity of illumination devices with broadband communication to provide connectivity. The most recent VLC communication standards specify OFDM as the underlying modulation due to its spectral efficiency and compatibility with existing broadband modems. However, a key challenge remains in realizing VLC modulators capable of generating OFDM signal compatible with the primary illumination function, while ensuring the efficacy of the luminaires.

In this Chapter, a novel method is proposed to integrate OFDM modulation into a switching power supply. Commutating diodes in the DC/DC converter are replaced by LEDs which are used for communication while the larger illumination string of LEDs is left unmodulated, preserving the quality of illumination and luminaire lifetime. Biasing the switching MOSFET to its saturation region during its off states allows for the MOSFET to act as an amplifier, amplifying the OFDM communication signal and injecting it to the LECD. As a result, energy efficient LED drivers capable of OFDM signal transmission is realized. Both simulation and experimental results are provided to demonstrate the feasibility of this approach, showcasing superior performance compared to existing literature in terms of component count, efficacy,

illumination quality, and reliability. Notably, based on simulation results, the efficacy of our approach surpasses the bias-T approach by approximately 6.25%.

3.2 Introduction

The ever-growing demand for wireless communication and limited RF spectrum has led to spectral congestion and has initiated interest in higher frequency bands for communications. In particular, OWC is a promising candidate to address the RF congestion problem as it considers the broad unregulated light spectrum. Due to the confinement of OWC signals by opaque boundaries, such links are particularly interesting in secure, dense indoor deployments such as the IoT. More recently, OWC links have been realized by leveraging the widespread use of LEDs in solid-state lighting (SSL) applications to realize *VLC* which imperceptibly modulates LEDs to simultaneously illuminate and provide connectivity. [132, 183, 184].

The concept of VLC involves utilizing visible light as a means of communication while maintaining the primary function of the lighting fixtures, i.e., illumination. Data are encoded by modulating the intensity of an LED at rates faster than the human eye can detect. At the receiver, a photosensitive diode converts the changes in light into an electrical current [185, 186]. A switching-mode power converter (SMPC) is typically used in the luminaire to regulate the brightness of the illumination. To realize VLC, the encoded information is amplified by a LPA, to deliver an AC signal which modulates the brightness of the luminaire.

Communication standards are essential for the deployment of VLC. For example, IEEE802.11 [135] sets protocols and regulations for wireless local area networks

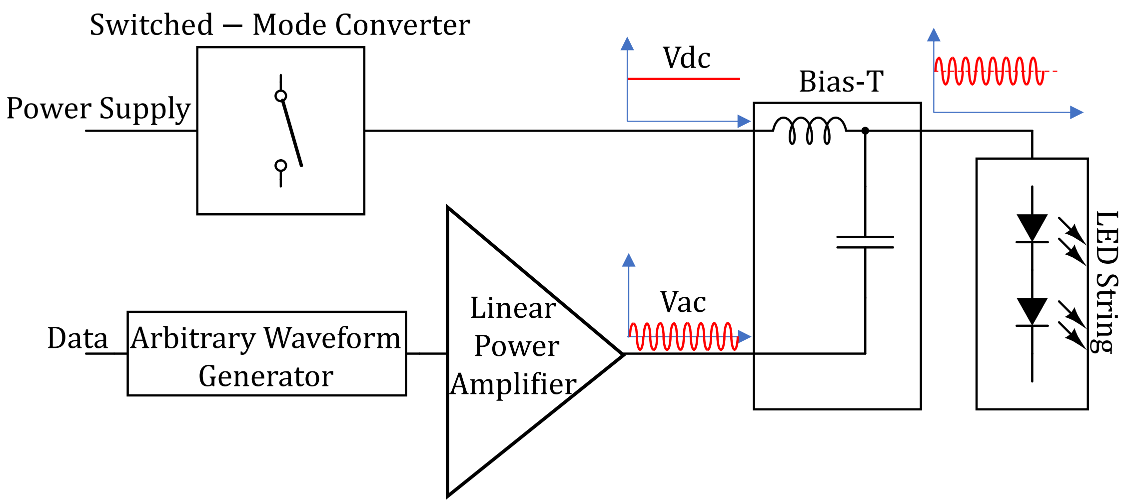

Figure 3.1: Conventional VLC transmitter with external signal modulation.

(WLAN), while IEEE802.11.bb [134] establishes standards for communication over the light medium. Similarly, IEEE802.15 specifies standards for wireless personal area networks (WPAN), and the sub-group IEEE802.15.13 [136] focuses on high-speed wireless communication via visible light. According to the latest updates from ITU-T G.9991 second amendment [85], VLC systems that comply with these standards are based on OFDM modulation popular in many radio frequency applications.

Wireless communications via VLC serves as a secondary purpose for luminaires, with their primary function being illumination. Therefore, while incorporating VLC into luminaires the impact on the quality of illumination must be minimized. One key challenge in integrating illumination and communication is to maintain a high *efficacy* [88]. Another challenge involves the *dimming capability* of the VLC system [94]. Moreover, modulation of the LEDs' brightness may result in *color shifting*, degradation of illumination quality, and faster *aging* of the LEDs over time [97]. Additionally, *flicker* [8], characterized by rapid and noticeable fluctuations in light brightness, can cause discomfort or pose health issues and should be minimized.

One of the most challenging aspects of developing a functional VLC system is implementing the transmitter, as it must find a balance between providing efficient illumination and enabling reliable communication. As such, research has focused on creating highly efficient transmitters that can deliver high-speed communication while minimizing complexity and component count. Any VLC transmitter needs a power converter to provide the LEDs with a DC current for illumination, and a means to inject the AC signal to the circuit. The design procedure can be divided into two approaches: *external modulation*, where the modulator is separate from the DC/DC converter, and *internal modulation*, which integrates the modulator into the DC/DC converter. It is important to note that these terms are coined for the specific context of this paper and should not be confused with terms such as external/internal optical modulation.

The *external modulation* approach shown in Fig. 3.1 is the most popular and consists of a typical DC/DC converter, such as buck and boost converters, to maintain the desired brightness level by generating a DC current. A linear amplifier then amplifies the modulated signal. A bias-T is often used to combine the two signals to drive the illumination LEDs. This is a widespread approach [99, 100, 187] and leads to a simple design with high overall data throughput. However, the efficiency of a class A, B, or AB amplifier can be as low as 10% [98] which substantially increases the losses in the system and therefore reduces the efficacy. In this regard utilization of switching mode power amplifiers has been studied in [101]. Although this method demonstrates significant efficiency, the inherent hardware and control complexity in the circuit design presents challenges in practical illumination applications [90]. In [105], a hybrid power amplifier is proposed where non-constant amplitude modulated data was split into two sinusoidal signals with fixed amplitudes but different phases to ensure the maximum efficiency operation of the linear amplifiers. However, this approach faced implementation challenges in avoiding mismatch between the LED strings [106].

In contrast, *internal modulation* approaches integrate the modulator and amplifier into the LED driver to overcome efficacy loss. In other words, modulation schemes are produced within the LED driver, eliminating the need for separate components such as an inefficient linear power amplifier. Consequently, this approach effectively reduces associated losses and enhances both efficacy and circuit simplicity. As a result, an LED driver is realized that can simultaneously provide DC and AC signal supply for the luminaires. However, internal modulation approaches pose a challenge as there is a trade-off between complexity and data rate. Various techniques have been suggested to address this issue. One such technique involves adding a switch to the LED string in parallel or in series to modulate the intensity of the illumination [108, 109]. This method is capable of high data rates and high efficacy, but the system's dimming capability is limited as the illumination level is proportional to the duty cycle, D. Moreover, the inability to reproduce pass-band modulation is another issue that substantially reduces bandwidth efficiency. Utilizing pulse width modulation (PWM) to alter the duty cycle is proposed in another study [102, 110]. Although it is shown to maintain good dimming capability along with high efficacy, the data rate is limited to a tenth of the switching frequency of the MOSFET (f_{sw}). In one recent study, the output ripple of the driver, typically filtered, is utilized to transmit data [103], however, this technique cannot implement OFDM as proposed in the standards above. In order to accommodate OFDM modulation, another DC/DC converter should be added synchronously to the system, leading to increased complexity, component count, and a complicated control scheme [107]. Another approach to reduce the complexity of the power circuit involves modulating a group of two consecutive pulses and extracting their first harmonic to reproduce pass-band modulation schemes [104]. However, this topology is incapable of OFDM, and the bandwidth is limited to half of f_{sw}. In other work, the Schottky diode in the converter was replaced by an LED, termed a LECD, to increase overall efficacy and separate the illumination and communication LED strings [154]. This approach is suitable for binary modulation but not spectrally efficient OFDM.

In this chapter, for the first time, we propose an internal VLC modulation approach, Fig. 3.2, to transmit advanced OFDM modulation required in current VLC standards (e.g., IEEE802.11bb) while preserving the simplicity, cost-effectiveness, and efficacy of the circuit and the luminaries. The approach in this work extends the concept of the LECD introduced in our earlier work [154] and modifies the gate signal of the switching MOSFET in a converter to allow it to operate in its linear mode rather than the cutoff in $(1 - D)$ intervals. By DC-biasing the MOSFET in the saturation region, the data to be transmitted is induced as high-frequency small signal fluctuations on the DC value, Fig. 3.3.b. The amplified current flowing through the drain-source of the MOSFET is filtered by the inductor and passes through the LECD, thus modulating its light intensity. Unlike [110], this method does not compromise the illumination as the illumination LED string is separated from the communication devices. In contrast to the PWM method [102], the data rate is not limited to a fraction of f_{sw}. Finally, different from the ripple modulation approach [107, 103], our approach has a simplified control method and is capable of OFDM modulation. This

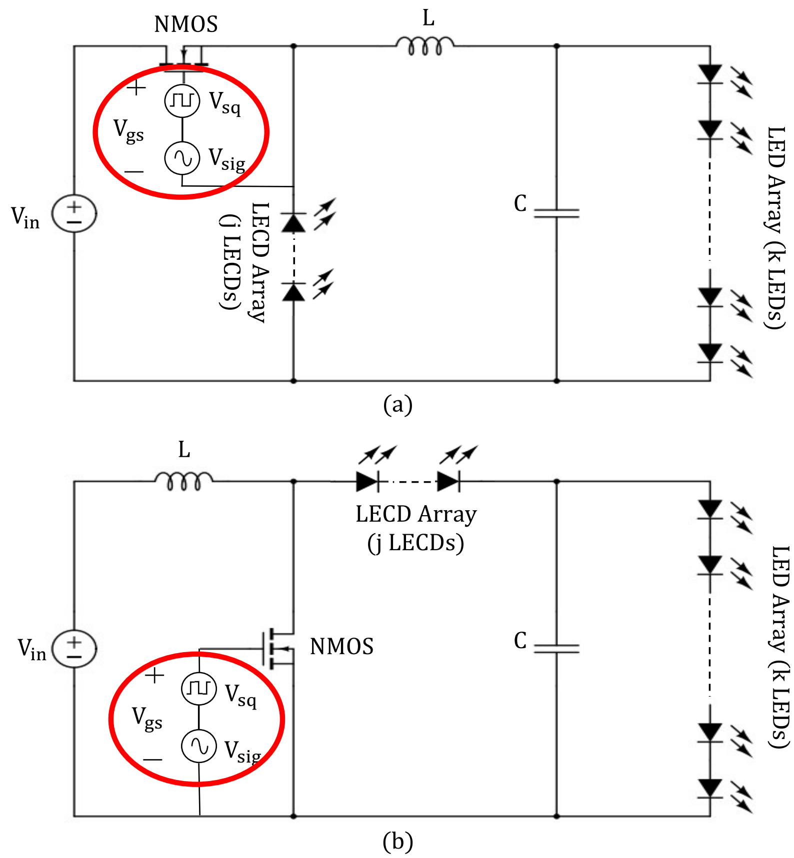

Figure 3.2: VLC enabled (a) buck and (b) boost converter with the Schottky diode replaced by LECDs.

method builds on previous research [154] in which an LED replaced the Schottky diodes in the buck/boost converter to enable data communication and enhance the overall efficacy. However, this method allows OFDM whereas [154] does not.

This chapter is organized as follows. Section 3.3 outlines the concept of integrating the amplifier in the MOSFET off-state and addresses concerns of preserving efficacy while maintaining high communication performance. Section 3.4 discusses the simulation analysis while Section 3.5 presents the experimental setup and results. Finally, Section 3.6 concludes the paper by comparing the proposed method and other

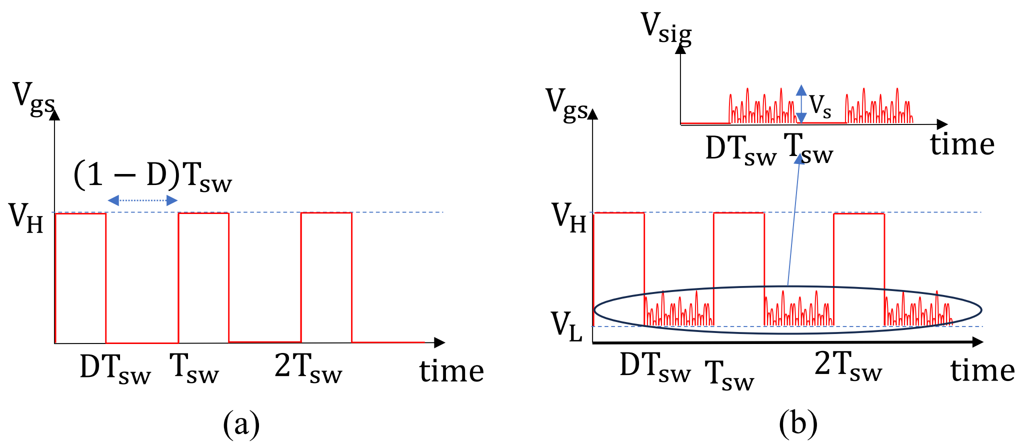

Figure 3.3: Gate-Source voltage in (a) Traditional DC/DC converter (b) Proposed method.

conventional data transmission methods in VLC systems and suggests potential future research. To enhance the readability of the manuscript, Table. 3.1 details the parameters and symbols used throughout this paper.

3.3 Principle of Operation

3.3.1 Concept

In [154] the Schottky diode in a typical DC-DC converter is replaced by an LECD to enable VLC. Thus the power typically dissipated in the Schottky diode of a conventional converter was harnessed to create modulated light through the LECD contributing to an improved efficacy. By adjusting the phase of the switching signal, low data rate communications were integrated into the power converter. In order to realize bandwidth efficient OFDM modulation necessary for higher rate VLC links, in this work the MOSFET in the converter acts as both a switching device and a means

Table 3.1: List of Parameters used throughout the paper

Parameter	Symbol	Unit
Square Waveform	V_{sq}	V
MOSFET Gate-Source Control Voltage	V_{gs}	V
Drain-Source Current	i_{ds}	A
Signal Source	V_{sig}	V
Converter Input Voltage	V_{in}	V
Samples Time Spacing	Δt	s
Efficacy	K	lm/W
Converter Input Power	P_{in}	W
Illumination Level	ϕ	lm
Junction Temperature	θ_j	C°
No. LEDs	k	—
No. LECDs	j	—
No. Subcarriers	N	—
Converter Switching Frequency/Period	f_s/T_{sw}	Hz/s
Signal Subcarrier Spacing	Δf_{sub}	Hz
Converter Output Voltage	V_{out}	V
LED/LECD Forward Voltage Drop	V_{LED}/V_{LECD}	V
Frequency/Time Domain OFDM Symbol	X/x	—
Clipped OFDM Symbol	$\bar{x}$	—
Low/High Voltage	V_L/V_H	V
Distance Between Transmitter and Receiver	d	m
Detector Physical Area	A	mm^2
Responsivity	R	A/W
Angle of Incidence	Ψ	$^\circ$
Optical Filter Gain	T_Ψ	—
Angle of Irradiance	ψ	$^\circ$
Bandwidth	BW	Hz
Concentrator Gain	g_Ψ	—
Lambertian Order	m	—

to amplify the modulated signal. Therefore, the gate-source signal (V_{gs}), Fig. 3.2, of the MOSFET in the converter is modified according to Fig. 3.3. The V_{gs} in the circuit in [154] or any other traditional DC/DC converter is a square waveform (V_{sq}) that oscillates between V_H and 0, [188, 83], as illustrated in Fig 3.3.a, with a frequency $f_{sw} = 1/T_{sw}$ and a duty cycle $D \in [0, 1]$. In contrast, in this work V_{gs} consists of V_{sq} and the data-bearing modulated signal V_{sig}, Fig. 3.3.b, defined as

$$
\begin{aligned}
V_{sq(t)} &= \begin{cases} V_H & t \mod T_{sw} \in [0, DT_s] \\ V_L & \text{otherwise} \end{cases} \\
V_{sig(t)} &= \begin{cases} 0 & t \mod T_{sw} \in [0, DT_s] \\ V_s & \text{otherwise} \end{cases} \\
V_s &: \ \text{OFDM time domain signal} \\
V_{gs(t)} = V_{sq(t)} + V_{sig(t)} &= \begin{cases} V_H & D.T_{sw} \\ V_L + V_{sig(t)} & (1-D).T_{sw} \end{cases}
\end{aligned}
\tag{3.1}
$$

Although switching MOSFETs are designed to operate either in cut-off or triode region, it is theoretically feasible to bias them in saturation mode and utilize them as linear amplifiers. As depicted in Fig 3.3.b, the MOSFET will be biased at V_L near saturation during the time interval of $(1 - D)T_{sw}$, in contrast to the conventional converter where it will be off during that interval, Fig 3.3.a. During the $(1 - D)T_{sw}$ interval, the modulated data is induced on the gate signal as a ripple, as illustrated in Fig 3.4.a. This ripple is then amplified and flows through the drain-source of the

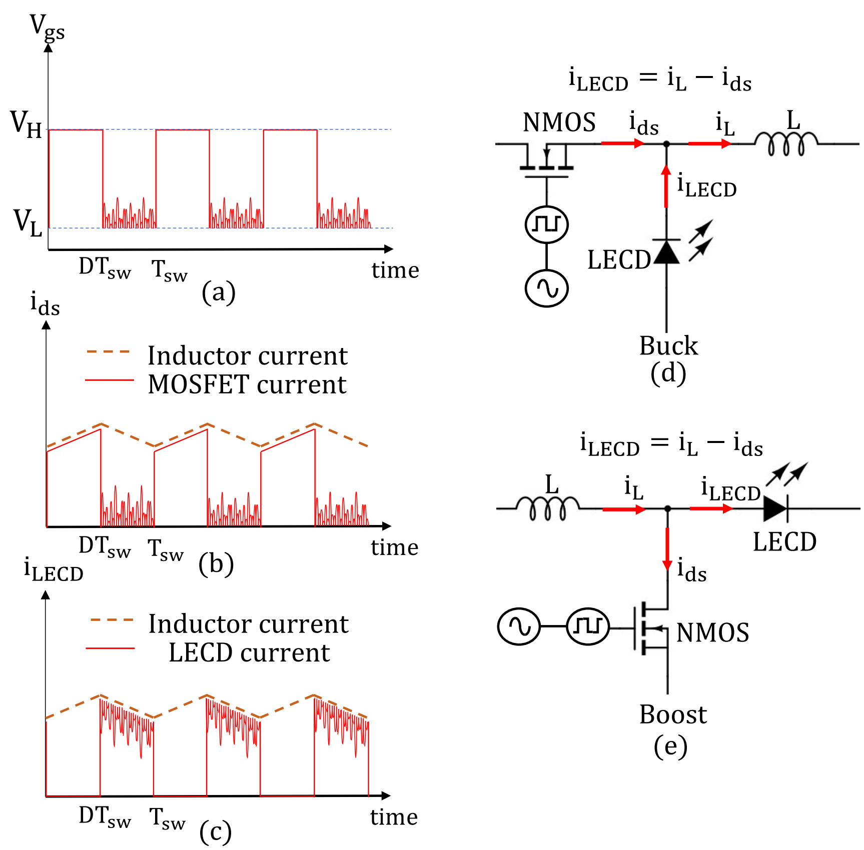

Figure 3.4: Communication signals in the proposed internal modulation technique. (a) Gate-source voltage of the MOSFET. (b) Drain-source current of the MOSFET. (c) Current flowing through the LECD. The relationship between currents depicted in (b) and (c) is illustrated in (d) and (e) for buck and boost converter respectively.

MOSFET(see Fig. 3.4.b) thus eliminating the necessity for a LPA to amplify the data. Due to the high frequency nature of the signal, the inductor will have high impedance and the current will close its loop through the LECD (see Fig. 3.4.c) hence modulating its light intensity. This results in the realization of a VLC transmitter capable of OFDM data transmission through its LECDs. The direction of the currents and the signals through the elements of the circuit are depicted in Fig. 3.4.d and Fig. 3.4.e for buck and boost configurations respectively. The high frequency equivalent circuit

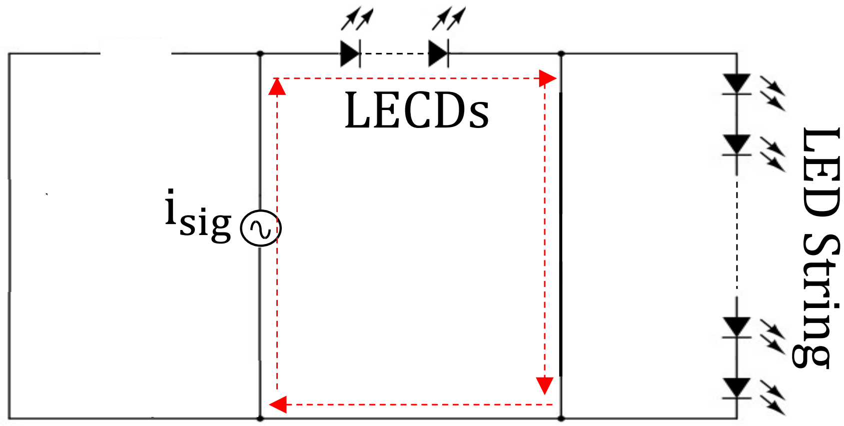

Figure 3.5: Amplified signal path in the equivalent high frequency model of the circuit.

of the boost converter in Fig. 3.5 illustrates the path of the signal in the circuit 3.2.

$$
\begin{aligned}
i_{ds}(t) &= \begin{cases} i_L(t) & t \mod T_{sw} \in [0, DT_s] \\ g_m \cdot i_{sig}(t) & \text{otherwise} \end{cases} \\
i_{LECD}(t) &= \begin{cases} 0 & t \mod T_{sw} \in [0, DT_s] \\ i_L(t) - g_m \cdot i_{sig}(t) & \text{otherwise} \end{cases}
\end{aligned} \tag{3.2}
$$

Additionally, it is important to highlight that during the $(1 - D)T_{sw}$ interval the LECD current, which mirrors the inductor current, assumes a ramp-shaped profile. This distinctive feature arises from the reduction in inductor current as it discharges within this time frame resulting in baseline wander of the communication signal.

This configuration eliminates the necessity for an external linear power amplifier since the MOSFETs function as amplifiers during their "off" periods. Consequently, this results in a reduction in the bill of materials. With the exception of the LECD replacing the Schottky diode, no supplementary components are introduced

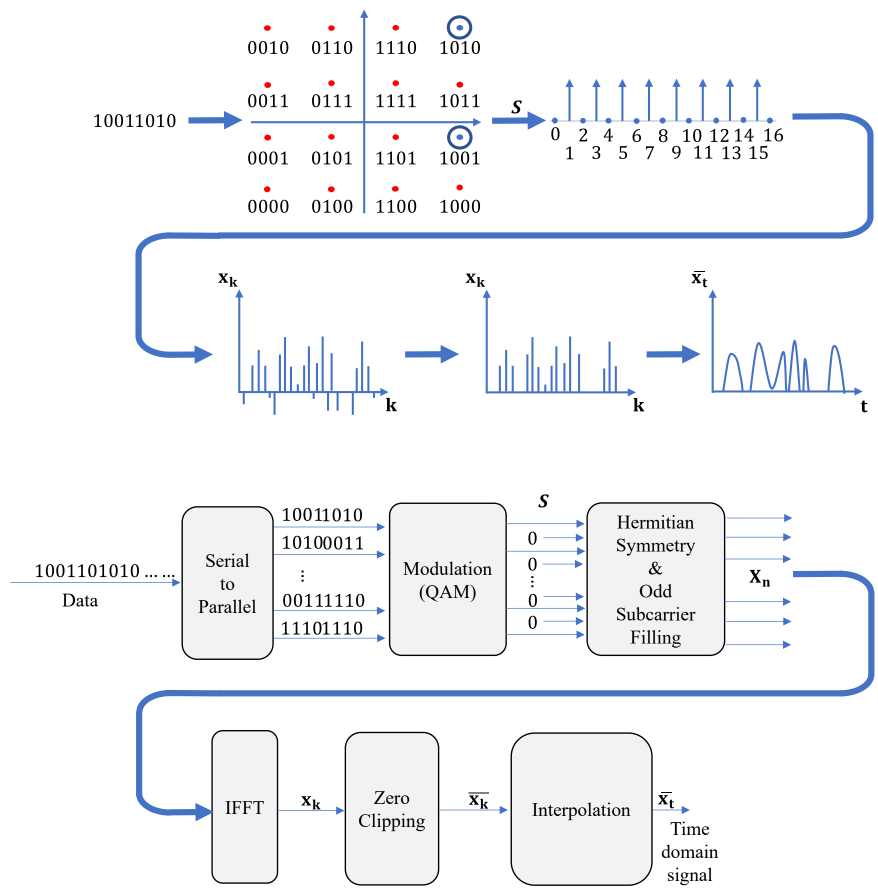

Figure 3.6: ACO-OFDM signal generation block.

to a DC/DC converter. This enhancement underscores the cost-effectiveness of this approach compared to traditional external modulation techniques, which typically involve the use of a DC/DC converter alongside a bias-T and a linear power amplifier. In the context of color shift and flicker, while the LECD may experience these effects due to receiving modulated high-frequency current, the majority of LEDs in this topology are in the illumination string and are supplied with unmodulated DC current. As a result, they are not subject to such effects, thereby ensuring a consistent and high-quality illumination output.

3.3.2 VLC Signal

The most recently ratified standards for VLC systems adopt OFDM signaling due to its high data rates, simplified one-tap equalization, and resilience to inter-symbol interference [189]. The principle of operation of an OFDM system involves dividing the transmit bandwidth into several smaller bandwidth carriers that are sent in parallel [190]. Signals modulated and transmitted by OFDM in RF channels are bipolar and complex-valued. In order to make such signals compatible with optical intensity channels where signals must be real and non-negative, several variants have been developed. Among them, DC-biased optical (DCO) OFDM and asymmetrically clipped optical (ACO) OFDM are the most popular and specified in VLC standards [85]. DCO-OFDM adds a DC bias to maintain non non-negativity of the signal while the ACO-OFDM achieves non-negativity by clipping negative components. Though both DCO- and ACO-OFDM can be transmitted using the proposed transmitter topology in Fig. 3.2, the added bias by DCO-OFDM induces greater conduction losses due to the higher DC current running through the MOSFET, thus ACO-OFDM is considered in the balance of this work.

The signal generation block of a 16-quadrature amplitude modulated (QAM) ACO-OFDM transmitter with N subcarriers is illustrated in Fig. 3.6. The incoming bits to be transmitted are divided into $N/4$ parallel sub streams each of which are input to a QAM modulator [143, 191]. The resulting QAM symbols are grouped to generate the frequency domain symbol, S, defined as

$$S = [S_0, S_1, S_2, S_3, ..., S_{\frac{N}{4}-1}] \tag{3.3}$$

The individual QAM symbols in S are assigned to subcarriers in the OFDM frame X in order to ensure that the output signal is both real and non-negative. In particular, ACO-OFDM defines the frequency domain symbol X as

$$X = [0, S_0, 0, S_1, ..., S_{\frac{N}{4}-1}, 0, S^*_{\frac{N}{4}-1}, 0...., S^*_1, 0, S^*_0] \tag{3.4}$$

or equivalently

$$X_n = \begin{cases} 0 & , n : \text{even} \\ S_{\frac{n-1}{2}} & , n < \frac{N}{2}, n : \text{odd} \\ X^*_{N-n} & , n > \frac{N}{2} \end{cases} \tag{3.5}$$

Notice that X is Hermitian symmetric and that only odd-index subcarriers are non-zero as illustrated in Fig. 3.6.

After the frequency-domain OFDM frame X is constructed, the signal is transferred to time domain by applying an inverse fast Fourier transform (IFFT) to yield time domain signal x with elements

$$x_k = \frac{1}{N} \sum_{m=0}^{N-1} X_m \exp\left(\frac{j2\pi km}{N}\right) \tag{3.6}$$

Notice further x is necessarily real due to the Hermitian symmetry of X but that still assumes negative amplitudes.

Consider defining the *clipped* OFDM signal $\bar{x}$ from x with samples

$$\bar{x}_k = \begin{cases} x_k & x_k > 0 \\ 0 & x_k \leq 0. \end{cases} \tag{3.7}$$

Notice that $\bar{x}$ is both real and non-negative and is thus compatible for intensity signaling on optical channels. It can be shown that since only odd subcarriers of X are modulated, the clipping noise generated in $\bar{x}$ lies only on the *even* subcarriers [144]. That is, the original data S in X is orthogonal to the clipping noise.

In order to transmit the OFDM symbol in a transmission time window $(1-D)T_{sw}$, as defined in Sec.3.3, the time spacing between $\bar{x}_k$ samples, Δt, is defined as

$$\Delta t = \frac{(1-D)T_{sw}}{N} = \frac{1}{N\Delta f_{sub}} \tag{3.8}$$

where Δf_{sub} is the frequency spacing between subcarriers in X. In order to transmit at least one OFDM symbol per T_{sw},

$$N\Delta t \leq (1-D)T_{sw} \longrightarrow \left\lfloor \frac{(1-D)T_{sw}}{N\Delta t} \right\rfloor \geq 1. \tag{3.9}$$

The clipped OFDM signal is then up-sampled and interpolated to create a time domain continuous signal, $x(t)$ for transmission on the optical channel.

In order to characterize the communication performance, a statistical model of the output signals is necessary. If N is sufficiently large, the samples of x in (3.6) can be shown to be well approximated by a zero mean Gaussian distribution with variance denoted σ^2. The resulting $\bar{x}$ in (3.7) can be shown to have the following half-Gaussian probability distribution function (pdf) [192]

$$f_{\bar{x}}(\tau) = \frac{1}{\sqrt{2\pi}\sigma} \exp\left(\frac{-\tau^2}{2\sigma^2}\right) u(\tau) + \frac{1}{2}\delta(\tau) \tag{3.10}$$

where $u(\cdot)$ is the Heaviside function and $\delta(\cdot)$ is the Dirac delta. Notice that half of the probability mass of the samples of $\bar{x}$ are at zero due to the clipping function.

Let μ_{ACO} and σ^2_{ACO} denote the mean and variance of $\bar{x}$ respectively. From (3.10), it can be shown that [235]

$$\begin{aligned} \sigma^2_{\mathrm{ACO}} &= \sigma^2 \left(\frac{\pi - 1}{2\pi}\right) \\ \mu_{\mathrm{ACO}} &= \frac{\sigma}{\sqrt{2\pi}} \end{aligned} \tag{3.11}$$

and thus that $\sigma_{\mathrm{ACO}} = (\sqrt{\pi - 1})\mu_{\mathrm{ACO}}$.

3.3.3 Illumination Performance

In order to maintain high performance for both illumination and communication, careful design of the gate signal of the switching MOSFET is essential. The two primary parameters of interest are the duty cycle and the signal variance of the communications signal. Additionally, when evaluating the overall effectiveness of a luminaire, it is important to consider its efficacy. Efficacy, often denoted as K, which is defined as:

$$K = \frac{\phi}{P_{in}} \tag{3.12}$$

where P_{in} is the input electrical power and ϕ is the luminous flux emitted by the luminaire.

The duty cycle of the power converter plays a crucial role in setting the brightness level of the luminaire by controlling the average current passing through the illumination LEDs. Additionally, the duty cycle also impacts the communication performance of the system. Comparing Fig. 3.7.a and Fig. 3.7.c illustrates that increasing D increases the amplitude of the DC current flowing through the LECDs and provides a higher dynamic range for the transmitted signal before the emergence of clipping of the ACO-OFDM symbol. This improved communication comes at the expense of a shorter transmission window, leading to a decrease in overall data throughput. However, given the improved SNR from the increased signal amplitude, higher order QAM modulation could be employed to improve the data throughput. It is important to note that since the brightness level of the luminaire is typically determined by the user or by application requirements, D is pre-determined and not a direct design parameter.

As discussed in Sec. 3.3, the OFDM data frame is transmitted during the $(1-D)T_{sw}$ interval when the switching element of the driver is "off". The bias point of the switching MOSFET in saturation must be carefully chosen as it fixes the amplification gain and affects the conduction losses in the signal transmission interval. According to (3.1) and Fig. 3.3, the effective bias voltage of the MOSFET depends on V_L and μ_{ACO} and is given as

$$V_{\text{bias}} = V_L + \mu_{ACO} \tag{3.13}$$

V_L is selected such that the MOSFET is on the edge of saturation, yet in the cut off region, thus maintaining minimum loss in the absence of a transmission signal. Although greater signal variance results in higher mean value from (3.11) and subsequently better amplification gain and SNR, if the amplitude of the signal exceeds that

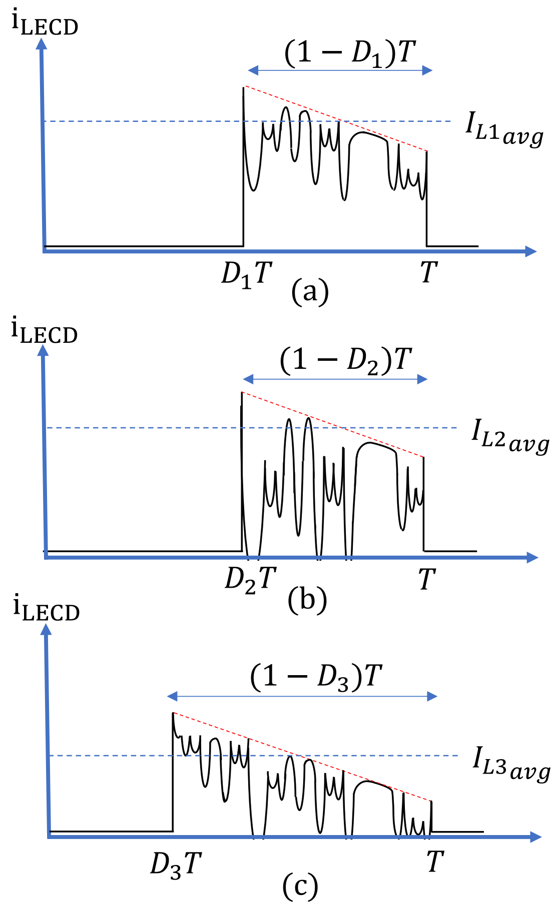

Figure 3.7: Clipping noise observed in both (b) and (c) due to an increased σ^2 and decreased D respectively compared to (a). Notice that (b) provides a better dynamic range while (c) allows for a longer transmission window.

of the LECD current, clipping noise will emerge, reducing the overall performance in terms of BER. This incident which results in the loss of data can be observed by comparing Fig. 3.7.a and Fig. 3.7.b.

3.3.4 Circuit Design Considerations

Switching elements used in DC/DC converters are typically MOSFETs, and their operation is controlled based on their V_{gs} shown in Fig. 3.3. Commercial MOSFETs are typically fabricated for two primary applications: amplification or switching. Those designed to be used as amplifiers are DC-biased in the saturation region and have a small AC signal superimposed on the gate voltage. Operating in the saturation region, where neither the drain-source voltage nor drain current is minimized, leads to losses associated with linear amplifiers. However, in the case of switching MOSFETs, V_{gs} is controlled by a square waveform, V_{sq} Fig. 3.3.a, to maintain the MOSFET in the cutoff or triode region. In switching applications, the MOSFET conducts either at its minimum V_{ds} or I_{ds} to minimize losses. Using switching MOSFETs as amplifiers leads to circuit design considerations which originate from the fabrication process and include:

1. *Thermal Runaway* [193–195]

   MOSFETs with V_{gs} values lower than their temperature coefficient point (TCP) maintain a positive correlation between junction temperature, θ_j, and drain current. In other words, there is a positive feedback loop between temperature and drain current. Therefore, rising temperature due to the losses results in higher drain current which subsequently leads to more losses and higher θ_j.

2. *Channel Length Modulation* [196]

   As a first approximation, in saturation region I_{ds} is typically modeled as being solely determined by V_{gs}. In reality, however, V_{ds} has an impact on I_{ds}. Larger value of V_{ds} will increase the current.

As illustrated in Fig 3.8, an increase in I_{ds} results in an increase in the θ_j which due to the TCP yields higher I_{ds}. Moreover, the increased I_{ds} results in an increased V_{ds} which also increases I_{ds} due to the channel length modulation. These two effects jointly increase θ_j, leading to increased conduction losses and system instability. Mitigating thermal instability concerns can be achieved through various means. One such approach involves the utilization of heatsinks. However, a more efficient strategy entails opting for topologies with lower V_{ds} values. For instance, when comparing the buck and boost converters for achieving the same output voltage, the boost converter, with its lower V_{ds}, becomes a more suitable option in this regard. This choice is reinforced by the fact that the Drain-Source voltage of the MOSFET could be as high as $V_{in} + V_{f_{\mathrm{LECD}}}$ for the buck converter and $V_{out} + V_{f_{\mathrm{LECD}}}$ for the boost converter, as depicted in Fig. 3.2. Consequently, it becomes evident that for the same output voltage, the drain-source voltage applied to the buck converter is higher than that of the boost converter, further emphasizing the advantages of the latter in this context.

3.3.5 Design Guidelines

Boost converters are extensively utilized in lighting applications, including LED display backlighting [197], solar-powered LED lighting [198], street lighting [199], and automotive headlights [200, 201]. While previous studies have investigated VLC in these applications, our research sets itself apart by presenting a broad approach to integrating a modulator into the boost LED driver, enabling simultaneous illumination and communication. Therefore, the simulations and experiments conducted in this study serve to demonstrate the feasibility of this concept. The proposed topology discussed in this study is adaptable to all lighting systems employing a boost converter

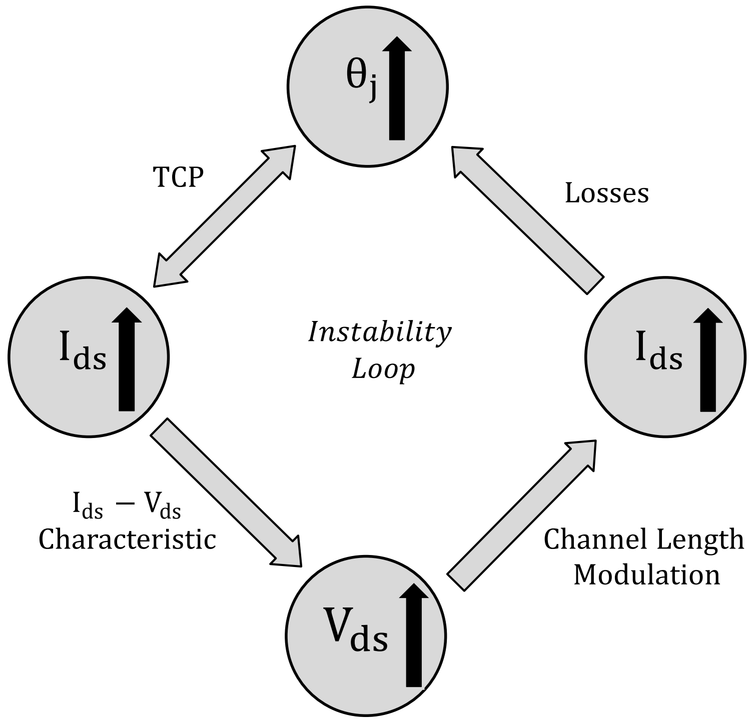

Figure 3.8: Positive feedback loop due to high V_{ds}.

as an LED driver. When designing a boost converter equipped with an integrated modulator, the following factors should be carefully considered.

The selection of the switching MOSFET is based on the desired f_{sw} and the required output power. The selection of the C and L depends on the acceptable output voltage ripple and inductor current ripple [202], respectively. The LECD used in the circuit can be selected as a typical illumination LED. However, illumination LEDs are not designed for operation in reverse bias and in scenarios involving high output voltage and a large number of illumination LEDs, it is essential to consider their breakdown voltage to ensure that it can withstand the reverse voltage applied during the DT_s. When selectingf_{sw}, it is crucial to take into account the transmission signal bandwidth since the transmission signal is induced on the LECD current Fig. 3.4, which is approximately equal to the inductor current during the $1-D$ portion of the cycle. The bias voltage V_L must be selected to be close but less than the threshold voltage specified in the data-sheet of the MOSFET in order to minimize conduction losses during the transmission window.

According to the available power supply and required output luminous flux the number of the LEDs, k, and LECDs, j, must be determined to ensure the desired dimming range is met when D is in the range of $40-80\%$ as the performance and efficiency of DC/DC converters drop at the two extremes of the duty cycle [204]. This decline can be linked to two factors: discontinuous mode operation at low duty cycles [205] and elevated conduction losses at high duty cycles [206]. Moreover, upon selecting j and k, their impact on the illumination and communication performance should be investigated. Considering a fixed total number of LEDs and LECDs, increasing the number of LECDs, j, enhances the communications SNR. However, this comes at the cost of a reduction in the total output lumens, given that LECDs illuminate only for a fraction of each switching period. This reduction in the DC current concurrently limits the maximum signal swing for the communication signal before clipping occurs. Moreover, the larger number of LECDs introduces a higher forward voltage drop, thereby constraining the dimming capability and reducing efficacy under the same DC voltage source and duty cycle. Conversely, a higher number of LEDs, k, in comparison to LECDs, j, results in a larger DC current through the circuit, allowing for a more extensive signal swing before encountering clipping issues, however, the SNR is expected to drop as the number of LECDs is now reduced.

In order to always maintain transmission of a whole number of OFDM symbols, the transmission interval should be greater than the length of one OFDM symbol, as in 3.9. The values of Δt, N for the communication signal are set by the standards [85], however, D and T_{sw} can be adjusted to either set dimming levels or transmit more than one OFDM symbol in each switching cycle. In the circuit design presented in this paper, (D) falls within the range of $40-80$ %, with a typical switching frequency of 10 kHz. However, the communication simulations and experimental results are all provided for a case of 40 % duty cycle under 10 kHz switching frequency which allows for 60 μs of OFDM symbol length. The subcarrier frequency spacing is considered 20 kHz which is equivalent to a symbol length of 50 μs.

3.4 Simulation Results

In this section, we propose a simulation study to demonstrate the feasibility of the approach presented in Sec. 3.3. The target is to design and implement a boost converter with integrated VLC that achieves a maximum luminous flux output of 1200 lm and is capable of dimming from 50 to 100%. Simulations are carried out over link distances of $10-100$ cm to facilitate comparison and validation against experimental results conducted in the experimental environment described in Sec. 3.5.

3.4.1 Simulation Setup

This section presents a brief overview of the design process, with a comprehensive design procedure and component selection discussed in Appendix. B. To begin the design, the available input voltage is considered to be 12 V. The dimming functionality should be effective within the range of $D \in [40\%, 60\%]$ in order to optimize converter efficiency. In practical terms, $D = 40\%$ should correspond to 50% dimming, while

Table 3.2: Simulation and Experimental Parameters for the VLC OFDM Boost Converter (cf. Fig. 3.2)

Parameter	Symbol	Value
Inductor	L	10 mH
Capacitor	C	470 μF
Duty Cycle	D	40% – 60%
Number of Subcarriers	N	256
Switching Frequency	f_{sw}	10 kHz
Light Emitting Diode	LED	7 Lumiled 3535L [179]
Switching Device	Sw	NMOS AO3442 [208]
Modulation Scheme		64QAM ACO-OFDM [85]
Light Emitting Commutating Diode	$LECD$	1 Lumiled 3535L
Input Voltage	V_{in}	12 V
Subcarrier Spacing	Δf_{sub}	20 kHz
Distance Between Transmitter and Receiver	d	0.1–1 m
Detector Physical Area	A	13 mm^2
Responsivity	R	0.25 A/W
Angle of Incidence	Ψ	0°
Signal Transmission of the Filter	T_Ψ	1
Receiver Angle with Respect to Transmitter	ψ	0°
Receiver Bandwidth	BW	5.5 MHz
Concentrator Gain	g_Ψ	1

$D = 60\%$ should correspond to 100% dimming. In summary, the electrical constraints for this system design can be described using (3.14) where the general equation for boost converter in [207] is modified to include the forward voltage drop of the LECD as

$$\begin{aligned} V_{in} \cdot DT_{sw} &= (V_{out} + V_{LECD} - V_{in})(1 - D)T_{sw} \\ V_{out} &= \frac{V_{in}}{1 - D} - V_{LECD} \end{aligned} \tag{3.14}$$

Using (3.14) and considering the constraints found above and voltage drop range of a typical LED, the range of V_{out} for the converter can be found to be

$$\begin{cases} V_{\text{in}} = 12 \text{ V} \\ 40\% \leq D \leq 60\% \\ 3 \text{ V} \leq V_{\text{LECD}} \leq 3.5 \text{ V} \end{cases} \longrightarrow 16.5 \text{ V} \leq V_{\text{out}} \leq 27 \text{ V} \tag{3.15}$$

Taking into account the available output voltage and referencing the $V - I$ and $\phi - I$ characteristics of LEDs readily available in the market allows for the informed selection of the type and quantity of LEDs and LECDs required to meet the luminous flux requirements. In this regard, a Lumiled 3535L LED [179] is selected where $k = 7$ illumination LEDs and $j = 1$ LECDs are necessary to meet the optical constraint. For a f_{sw} up to 100 kHz and given the maximum current limit, an NMOS AO3442 [208] is selected as the switching device. Considering the nominal voltage and current in the circuit and an acceptable ripple of 5% for the inductor current and output voltage, following conventional guidelines [202], the inductor and capacitor values are selected as 10 mH and 470 μF respectively.

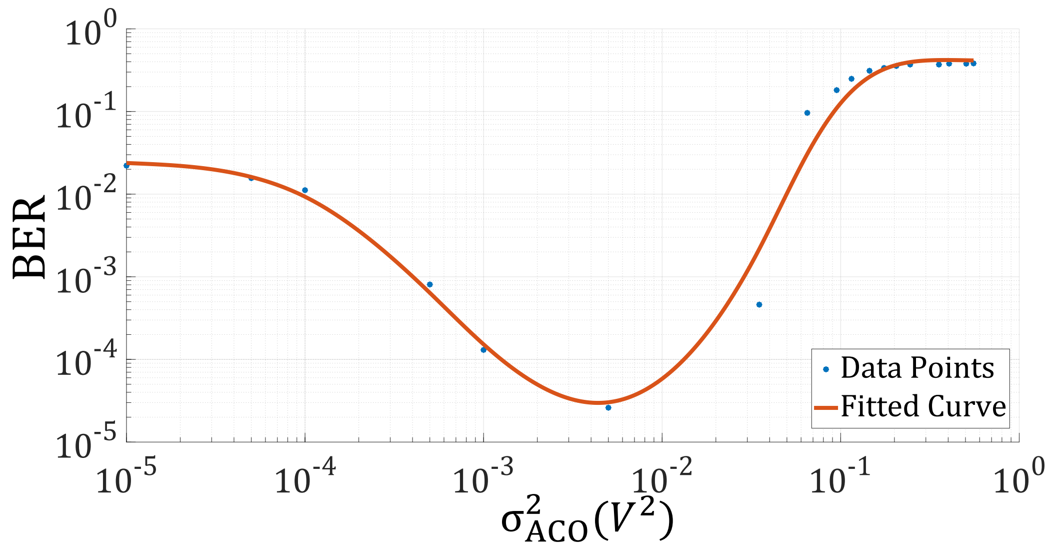

Figure 3.9: Simulated BER versus σ^2_{ACO} for a fixed distance of 10cm.

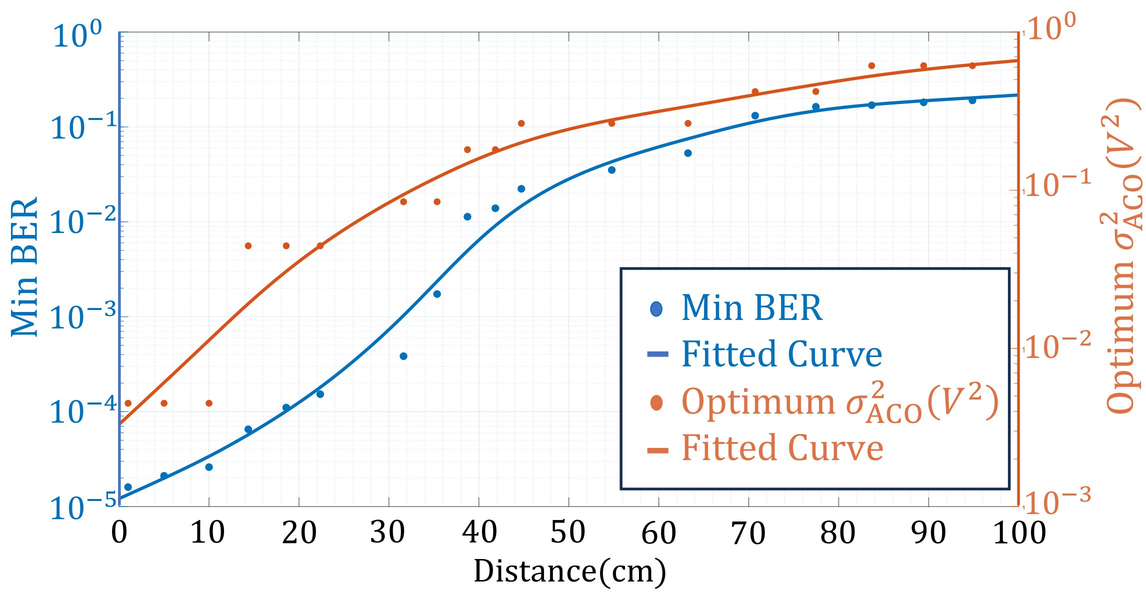

Figure 3.10: Simulated optimum BER and σ^2_{ACO} versus link distance.

The parameters of the communication system are selected in accordance with an established VLC standard [85]. In particular, the transmission signal contains 256 subcarriers modulated with 64-QAM ACO-OFDM modulation and $\Delta f_{sub} = 20$ kHz. The bias voltage V_L of the MOSFET in Fig. 3.3 is set to 2.2 V, considering that the threshold voltage specified in the datasheet is 2.3 V. Table. 4.2 presents a summary of the components and parameters utilized for simulating the boost converter illustrated in Fig. 3.2.b.

The variance σ^2_{ACO} is a critical parameter which determines the communication performance as measured by the BER [191]. As illustrated in Fig. 3.7, σ^2_{ACO} must be chosen to balance increased signal power with clipping distortion. In order to find the optimum σ^2_{ACO}, simulations are performed for different variances while maintaining a fixed distance between the transmitter and receiver (i.e., 10cm)

In the simulations, effort is taken to model the experimental setting to allow for comparison of the results. The electrical current through the LECD is converted to luminous flux using the relation

$$\phi_v(I) = -0.0001I^2 + 0.3093I + 3.647 \tag{3.16}$$

which is a quadratic fit [227] according to the datasheet of the LECD. The propagation between the transmitter and the receiver is modeled as a flat fading channel with fixed propagation delay and DC gain using the classical line of sight model [44]

$$H_{(0)} = \begin{cases} \frac{(m+1)A}{2\pi d^2} cos^m(\psi) T_s(\Psi) g(\Psi) cos(\Psi), & 0 \leq \Psi \leq \Psi_c \\ 0, & \Psi > \Psi_c \end{cases} \tag{3.17}$$

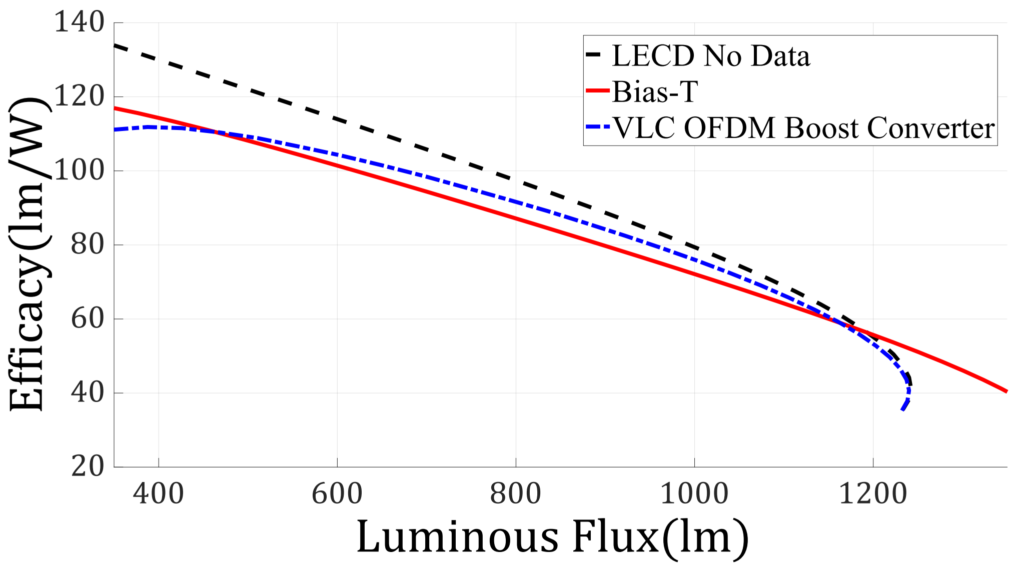

Figure 3.11: Simulated efficacy for different dimming levels.

The parameters $m, d, \Psi, \psi, T_s(\Psi), g(\Psi)$, and Ψ_c used in 3.17 are defined in Table. 4.1 and their values are chosen to correspond to the available laboratory equipment. The received optical intensity is then converted back to current through a PDA36A(-EC) optical receiver from Thorlabs [209]. For amplification, the 10 dB setting is selected for the photodetector, and corresponding responsivity, active detection, and bandwidth are listed in Table. 4.2. The receiver associated noise component is modeled as a signal-independent, additive white Gaussian noise with a root mean square (RMS) value of 280 μV.

3.4.2 Communication Results

Figure. 3.9 shows a graph displaying the BER as a function of σ^2_{ACO}, obtained by sending 10^7 bits using 64 QAM ACO OFDM across 256 subcarriers over a 10 cm link with a constant $D = 44\%$. Assuming high ambient noise of the indoor VLC

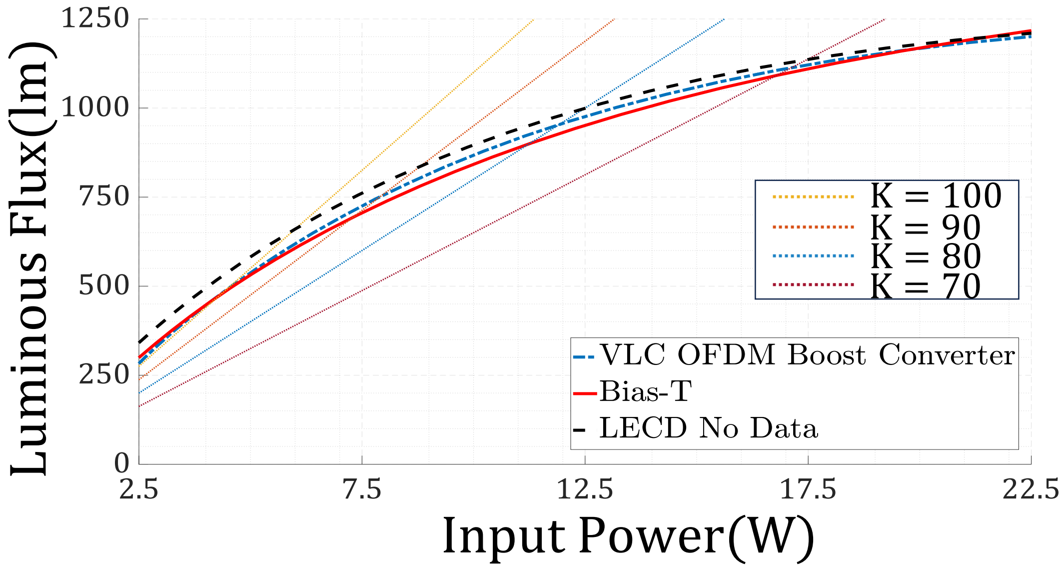

Figure 3.12: Simulated luminous flux for different input electrical power with lines of constant efficacy indicated.

channel, the noise is dominated by the shot noise modeled as a white additive Gaussian noise [44] and the corresponding SNR can be determined according to the optical power of the signal and the noise value [14]. Notice that, as expected, increasing σ^2_{ACO} improves BER to an optimal point after which performance degrades due to increased clipping distortion. It is crucial to highlight that a duty cycle of 44% was consistently maintained across all simulations to ensure the transmission window duration is sufficient for transmitting a single ACO OFDM symbol. Throughout the subsequent analysis, D remains fixed at this value to uphold consistency.

Although the previous simulation was conducted for a fixed distance of 10 cm, Fig. 3.10 plots the minimum BER and optimum σ^2_{ACO} as a function of link distance. As the distance between the transmitter and receiver increases, the BER also increases. Notice also that the optimum σ^2_{ACO} increases with link distance. This phenomenon arises due to the balance between the SNR reduction due to an increase in link length with the induced clipping distortion.

3.4.3 Illumination Results

To evaluate the performance of the VLC OFDM boost converter in terms of illumination parameters, a comparison is made with two different approaches. The first system is externally modulated approach using an amplifier and bias-T, as shown in Fig. 3.1. The amplitude of the communication signal is adjusted to have the same optical power as the VLC OFDM Boost Converter given that all LEDs in the illumination string are modulated in the externally modulated approach. The second approach employs an unmodulated LECD rather than a conventional commutating diode as first proposed in [154] and denoted 'LECD No Data'. The duty cycle in all methods is swept to find the efficacy (3.12) for each certain illumination level. The optimum variance, obtained from Fig. 3.9 for a 10cm distance, is used as the transmission signal. Figures 3.11 and 3.12 are generated by deriving D, ϕ, and P_{in}, and subsequently plotting efficacy against luminous flux and luminous flux against input power, respectively.

Fig. 3.11 illustrates the relationship between simulated efficacy and illuminance, achieved by varying the parameter D for dimming levels from $50 - 100\%$. It is noteworthy to highlight that the comparison of efficacy is performed under the condition of an identical transmitted output signal, thereby ensuring an equivalent BER in each scenario. Put differently, the assessment of efficacy is carried out across the different topologies each transmitting identical communication signals. As discussed in Sec. 3.3.5, it is observed that the efficiency of the converters diminishes at the extreme ends of the range of duty cycle, D. Notably, both the VLC OFDM Boost

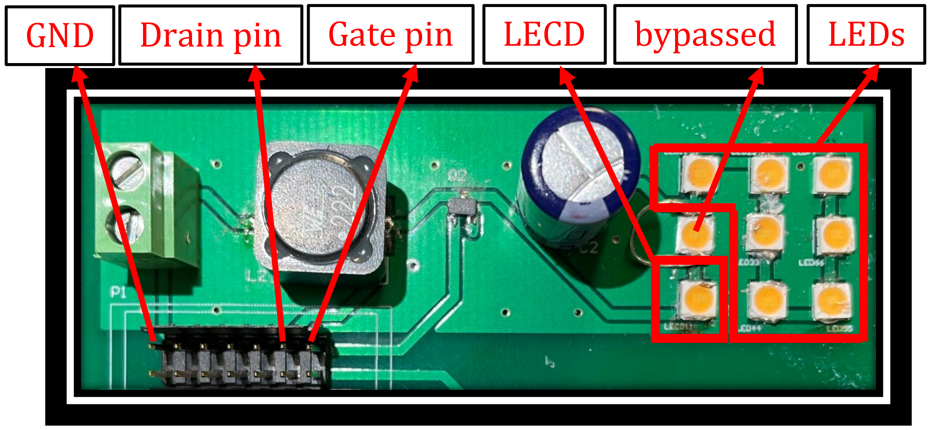

Figure 3.13: Boost converter printed circuit board.

Converter and LECD No Data, exhibit a more pronounced decrease at these extreme D values. This observation can be attributed to the fact that, to match the light output of a conventional boost LED driver, the VLC OFDM Boost Converter is required to operate at a higher D. This characteristic has been thoroughly examined in [154]. However, it is important to emphasize that the initial design constraints ensure that the D remains within the range of 40 to 60% for the required dimming range of 50 to 100% of a maximum luminous flux of 1200 lm. Consequently, any decrease in effectiveness beyond 1200 lm or before 600 lm is not relevant since this is outside the operating range of the converter. As a result and as confirmed by the data presented in Fig. 3.11, the VLC OFDM boost Converter provides a higher efficacy, up to 6.25%, in the operating range than the externally modulated approach.

Fig. 3.12 not only shows the relationship between output lumens and input power for various approaches discussed earlier but also includes lines of constant efficacy for use as tools in system design. In cases where there is an illumination constraint on the minimum required efficacy, this graph allows designers to discern their maximum attainable output lumen flux and the corresponding required input power to achieve it. If the specified desired output brightness and the minimum efficiency do not correspond to any of the depicted graphs, it suggests that under the circuit design constraints, such as j, k, and V_{in}, it is not possible to achieve the desired brightness with the specified efficiency. Consequently, design adjustments to parameters/components would be needed to meet the required criteria. Fig. 3.12 provides a basis for choosing which approach aligns better with the desired efficacy levels for a specific application. Furthermore, considering the design constraint specified for the output luminous flux, falling within the range of $600 - 1200$ lm as discussed in Sec. 3.3.5, the graph illustrates that the VLC OFDM boost Converter consistently demands less input power for each dimming level, signifying superior efficacy compared to the alternative approach. It is worth noting that even though the increase in efficacy may seem small, it holds significant value especially in the context of LED drivers which operate near 95% efficiency [210]. These incremental improvements are crucial, given the ongoing research efforts to push efficiency beyond the 95% threshold.

3.5 Experimental Results

Fig. 3.13 presents the implemented printed circuit board of the VLC-OFDM boost converter, which was used to validate the previously discussed simulation results according to Fig. 3.14. Initially, both optical and electrical measurements were conducted to confirm the findings regarding efficacy. To accomplish this, a Tektronix AWG2021 arbitrary waveform generator [211] was utilized to generate the signal and an integrating sphere and a PDA36A(-EC) optical receiver from Thorlabs [209] were employed to collect all the emitted light from the LEDs. Notice that the optical receiver is uncalibrated and thus results presented are in arbitrary units, allowing

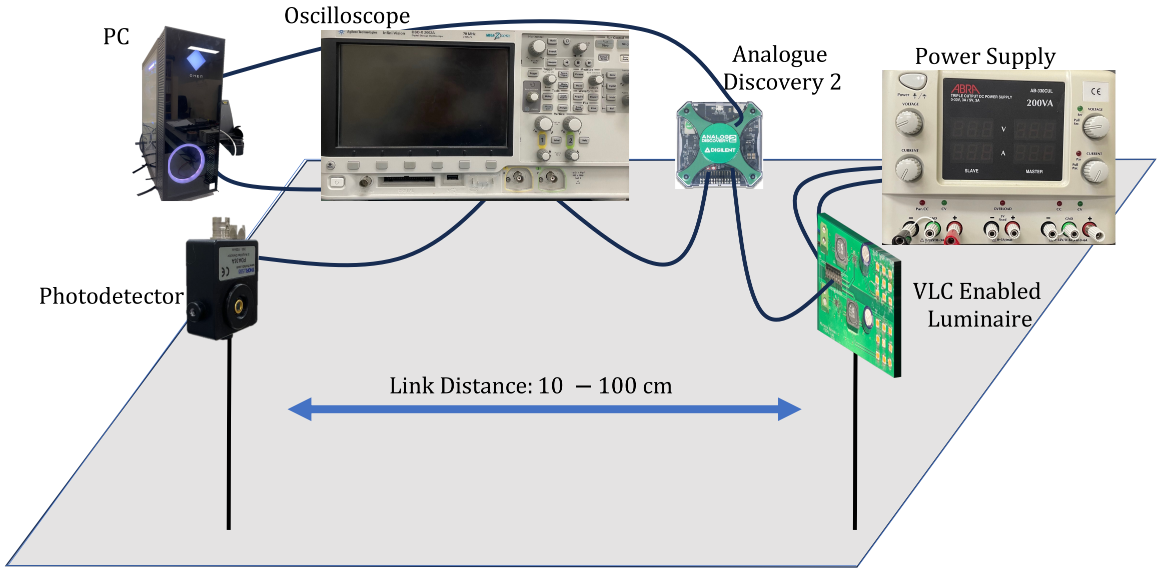

Figure 3.14: Diagram displays the experimental setup used to collect measurements.

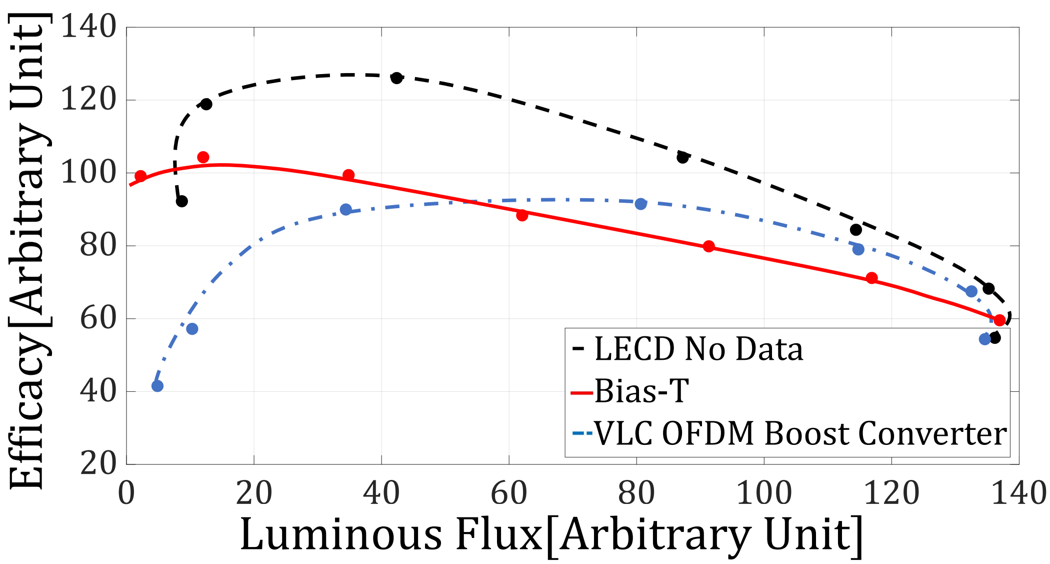

Figure 3.15: Measured efficacy comparison when $\sigma^2_{ACO} = 3.6 \times 10^{-4}V^2$, $N = 256$, T_{sw}= 100 μs, Δf_{sub}= 10 kHz.

for a relative comparison between approaches. The three approaches tested included the VLC OFDM boost converter, LECD No Data, and externally modulated bias-T method. For the externally modulated approach, the LECD in the setup was replaced with a commutating diode and the communication signal was combined with the illumination current through a 100 K-4200 MHz RF wideband coaxial feed bias-T [212]. The measurement of efficacy versus duty cycle was carried out and is depicted in Fig.3.15, under the same conditions as detailed in Sec. 3.4, utilizing the components with parameters listed in Table. 4.2. To evaluate and compare the optical performance of the approach, the LEDs in the setup were precisely aligned to ensure the entirety of their light output entered the integrating sphere. Subsequently, D was adjusted within the range of 40 to 60%, aligning to the data provided in Sec. 3.3.5. During these adjustments, the input power and total output luminous flux were recorded. Importantly, the data points presented in Fig.3.15, along with their fitted curve, demonstrate behavior consistent with the simulated results in Fig. 3.11.

Next, communication measurements were undertaken, with the link distance set at a fixed 10 cm, and the optimal variance for this distance, as indicated by Fig.3.9, was utilized. The electrical configuration matched the specifications outlined in Table 4.2. The communication signal employed was a 64 QAM ACO-OFDM signal consisting of 256 subcarriers which is defined in the VLC standard [85]. The value of signal variance is set to $\sigma^2_{ACO} = 4 \times 10^{-3} V^2$. To capture the signal, the PDA36A(-EC) was connected to an oscilloscope [213]. Following this, the acquired signal was imported into Matlab [216] for subsequent decoding. A cyclic prefix equal to 1/10 of the symbol length was added to the beginning of the transmitted signal as is conventional in OFDM systems [217].

Reading the V_{gs} (see Fig 3.3) from the gate pin, it is imported to MATLAB to be decoded and compared with the received signal to find the BER. In order to

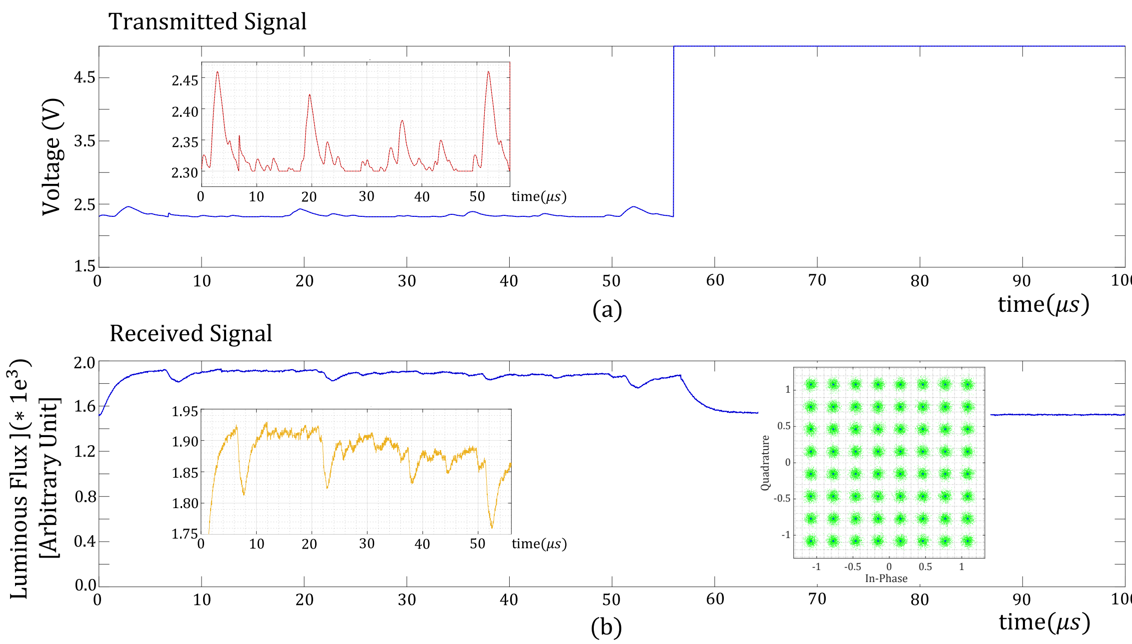

Figure 3.16: (a) Measured transmitted electrical at MOSFET (V_{gs}). (b) Measured received optical signal from the photodetector with the constellation diagram displaying both received and transmitted modulated bits, $T_{sw} = 100\mu$s, $D = 44\%$.

find the BER, 800 symbols were transmitted, and received data frames were collected, resulting a total of over 1.23 million bits transmitted over the channel. Fig. 3.16 shows an example of the transmitted and received frame. The measured BER $= 4 \times 10^{-5}$ which shows close agreement with simulation results in Fig. 3.9. From the graph, it is evident that the transmission window measures 56 μs, while the duration of the symbol transmitted is 50 μs. This difference is deliberately made to account for the delay during the MOSFET's transition from triode to saturation, thereby safeguarding against data loss. Notice that the received optical modulated signal in Fig.3.16.b exhibits an inverted polarity as compared to the modulated signal present at the gate of the MOSFET Fig 3.16.a. This polarity inversion stems from the opposite direction of the drain-source current during the $1 - D$ portion of the cycle which subtracts from the DC current in the LECD, as illustrated in Fig. 3.4. Notice also inset in Fig 3.16.b is a constellation scatter plot for the received 64-QAM signals where the blue points indicate the transmitted signals and the green represent the received signals.

3.6 Conclusions

This study demonstrates a cost-effective LED driver with integrated VLC, implementing advanced OFDM schemes from recent standards. Integrating the modulator with the power device and using the MOSFET for switching and amplification eliminates the need for an RF amplifier and bias-T, reducing component components by 33% and improving efficacy by 6.25%.

Our proposed scheme was adaptable to both ACO-OFDM and DCO-OFDM. ACO-OFDM was preferred in this study due to its higher optical power efficiency, as DCO-OFDM requires a larger DC bias, leading to higher conduction losses from the MOSFET's elevated DC operating point and increased DC current.

The proposed design separates illumination LEDs from communication LEDs, extending the lifespan of illumination LEDs and improving lighting quality by reducing flicker and color shifting. While this study used identical LEDs for both functions, purpose-built LECDs with extended lifetimes could be used without compromising illumination performance, as they are fewer in number, 1 to 7 ratio in this case, and mitigate total circuit failure caused by short-circuit failures in LECDs.

Future work will focus on optimizing the ratio of LEDs to LECDs in a luminaire to balance trade-offs between communication and illumination performance addressed in Sec. 3.3.5. Another avenue for future improvement is the application of hybrid modulation techniques. By combining fast modulated signals, such as OFDM, with slow-paced simple signals transmitted using PPM/OPPM modulation, it is possible to achieve enhanced data transmission rates while preserving the simplicity and efficiency of the overall system. Exploring hybrid modulation schemes can offer new possibilities for increasing the capacity and versatility of VLC systems.

Additionally, in the method proposed in this chapter, the switching frequency of the MOSFET is not the limiting factor, as signal transmission occurs during the interval $(1 - D)T$. Unlike the design presented in Chapter 2, where high-frequency switching devices could enhance data rates, here the bandwidth of the LED serves as the primary bandwidth limitation in this chapter. Future research could focus on using Micro-LEDs [214] or RGB LEDs [215] as LECDs to increase the bandwidth of the system.

Chapter 4

An Integrated Illumination LED Driver and Optical Wireless Communications Repeater

One important aspect of a functional VLC system is the provision of an uplink channel and connectivity to the backbone network, as highlighted in Sec.1.3.3 and Sec.1.3.4. This chapter introduces an optical repeater topology by employing a multi-phase boost converter as an LED driver, where the Schottky diodes in each phase are replaced with photodetectors. This configuration enables data transmission from the user to VLC access points (luminaires) via IR signals and allows for the realization of an optical uplink channel. The received signal is amplified and can be retransmitted across different wavelengths. Additionally, luminaires can communicate with the backbone network through an optical modem in the IR spectrum. The illumination and communication performance of this approach is evaluated through simulations and validated by experimental measurements of efficacy, amplification gain, and BER in a laboratory setup.

 Additional contribution to this work that was also submitted is provided in Appendix A which further investigates the theoretical calculations regarding the noise figure of the optical repeater introduced in Chapter 4.

4.1 Abstract

VLC leverages optical bands to meet the escalating demands for wireless communication. This paper presents a new approach to address the challenges encountered in establishing an optical uplink and downlink relay for VLC systems. A multi-phase boost converter topology is developed to realize a repeater capable of receiving and amplifying infrared uplink signals and re-transmitting them across both infrared and visible spectra. Conventional commutating diodes within each phase of the converter are replaced with photodiodes, enabling the detection of infrared (IR) signals. The resultant photocurrent modulates the intensity of multiple emitters at output, enabling spatial summation and amplification of the re-transmitted signal. By using emitters in infrared and visible bands, applications such as fronthauling and backhauling can be realized within VLC networks. These applications facilitate the interconnection of luminaires to backbone networks. Simulation and experimental results indicate that the integration of the repeater into a luminaire through this approach does not

adversely impact the efficacy of the luminaire and for the tested configurations the repeater is capable of an end-to-end optical gain of 7 for IR signals with amplitudes of $1 - 10$ mW.

4.2 Introduction

The rise of mobile and IoT devices is driving a demand for wireless data, resulting in RF spectrum congestion [236], especially in crowded indoor and IoT environments. OWC, utilizing unregulated light spectrum, offers a solution. VLC, a type of OWC, uses LED illumination for interference-free communication [218] in high-density, short-range settings. However, implementing a VLC system is complicated. Luminaires need both power and data connectivity, challenging both front and back-hauling. Moreover, the uplink channel in VLC is problematic for battery-powered handheld devices due to SNR limitations. Research focuses on circuit designs to alleviate these issues while preserving illumination quality.

Bi-directional VLC, where data transmission occurs simultaneously in both the uplink and downlink, is of paramount importance for achieving comprehensive communication capabilities [219]. While there has been extensive research focused on optimizing downlink communications in the context of VLC [99, 105, 106, 103, 154, 155], the uplink channel has received considerably less attention. Optical wireless uplinks are most often realized in the infrared spectrum to make them imperceptible to users, avoid interference with the visible light signals used for downlinks, and comply with strict power constraints in generating uplink signals [116, 117, 120].

In addition to establishing an uplink channel connecting users to the VLC access points, transmission of data between these access points and the central data

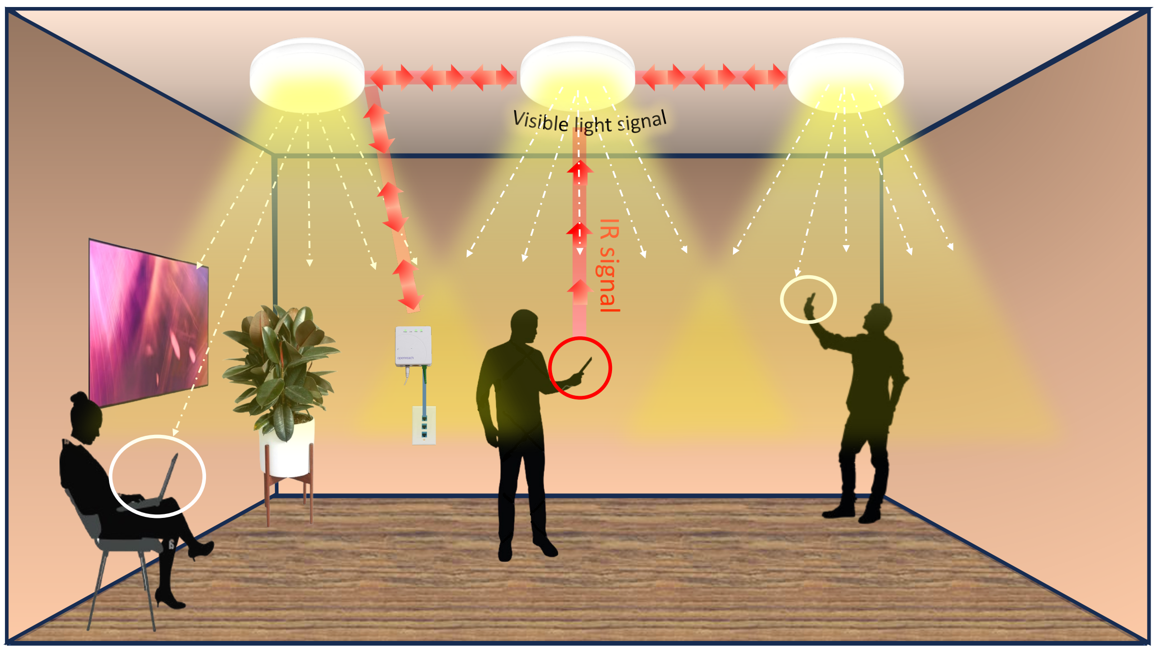

Figure 4.1: The transmitted IR signal from the user in the middle of the room is amplified and broadcast through visible light. IR transmission allows for the transmission of data between the luminaires as well as communication with a data source through the optical modem mounted on the wall.

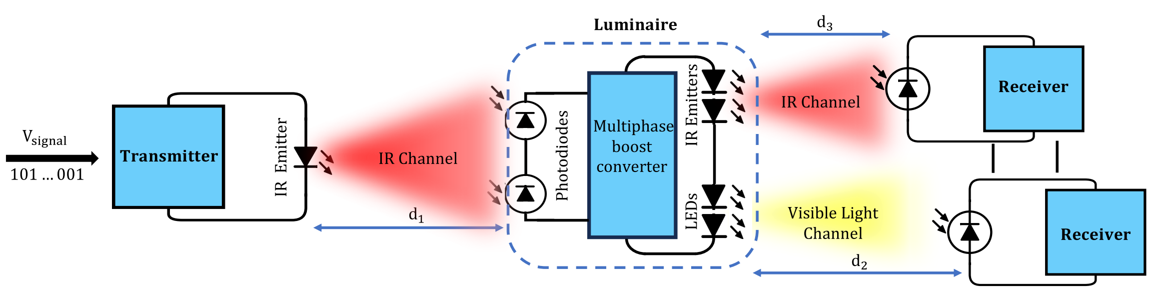

Figure 4.2: Simplified model of the proposed repeater. The IR signal is received, amplified, and re-transmitted in infrared and visible spectra.

infrastructure, referred to as fronthauling and backhauling, holds significant importance [122]. Integration of power line communications (PLC) with VLC has been considered as a potential backhauling physical medium in [123–125]. However, this method has disadvantages such as susceptibility to disturbances on the powerline and vulnerability to RF interference [16]. In [126], the design and implementation of a cascaded system of fast ethernet and power-over-ethernet (PoE) with VLC are presented which has similar drawbacks as for PLC channels. In order to avoid such infrastructure costs associated with wired solutions, wireless alternatives have been explored. Among wireless backhauling solutions, integration of VLC with high bandwidth FSO links for backhaul is presented in [127, 128] which necessitates precise link alignment. The use of mmWave has also been considered in [129] which is capable of high data rates, but has drawbacks including the need for special hardware for implementation, and security weakness as these signals can penetrate through walls. Another solution was presented in [220] where line-of-sight (LOS) VLC links between auxiliary LEDs and photodetectors have been used as the backhaul structure. However, LOS restrictions and interference caused by the backhaul link on the user data are drawbacks of this method. A mirror-aided non-LOS VLC backhaul link has been proposed in [130] to overcome the LOS constraint. Nevertheless, this method adds to the components and leads to complexity in implementation. While there are many approaches to address front and backhauling in VLC, all previous approaches require specialized implementation setups, making them either not widely available or expensive to deploy.

In this chapter, for the first time, the design of an optical repeater integrated into the LED driver of a luminaire is investigated. As Fig. 4.1 depicts, information transmitted from a handheld device in the center of the room is sent to ceiling-mounted repeater-enabled luminaires via IR uplink signals. The signal received by the luminaire is amplified and broadcast in the room in the visible band, while also being relayed to adjacent luminaires through IR to further increase the coverage. Additionally, data exchange between luminaires and an optical transceiver, linked to a central data infrastructure, could be implemented through IR presenting an optical backhauling solution to the optical network.

Fig. 4.2 presents a simplified model showing the integrated luminaire power converter and communications repeater presented in this paper. The LED driver is realized as a multi-phase boost converter wherein the Schottky diodes are substituted by photodiodes capable of detecting optical signals when under reverse bias. These photodiodes generate an electrical photocurrent proportional to the intensity of the received IR signal. This current is superimposed on the DC current supplied by the LED driver for illumination, thereby modulating the intensity of the visible LEDs output. While visible LEDs for illumination are used as emitters, additional IR LEDs can also be added to the output stage to facilitate data transmission in the IR domain. Given that multiple emitters can be linked in series, spatial summation of the optical signals from the emitters results in signal amplification.

Unlike [118], our method only utilizes the optical spectrum which can be employed as an uplink channel in an RF-sensitive environment without interference. In contrast to [16], the proposed method can be integrated into existing lighting infrastructure without changes to the cabling or electrical installation of the building, hence offering a cost-effective backhauling and fronthauling solution. To the knowledge of the authors, this is the first work to consider the design of a repeater that has infrared input and both visible/IR output which allows for broadcast as well as enabling optical front/backhauling to connect the VLC-enabled luminaires to the backbone networks.

4.3 Principle of Operation

4.3.1 Concept

A multi-phase boost LED driver for a luminaire is illustrated in Fig. 4.3. The Schottky diode typical in each phase of such converters is replaced by a photodiode to create a means of receiving an optical signal, x_{sig}. The operation of the repeater remains unaffected by the type of modulation of the received signal, provided it is intensity-modulated. Examples of modulation schemes that can be used for intensity modulation of light include on-off keying (OOK), pulse position modulation (PPM), or direct-current-biased optical (DCO) and asymmetrically clipped optical (ACO) OFDM [135, 134, 136, 85]. The following explanation of the topology will use the example of a 2-phase boost converter, however, it can be expanded to an N-phase boost converter.

In the case of $N = 2$, two 180° out-of-phase square waveforms with the same amplitude and duty cycle drive the MOSFETs of the synchronous 2-phase boost converter, as seen in Fig. 4.5.a. According to Fig. 4.4, when the MOSFET of a phase is on, the corresponding photodiode is reverse-biased, generating a photocurrent, i_{sig}, upon infrared (IR) signal reception, x_{sig}. This is called the *detection mode* state. When the MOSFET is off, the photodiode becomes forward-biased, conducting the inductor's DC current to the output LEDs. This is the *conduction mode* state. As

Table 4.1: List of Parameters used throughout the paper

Parameter	Symbol	Unit
Repeater input/output DC voltage	V_{in}/V_{out}	V
Duty cycle	D	—
Low/high voltage	V_L/V_H	V
Inductor current ripple	ΔI_L	A
No. phases in the converter	N	—
Converter switching frequency/period	F_{sw}/T_{sw}	Hz/s
Efficacy	η_{ef}	lm/W
MOSFET gate-source control voltage	V_{gs}	V
Luminous flux	Φ	lm
No. LEDs at the output	j	—
No. PDs in each phase	k	—
Optical signal mean	μ	W
Optical signal variance	σ^2	W^2
Transmitted optical power from T_x	P_{Tx}	W
Received optical power at R_x	P_{Rx}	W
Signal subcarrier spacing	Δf_{sub}	Hz
PD generated current	i_{PD}	A
PD detection physical area	A_1	mm^2
Responsivity of PD	R_1	A/W
IR transmitter distance from repeater	d_1	m
VLC receiver distance from repeater	d_2	m
No. subcarriers	M	—
End to end gain	G_{e2e}	—
Repeater gain	G	—
VLC channel gain	H_2	—
IR channel gain	H_1	—
VLC detector physical area	A_2	mm^2
Lambertian Order	m	—
Optical Gain of LED	Q	lm/A
Angle of irradiance	ϕ_1, ϕ_2	$^\circ$
Angle of incidence	ψ_1, ψ_2	$^\circ$
Field of view	Ψ_1, Ψ_2	$^\circ$

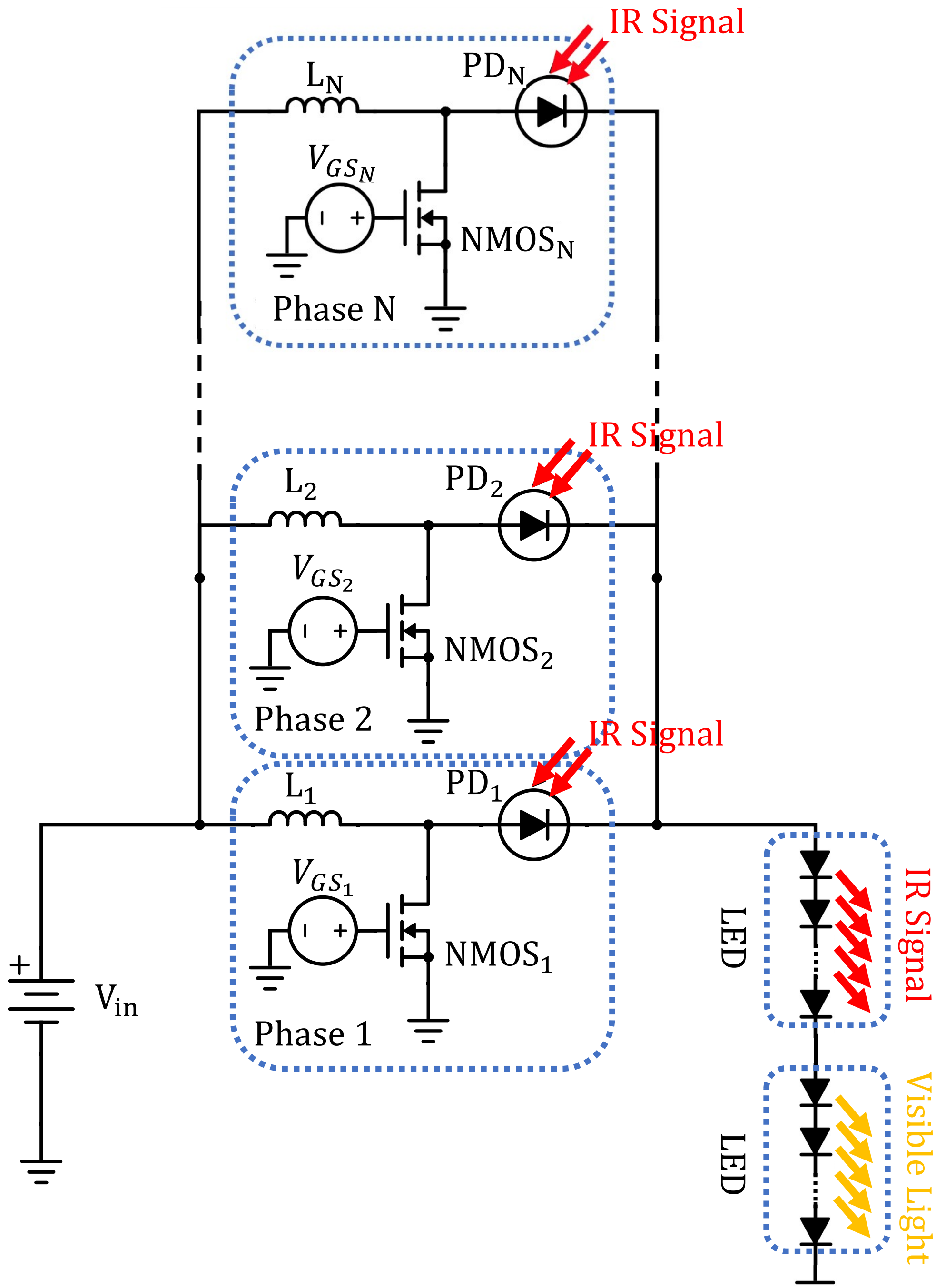

Figure 4.3: Integrated repeater into multi-phase boost LED driver with N phases and two strings of LEDs, IR and visible, connected in series at the output.

in Fig. 4.5.b, the current of a photodiode at any instance is either equal to that of the inductor or the negative of the generated photocurrent, and the output current flowing through the LEDs is equal to the combined sum of the currents from the photodiodes, i.e.,

$$
\begin{aligned}
&i_{sig}(t) = R_1(\lambda)x_{sig}(t) \\
&t \in [0, DT_{sw}] = \begin{cases} i_{PD1}(t) = -i_{sig}(t) \\ i_{PD2}(t) = i_{L2}(t) \end{cases} \\
&t \in [DT_{sw}, T_{sw}] = \begin{cases} i_{PD1}(t) = i_{L1}(t) \\ i_{PD2}(t) = -i_{sig}(t) \end{cases} \\
&i_{LED}(t) = i_{PD1}(t) + i_{PD2}(t)
\end{aligned}
\tag{4.1}
$$

where R_1 is the responsivity of the photodiode, which depends on the wavelength of the incident, λ. Therefore, as depicted in the last graph of Fig. 4.5.b, the current of each LED at the output will be equal to the DC current of the inductor superimposed by the photodiodes generated current. Since multiple LEDs are connected in series at the output, their light intensities are combined spatially [221], resulting in the transmission of the amplified received signal. It is important to note that the graphs in Fig. 4.5 illustrate the scenario where $D = 50\%$. However, this is not always the case when dimming is imposed, and other scenarios will be examined in detail in subsequent sections.

In the more general scenario where the LED driver consists of N phases, the gate-source signals of the MOSFETs, V_{GSi}, are square waveforms with a duty cycle of D, and a phase-shift of $\frac{2\pi}{N}$. When the MOSFET of a phase is in detection mode

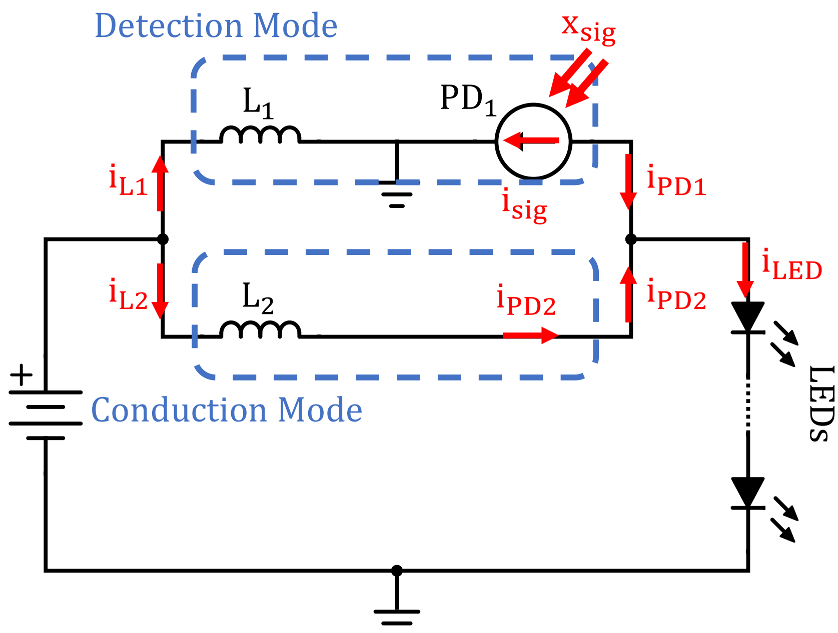

(a)

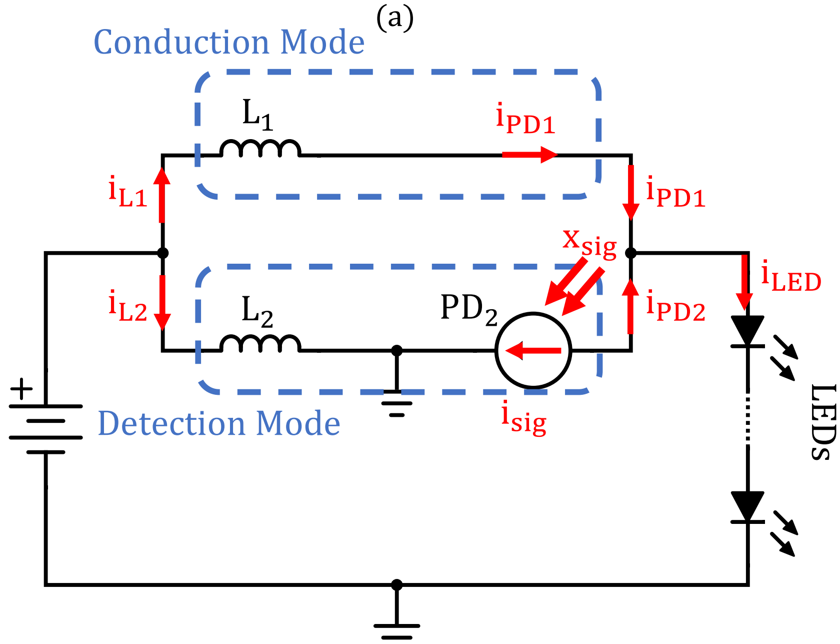

(b)

Figure 4.4: Proposed 2-phase boost repeater structure. (a) illustrates the scenario where phase 1 is in detection and phase 2 is in conduction mode. (b) depicts the case where phase 1 is in conduction and phase 2 is in detection mode.

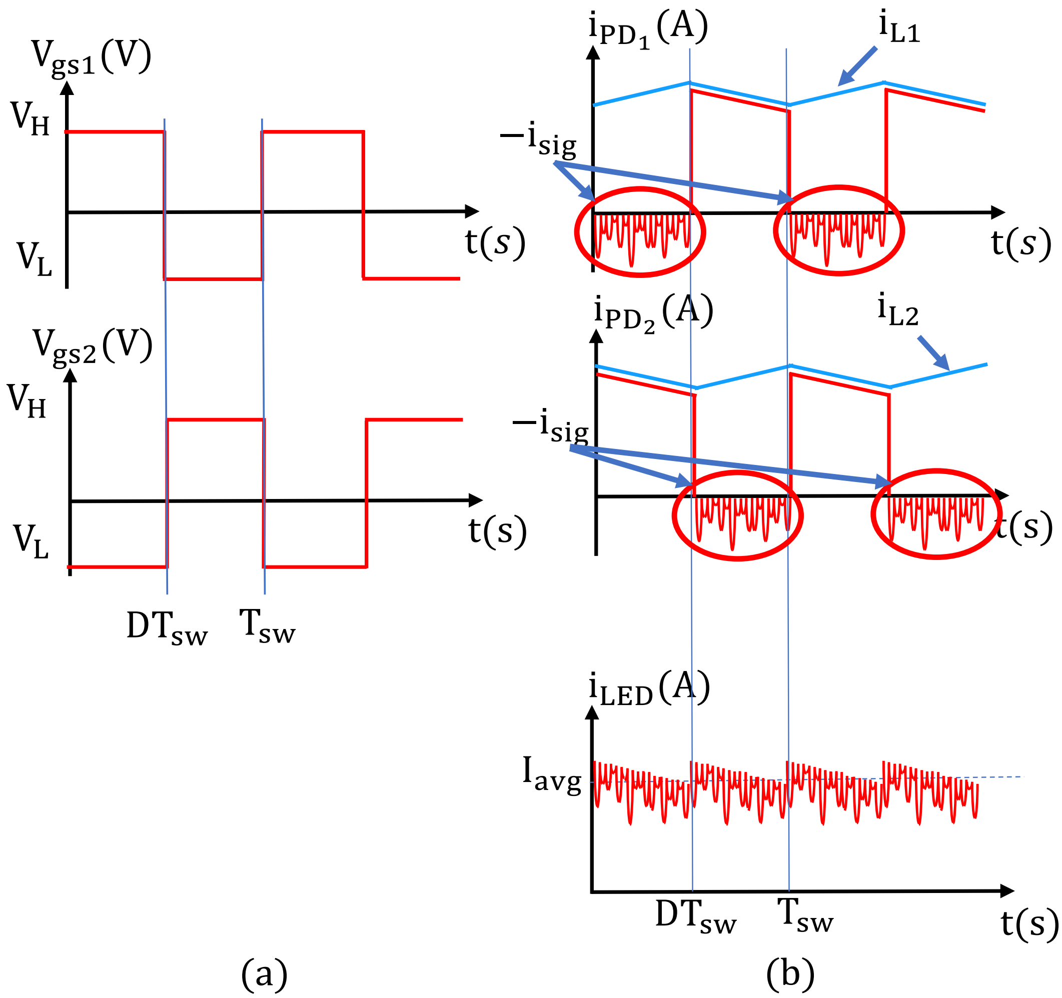

Figure 4.5: Key voltages and currents of the circuit in Fig. 4.4. The gate signals of the MOSFETs are illustrated in (a), while (b) represents the currents in the photodiode and inductor of each phase and the LEDs at the output.

it generates a photocurrent according to the received signal, and when in conduction mode it carries the DC current required to illuminate the LEDs. As in the previous case, the current flowing through the LEDs at the output, at any given moment, is the combined sum of the currents from all the photodiodes:

$$\begin{aligned} &i_{LED}(t) = i_{PD_1}(t) + i_{PD_2}(t) + ... + i_{PD_N}(t) \\ &i_{PD_i}(t) = \begin{cases} -i_{sig}(t) & ,V_{gs_i} = V_H : \ \text{Detection} \\ i_{L_i}(t) & ,V_{gs_i} = V_L : \ \text{Conduction} \end{cases} \end{aligned} \tag{4.2}$$

As depicted in Fig. 4.3, the emitters at the output could be a combination of LEDs in visible and infrared bands so that the signal can be simultaneously transmitted at different wavelengths to address broadcast as well as backhauling/fronthauling in VLC systems. The emitters used at output in the discussion of this chapter are considered to be visible LEDs unless otherwise stated.

4.3.2 Illumination Performance

In working to integrate an optical communication repeater into a luminaire, it must be emphasized that illumination is the primary role of the luminaire and cannot be compromised. Key metrics include efficacy (η_{ef}), as well as dimming capability and flicker-free illumination.

Switched-mode power supplies, especially those designed for LED drivers, are engineered to minimize fluctuations in the output, ensuring consistent and flicker-free illumination. Typically, these converters incorporate a capacitor in the final stage to filter out any remaining fluctuations, see Fig. 4.6.a. Moreover, in boost converters,

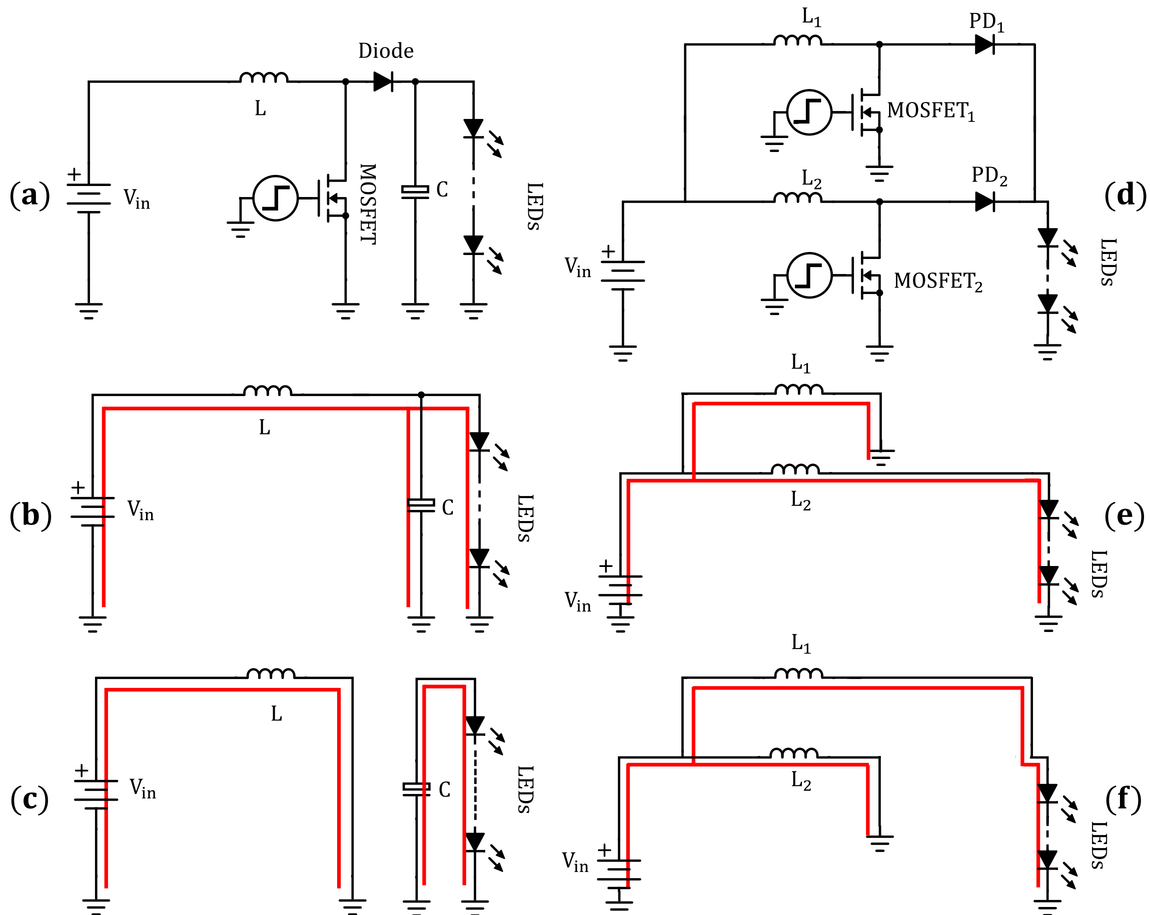

Figure 4.6: Structure of a single phase and 2-phase boost converter is depicted in (a) and (d) respectively. The current path through the circuit is illustrated in (b) and (c) when the MOSFET is off and on respectively. The current flow in the circuit of the 2-phase boost is shown in (e) when MOSFET 1 is on and in (f) when MOSFET 2 is on.

the capacitor plays a pivotal role in maintaining a stable output current to power the LEDs. As depicted in Fig. 4.6.b, during the off state of the MOSFET, the discharge current from the inductor is split between the LEDs and the capacitor, thus charging the capacitor. Consequently, during the on-state of the MOSFET and when the diode is reverse-biased the current for the LEDs is drawn from the capacitor, see Fig. 4.6.c. However, since intensity modulation of the LEDs is necessary for data transmission, the capacitor must be eliminated which disrupts the consistent current flow to the LEDs. Nonetheless, in designs incorporating multiphase boost converters, like the 2-phase boost converter in Fig. 4.6.d, strategic manipulation of duty cycles allows for the uninterrupted supply of output current through the discharge of other phase inductors while one phase is charging. In other words, when one phase is in detection mode, there will be another phase in conduction mode to make up for the current that once was supplied by the capacitor, see Fig. 4.6.e and Fig. 4.6.f.

Given that the same V_H and V_L values, as well as identical pulse width, are assumed for the V_{gs} of all phases in an N-phase boost converter, and there is a delay of $\frac{T}{N}$ seconds for the V_{gs} of each phase relative to the preceding one, the set of possibilities for D can be categorized as:

$$\begin{cases} D \in \left[0, \frac{1}{N}\right) & (I) \\ D = \frac{1}{N} & (II) \\ D \in \left(\frac{1}{N}, \frac{N-1}{N}\right] & (III) \\ D \in \left(\frac{N-1}{N}, 1\right] & (IV) \end{cases} \tag{4.3}$$

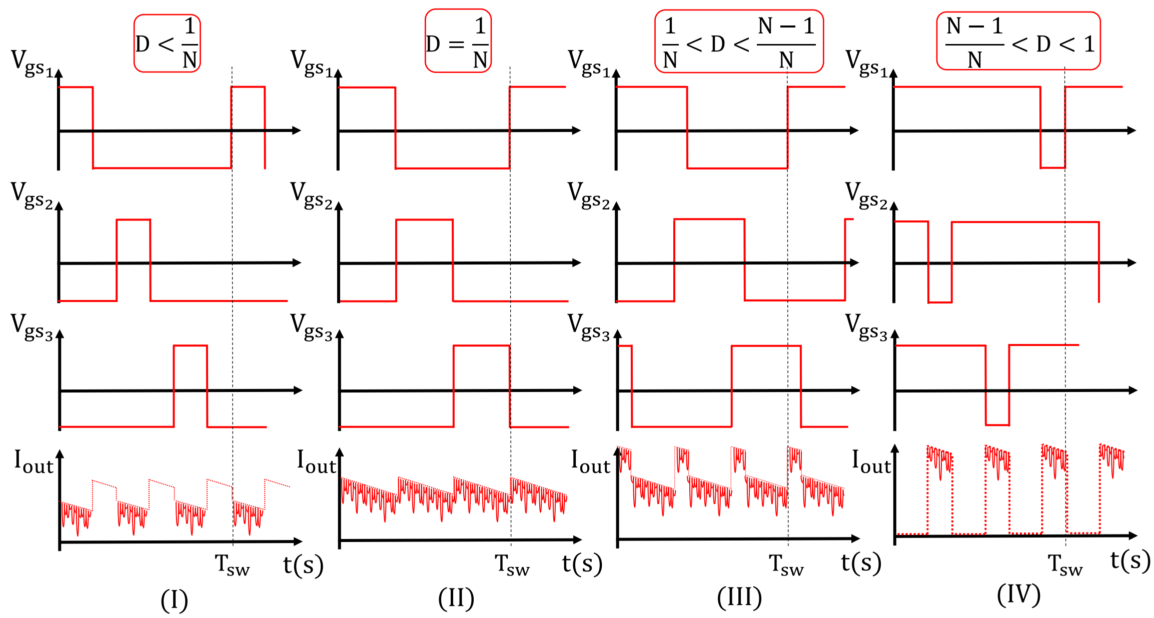

Figure 4.7: Various scenarios for the duty cycle (D) in a 3-phase repeater boost converter with N representing the number of phases. Scenario (I) involves instances where none of the photodiodes are in reverse bias. In Scenario (II), one photodiode is consistently reverse-biased at each instance for signal detection. Scenario (III) depicts instances where more than one photodiode is engaged in signal detection. Scenario (IV) entails instances where all photodiodes are simultaneously in reverse bias.

Fig. 4.7 illustrates examples of the gate-source signals and output current of a 3-phase boost converter, serving as a means to facilitate the analysis of the repeater performance concerning both illumination and communication across various scenarios outlined in Eq. 4.3.

1. Scenario (I):

   Illustrated in Fig. 4.7.a and characterized by $D < \frac{1}{N}$, in this scenario instances occur where $V_{GS} = V_L$ across all phases, indicating that according to Eq. 4.2, they are all in conduction mode, resulting in no signal reception. The uninterrupted current flow through the LEDs is guaranteed in this case, however, detection of a signal is only possible in DT_{sw} intervals of the switching period.

2. Scenario (II):

   Under this scenario depicted in Fig. 4.7.b, where $D = \frac{1}{N}$, only a single phase operates in detection mode at any given time, with the remainder in conduction. Consequently, consistent signal detection and uninterrupted current flow through the LEDs are sustained. Additionally as observed in Fig. 4.7 this case exhibits the least fluctuation of DC current through the LEDs, suggesting minimal flicker.

3. Scenario (III):

   In the third case, defined by $\frac{1}{N} < D \leq \frac{N-1}{N}$ and portrayed in Fig. 4.7.c, one or more phases are in detection mode simultaneously, yet there is always at least one phase in conduction mode. Although detection of the signal is possible at all times during a switching period, signals detected in shorter intervals are amplified due to the involvement of multiple phases in detection. While this may enhance the SNR and overall amplification gain, the complexities involved in decoding at the receiver end render signal detection during these intervals less favorable.

4. Scenario (IV):

   Scenario IV, characterized by $\frac{N-1}{N} < D \leq 1$, is depicted in Fig. 4.7.d. It is observed that there are instances where all phases are in detection mode while none are in conduction, leading to no illumination. Considering that the repeater is situated within a luminaire requiring uninterrupted illumination, this scenario is deemed undesirable. Additionally, it is important to note that although having all phases in detection mode may initially appear advantageous for communication purposes, there is no reception of signal during this interval due to the loss of photodiodes' reverse-bias as the output current and voltage drop to zero.

It can be concluded that operating in scenario (II) is the most desirable and scenario (IV) the least. The duty cycle D resulting to the maximum illumination can be set in the design procedure to be equal $\frac{1}{N}$ to avoid operation in scenarios (III) and (IV) while ensuring that the nominal operation of the luminaire occurs in scenario (II). However, the dimming capability of the luminaire is also often of importance, thus adjusting D to lower values than $\frac{1}{N}$, is required.

In order to maintain an integer number of symbols in all the detection intervals in scenario (I) the length of the detection window, should be divisible by the length of one received symbol, i.e.,

$$DT_{sw} \mod T_{sym} = 0 \tag{4.4}$$

Since the length of an OFDM symbol is set by the communication standards [85, 87], and D is set according to brightness required, the only remaining variable to adjust is T_{sw}. Through adjusting the switching frequency of the converter, one can satisfy the criteria in Eq. 4.4.

4.3.3 Gain Analysis

Given the proposed topology is utilized as an amplifying repeater, one of the critical parameters for evaluation is the optical gain, denoted as G. This value represents the ratio of the optical power of the signal emitted from the LEDs of the repeater, P_{Ro}, to the optical power of the received infrared signal at the photodiodes of the repeater, P_{Ri}. The end-to-end optical gain of an optical wireless channel, represented as G_{e2e} and illustrated in Fig. 4.8, is defined as the ratio of P_{Rx} of the signal received by R_x, located at a distance d_2 from the repeater, to P_{Tx} transmitted by the T_x positioned at a distance d_1 from the repeater. The gain can be calculated as follows:

$$G_{e2e} = \frac{P_{Rx}}{P_{Tx}} = H_1 \times G \times H_2 \tag{4.5}$$

where H_1 is the infrared uplink channel gain, G, is the repeater optical gain, and H_2 is the visible light downlink channel gain. When modeling H_1 and H_2, the Lambertian emission pattern is considered for all LEDs, and the line-of-sight path is assumed to dominate over other reflective paths. Therefore, H_1 and H_2 are both modeled as a flat fading channel with a constant propagation delay [44].

As mentioned in Sec. 4.3.1, this repeater topology is modulation-agnostic. For the purposes of this study, the signal is considered to be modulated by ACO-OFDM. An ACO-OFDM signal with mean optical power (μ_{ACO}) of P_{Tx} is transmitted by the

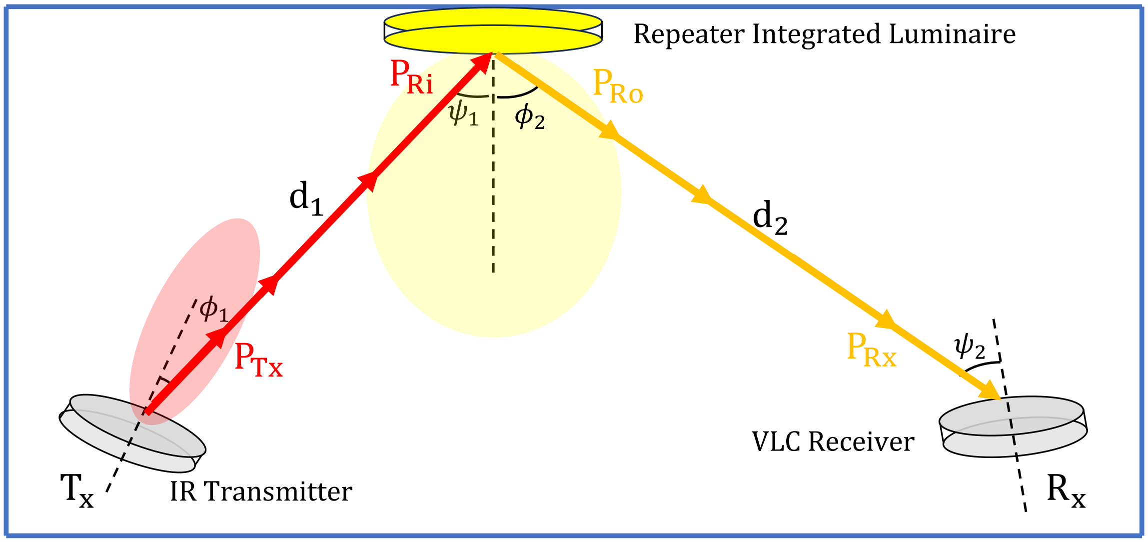

Figure 4.8: Position of the transmitter, repeater, and the receiver in a room. The optical power of the signal transmitted by T_x is P_{Tx} and the optical power of the signal received at R_x is P_{Rx}.

user at T_x, propagates through the IR channel with a DC gain of H_1, and is received by the repeater [44].

$$H_1 = \begin{cases} \frac{(m_1+1)A_1}{2\pi d_1^2} cos^{m_1}\phi_1 T_{1(\psi_1)} g_{1(\psi_1)} cos\psi_1, & 0 \leq \psi_1 \leq \Psi_1 \\ 0, & \psi_1 > \Psi_1 \end{cases} \tag{4.6}$$

Note that the symbols employed in the equation are detailed in Table 4.1.

In the repeater, the photodiodes produce an electric current which is directly proportional to the optical power of the signal received at the repeater.

$$I_{PD} = k \times P_{Ri} \times R_{1(\lambda_1)} \tag{4.7}$$

Here, k is the number of photodiodes in each phase and $R_1(\lambda_1)$ is the responsivity of the photodiode at wavelength λ_1. The received signal photocurrent sums with the DC current of the output LEDs, however, the polarity of the signal is reversed as illustrated in Fig. 4.4.b. Assuming that the amplitude of the photo-generated current from the photodiode is small relative to the DC current through the LEDs, the DC operating point of the LEDs is maintained. Thus, P_{Ro}, the output optical power of the repeater can be determined.

$$P_{Ro} = j \times I_{PD} \times Q_{(I_{DC})} \tag{4.8}$$

Here j represents the number of output LEDs, and $Q(I_{DC})$ denotes the optical gain of the LED. Using Eq. 4.7 and Eq. 4.8, the optical gain of the repeater, G can be defined found as:

$$\begin{aligned} P_{Ro} &= j \times k \times P_{Ri} \times R_{1(\lambda_1)} \times Q_{(I_{DC})} \\ G &= \frac{P_{Ro}}{P_{Ri}} = j \times k \times Q(I_{DC}) \times R_1(\lambda) \end{aligned} \tag{4.9}$$

In practice, the optical gain is not typically listed in the datasheets of visible light LEDs. Instead, these datasheets use lumens, a photometric unit that considers the human eye's varying sensitivity to different wavelengths of light. A typical approximation assumes that the LEDs emit monochromatic light at a wavelength of 555 nm. According to the luminosity curve, this is the wavelength to which the human eye is most sensitive, where 1 lumen is equivalent to 1/683 W [222].

Next, the visible light signal emitted by the LEDs will propagate through and be conveyed to the receiver located at R_x. The gain of the visible light channel can be determined by:

$$H_2 = \begin{cases} \frac{(m_2+1)A_2}{2\pi d_2^2} cos^{m_2}\phi_2 T_2(\psi_2) g_2(\psi_2) cos\psi_2, & 0 \leq \psi_2 \leq \Psi_2 \\ 0, & \psi_2 > \Psi_2 \end{cases} \tag{4.10}$$

The variables $m_2,\ A_2$, and d_2 are defined in Table. 4.1. Using Eq. 4.5, $\frac{P_{RX}}{P_{Tx}}$, also known as end-to-end optical gain, G_{e2e}, can be calculated using the expressions found for $H1,\ G$, and H_2 in Eq. 4.6, Eq. 4.9, and Eq. 4.10 respectively. For a specific case where the values of $\lambda,\ \phi_1,\ \psi_1,\ \phi_2$, and ψ_2 are constant, the gain can be simplified to:

$$G_{e2e} = \frac{P_{Rx}}{P_{Tx}} = \frac{\gamma}{d_1^2 d_2^2} \times j \times k \times Q(I_{DC}) \tag{4.11}$$

The constants in the gain equation are denoted by γ. It can be observed that the amplifier's gain depends on the number of photodiodes, the number of LEDs, and the LED's DC current, which indicates the luminaire's dimming level. Since the dimming level is determined by the duty cycle, we can conclude that the gain is a function of j, k, and D.

4.3.4 Bandwidth and Noise Analysis

The bandwidth of an optical repeater is a pivotal factor in the performance analysis of optical communication systems as it directly affects the ability of the repeater to convey high data rate signals and maintain signal integrity over extended distances.

As discussed in Sec. 4.3.1 and Sec. 4.3.3, the repeater operates on a simple optical-to-electrical and electrical-to-optical conversion and consequently its design and components do not inherently limit the bandwidth. In our scenario, bandwidth is primarily constrained by the photodiodes and LEDs. Here, the phosphor-coated LEDs serve as the limiting factor with their bandwidth restricted to a few MHz, whereas the photodiode offers a bandwidth reaching up to 50 MHz. are the main bandwidth limiters. While increasing the bandwidth to GHz levels may introduce challenges related to routing and board tracks on the printed circuit board, the repeater topology does not intrinsically constrain bandwidth, as no signal processing happens within the repeater topology,and should be adequate for the recommended available bandwidth of 50 MHz in the high-bandwidth physical layer (HB-PHY) [87]. For example, a 256 subcarrier, 64 QAM ACO-OFDM modulated signal with a $\Delta f_{sub} = 100$ kHz can achieve a data rate of 76.8 Mbps which lies inside the range of rates between 23 Mbps and 2.192 Gbps specified in [87].

The noise figure of an optical repeater determines the impact of the repeater on the overall SNR and, consequently, the BER of the system, both of which are critical for communication quality. The primary noise sources in this topology are the thermal noise of the MOSFET operating in the triode region and the shot noise of the photodiode due to the high ambient noise in VLC settings. As illustrated in Fig. 4.9, except for I_n, which represents the shot noise of the reverse-biased photodiode, all other noise sources are significantly filtered by the inductors in their paths to the output. Consequently, the noise introduced to the system by the repeater (N_A) is considerably less than the input noise (N_i), leading to the conclusion that the noise

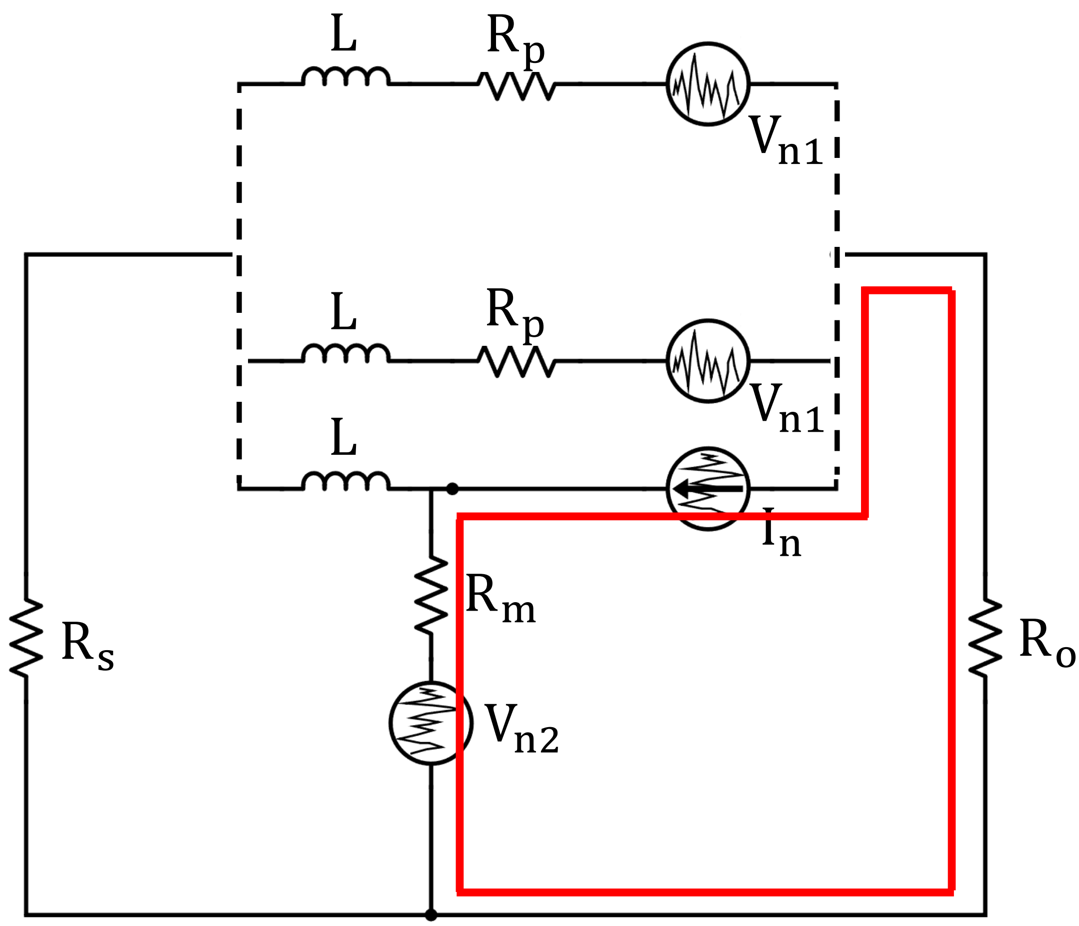

Figure 4.9: Noise equivalent of the repeater. V_{n1} represents the shot noise of the photodiodes in forward bias, and V_{n2}, signifies the thermal noise of the MOSFET operating in triode region. I_n indicates the shot noise of the reverse-biased photodiode while detecting signal.

figure of this repeater is effectively 0 dB, i.e.,

$$NF = 10 \log \left(\frac{SNR_i}{SNR_o} \right) = 10 \log \left(1 + \frac{N_A}{N_i} \right) \approx 0 \text{ dB} \tag{4.12}$$

where N_A and N_i refer to the noise added by the repeater and the noise delivered to the repeater respectively. A thorough analysis of the noise figure, including the theoretical calculation of the noise figure can be found in the supplemental files attached to the article.

4.3.5 Circuit Design Considerations

In the integration of a communications repeater into the power converter, several issues must be addressed to ensure both efficient electrical operation while meeting optical constraints.

1. Uninterrupted Illumination

   As mentioned in Sec. 4.3.2, the capacitor typically added to the final stage of boost is removed to allow modulation at the output. In this case, the scenarios outlined in Fig. 4.7 must be considered through careful handling of the duty cycle to ensure constant uninterrupted illumination is maintained.

2. Output Ripple

   The selection of the inductor size is determined based on constraints like the permissible ripple in the output current and the desired level of illumination specified by the application, along with considerations of the available input power source. According to [207] the ripple of the inductor current can be determined by

$$\Delta I_L = \frac{V_L \times (1 - D) \times T_{sw}}{L}. \tag{4.13}$$

This equation suggests that to reduce current ripple at the output, one can use a larger inductor size, increase the duty cycle, or raise the switching frequency. As indicated in Fig. 4.4.d, $V_L = V_{out} - V_{in}$ when the MOSFET is off, therefore, minimizing the difference between output and input voltage also contributes to reducing output ripple.

3. Photodiode Forward Current

   While photodiodes are functionally similar to Schottky diodes, they are not designed for operation in forward-bias. In the case of a large load current, photodiodes can be operated in this regime often with several in parallel to share the phase current and prevent circuit failure. Since datasheets typically do not include information regarding the maximum value for forward-biased current for photodiodes, in practice, and in our experiments in Sec. 4.5, this must be tested experimentally.

4. Eye Safety

   Infrared radiation possesses the capacity to traverse the human cornea and potentially cause thermal damage to the retina. Adherence to eye safety protocols is imperative, as set forth by the International Electrotechnical Commission (IEC) [223]. Compliance with IEC Class 1 allowable exposure limit (AEL) signifies the assurance of eye safety across all operational scenarios for IR LEDs.

4.3.6 Design Methodology

Buck converters are common in household lighting due to the lower operating voltage of luminaires compared to building electrical supply [224]. While boost converters are less common in grid-powered lighting, they are widely used in high-intensity lighting, display backlighting, automotive lighting, and off-grid smart homes with green energy sources like wind turbines and solar panels and is the focus of this work [225]. This section highlights the choice of a 2-phase boost converter for its simplicity and cost-effectiveness. Adding additional phases increases complexity and costs, which runs counter to the aim of creating an efficient, affordable LED driver for luminaires. However, for high current loads, more phases can reduce component stress, allowing higher nominal ratings with the same components. Additionally, If a high switching frequency is necessary to minimize ripple, adding phases is an option for a given MOSFET. For instance, a 3-phase and a 2-phase boost converter both switching at F_{sw} are similar to single-phase converters operating at $3F_{sw}$ and $2F_{sw}$ respectively.

Referring to established communication standards [85], the duration of OFDM symbols is predetermined. As discussed in Sec. 4.3.2 and shown in Fig. 4.7, an optimal scenario exists when $D \leq \frac{1}{N}$, in this context equating to $\frac{1}{2}$ as $N = 2$. As the first design constraint revolves around the desired illumination level and dimming range, it is imperative to ensure that the nominal illumination level occurs at $D_{max} = 50\%$, and the minimum dimming level is achieved at $D_{min} = 30\%$, considering that the converter efficiency diminishes at low duty cycles. Consequently, the switching frequency should be chosen such that the length of each detection phase is longer than the length of one OFDM symbol, i.e. $\frac{D_{min}}{F_{sw}} \geq T_{symbol}$. Based on the available input voltage and the determined range for D, nominal converter voltages can be

Table 4.2: Simulation and Experimental Parameters for the 2-phase Boost repeater (cf. Fig. 4.3 & 4.8)

Parameter	Symbol	Value
Inductor	L	6 mH per phase
Photodiode	PD	2 MT03-004 per phase
Light emitting diode	LED	7 Lumiled 3535L
IR emitter	IR LED	4 SFH-4727AS
Switching device	Sw	NMOS AO3442
Input voltage	V_{in}	13 V
Duty cycle	D	40% – 50%
Switching frequency	F_{sw}	10 kHz
Distance between repeater and transmitter	d_1	1 m
Distance between repeater and receiver	d_2	1 m
No. subcarriers	M	256
Subcarrier spacing	Δf_{sub}	20 kHz
Modulation Scheme		64 QAM ACO OFDM
Mean value of the signal	μ_{ACO}	1 – 10 mW

ascertained, which, coupled with the frequency, facilitate a deliberate selection of the MOSFET. The inductor size will then be determined based on the permissible ripple on the output current, typically set at 5% [202]. Based on the output voltage range, being $V_{out} \in [\frac{V_{in}}{1-D_{min}}, \frac{V_{in}}{1-D_{max}}]$, the number of the LEDs needed to maintain the dimming with the specified V_{out} range can be determined.

4.4 Simulation Results

In this section, we investigate the design and simulation of a repeater intended for use as luminaire within a typical workplace environment, such as an office. Compliance with occupational safety and health administration (OSHA) [226] standards

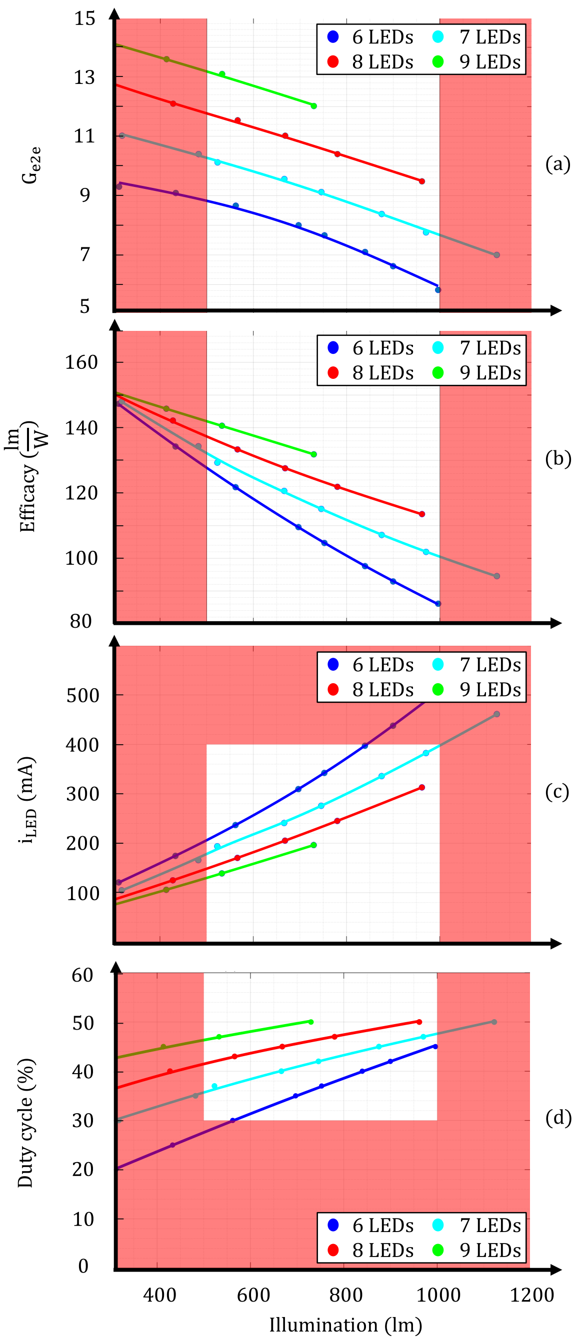

Figure 4.10: Performance comparison for different numbers of LEDs. (a). Gain vs illumination (b). Efficacy vs illumination (c). Current vs illumination (d). Duty cycle vs illumination. The shaded area in red represents the region where the repeater should not operate and helps to determine the best combination of LEDs to select

dictates that an open-space office necessitates an illuminance of 30-foot candles, approximately equivalent to 320 lux. Assuming a room height of 3 meters and ceiling-mounted lighting, it can be determined that three LED lightbulbs, each emitting 1000 lm with a beam angle of 60°, would adequately illuminate the workspace. Considering 500 lm or 50% dimming range is desired, the target will be the design and simulation of a repeater with a nominal brightness of 1000 lm and a dimming capability of 50%.

This design approach is exemplified by the scenario of a user positioned in the middle of the room, as shown in Fig. 4.1, where IR signal is transmitted to the luminaire and is broadcast in the room via visible spectrum. Similar design methodologies can be applied for the back/front hauling links, ensuring consistent and adequate illumination throughout the office space.

4.4.1 Simulation Design

This section presents a brief overview of the design process, with a comprehensive design procedure and component selection discussed in Appendix. C. In order to begin the design, the input voltage is considered to be 12 V, consistent with the voltage provided by commercially available solar panels [198], and the dimming should be achieved with $D \in [30\%, 50\%]$. Using the input voltage and the specified range for D, the maximum output voltage can be determined via Eq. 4.14 which is the general equation for boost converters that relates V_{out} to V_{in} and D [207]:

$$\begin{aligned} V_{out} &= \frac{V_{in}}{1-D} \\ V_{out-max} &= \frac{12}{0.5} = 24\text{V} \quad , D_{max} = 50\% \end{aligned} \tag{4.14}$$

For a F_{sw} up to 100 kHz and according to the voltages in the circuit, see Eq. 4.14, an AO3442 NMOS [208] is selected as a switching device for each phase. Regarding the inductor, considering 5% acceptable ripple in the current [202], according to conventional design guidelines, a 10 mH inductor has been selected for each phase. As for the optical devices, simulation models are populated with the parameters as listed on the datasheets for the experimental setup, Table. 4.8. Furthermore, $d_1,\ d_2$ are both set to 1 m, and $\phi_1,\ \phi_2,\ \psi_1,\ \psi_2$ are all set to 0°.

The number of LEDs in the luminaire affects both the illumination and the gain of the repeater. According to $V_{out-max}$ derived from Eq. 4.14, and given that the typical forward voltage drop across an LED ranges from 2.5 V to 3.5 V [203], it can be inferred that the available output voltage can support approximately $\lfloor\frac{24}{3.5}\rfloor = 6$ to $\lfloor\frac{34}{2.5}\rfloor = 9$ LEDs. Based on the $v - i$ and $\Phi - i$ characteristic of available LEDs, six Lumiled 3535L LEDs [179] are capable of delivering up to 1000 lm when operated at their maximum ratings. The luminous flux versus current $(\Phi - i)$ curve for this LED can be modeled by the following quadratic fit [227]

$$\begin{aligned} \Phi(i) &= -0.0001i^2 + 0.3093i + 3.647 \\ \frac{\partial\Phi}{\partial i} &= -0.0002i + 0.3093 \end{aligned} \tag{4.15}$$

As illustrated in Eq. 4.9, a greater number of output LEDs results in higher repeater amplification gain G. Additionally, as indicated by Eq. (4.15), higher DC currents through the LEDs reduce their optical gain, implying that increasing the number of LEDs yields better efficacy since they can provide the same illuminance with lower current. Therefore, as long as the absolute ratings of the LEDs are not exceeded and the dimming range within the desired duty cycle is maintained, using more LEDs is preferable.

Fig. 4.10 presents a comparative analysis of the design space for a 2-phase boost converter with different numbers of LEDs (6, 7, 8, and 9) at the output. The comparison encompasses parameters such as gain, efficacy, load current, and operating duty cycle, all within a dimming range of $500 - 1000$ lm. As indicated by Eq. (4.9) and corroborated by Fig. 4.10.a, increasing the number of LEDs enhances G_{e2e}. Additionally, Fig. 4.10.b shows that a higher LED count corresponds to increased efficacy, due to the higher conversion rate of current to luminous flux at lower current levels, as described by Eq. 4.15. However, it is crucial to ensure that the desired dimming range is achievable within the LEDs' nominal current limits, $i_{LED} \leq 400$ mA per the datasheet. According to the design constraints made in Sec. 4.3.6, D in all these simulations has been limited to 50% and therefore Fig. 4.10.c highlights that configuration with 6 LEDs fails to attain the illumination target while maintaining $i_{LED} \leq 400$ mA. Finally, Fig. 4.10.d illustrates that options with 6, 8, and 9 LEDs cannot cover the full dimming span while keeping $D \in [30\%, 50\%]$. Consequently, it can be deduced that a combination of 7 LEDs represents the most suitable configuration for this scenario. This graphical representation presented in Fig. 4.10 is a valuable tool in design, assisting in selecting the optimal number of LEDs for specific application requirements.

The photodiodes in each phase are connected in parallel, and do not significantly affect the efficacy by accumulated forward voltage drop. However, using more photodiodes can slightly reduce efficacy due to small power losses in the additional photodiodes and a decrease in LED efficacy when modulated by higher amplitude signals. Furthermore, the parallel connection of mismatched photodiodes will result in

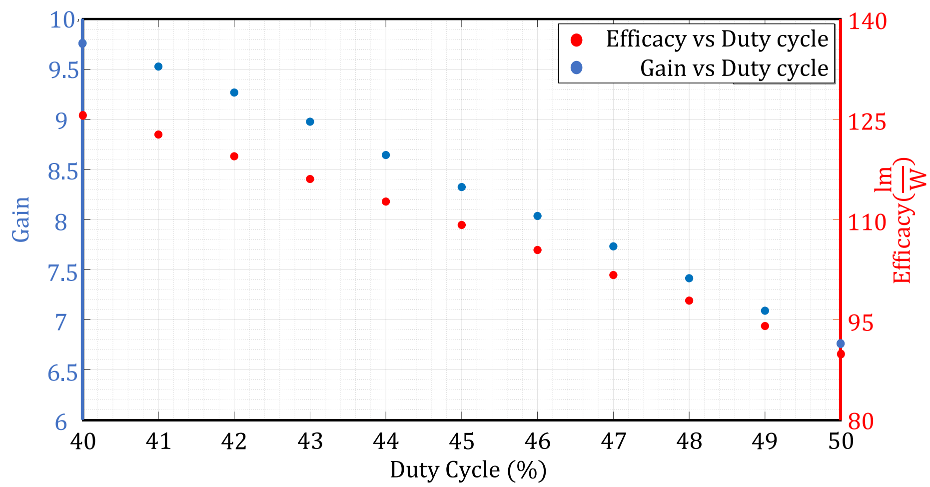

Figure 4.11: Simulated Gain and efficacy versus Duty cycle for a received signal power of 10 mW. The 2-phase boost converter is switching at $F_{sw} = 5$ kHz with $D \in [40\%, 50\%]$ and other specifications of the simulation are detailed in Table. 4.2.

one turning on sooner than the others, ceasing communications. Additionally, the combined capacitances of parallel photodiodes add reducing the bandwidth of the repeater. On the other hand, a higher number of photodiodes (k) helps to prevent excessive forward DC current from damaging any single photodiode [233]. Moreover, this also leads to increased amplification gain, as indicated by Eq. 4.11. In this study, one photodiode is used in each phase of the converter [234].

Though the repeater topology is modulation agnostic, for these experiments and simulations a signal employing ACO-OFDM modulation with a 256-subcarrier and 64-QAM is used. The length of each symbol is 50 μs, corresponding to a subcarrier spacing (Δf_{sub}) of 20 kHz. Due to the bandwidth constraints of the laboratory equipment, this subcarrier spacing is used for experimental results, and the simulations are conducted with the same value to ensure comparability. Given the use of ACO-OFDM, the signal variance (σ^2_{ACO}) is directly proportional to its mean value (μ_{ACO}) [235], which ranges from 1 mW to 10 mW. The chosen parameters, including a 1 m

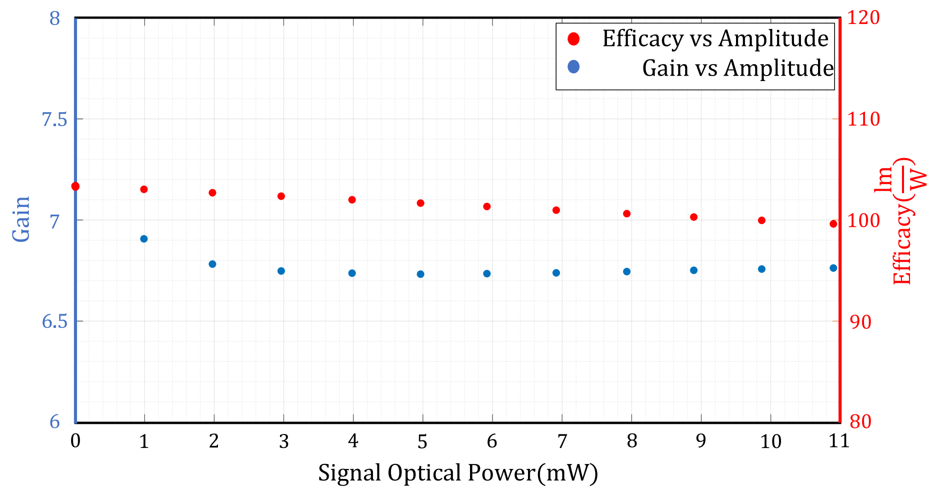

Figure 4.12: Simulated Gain and efficacy versus optical power of the IR signal at T_x. The 2-phase boost converter is switching at $F_{sw} = 5$ kHz with $D = 50\%$ and other specifications of the simulation are detailed in Table. 4.2.

distance for both infrared (IR) and visible light links, reflect the available space in the experimental setup within a laboratory environment and are established to allow for comparison. Additional parameters and their respective values for the simulations and experiments are detailed in Table 4.2. Subsequent sections will investigate the impact of duty cycle and IR signal optical power on repeater performance.

4.4.2 Duty Cycle

Fig. 4.11 is created by varying D from 40 to 50%, with the transmitted optical power (P_{Tx}) held steady at 10 mW, to document the received and transmitted optical power as well as the input electrical power. This data is then used to plot efficiency and optical gain as a function of D, demonstrating the simulated effect of the duty cycle on efficiency and total gain while maintaining the signal's optical power at 10 mW. It is observed that both efficacy and gain decrease with increasing duty

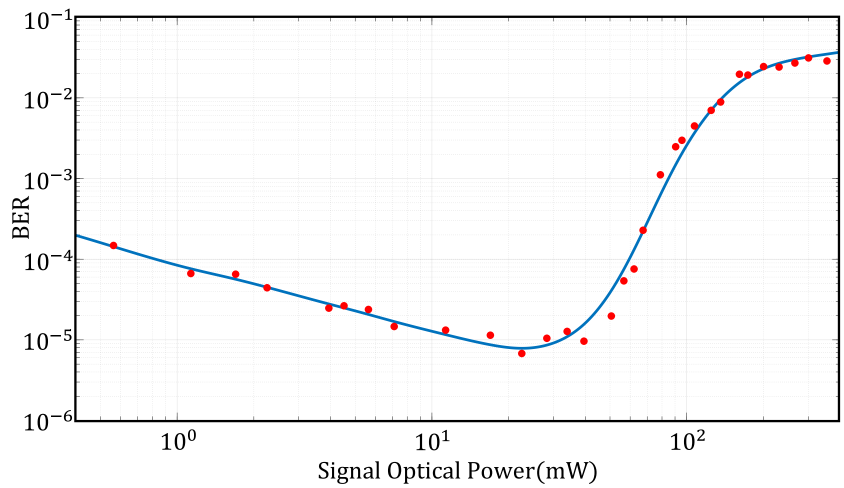

Figure 4.13: Simulated BER of the transmitted signal by the repeater versus the power of the IR signal at T_x. The signal is a 64 QAM ACO OFDM with 256 subcarriers. Further specifications of the simulation are detailed in Table. 4.2.

cycle. The decline in efficacy can be attributed to two primary factors: heightened conduction loss and diminished LED efficacy. With an increase in duty cycle, both the current passing through the MOSFET in its on-state and the duration of this current flow rise, consequently increasing the root mean square (RMS) of the current through the MOSFET. Therefore, according to [229], conduction loss increases, expressed as

$$P_{con} = I_{rms}^2 R_{DS} \tag{4.16}$$

Here, R_{DS} represents the equivalent resistance of the MOSFET in its on-state. Additionally, as previously discussed in Eq.4.15, the LED's efficacy decreases at higher currents, leading to a reduction in both efficacy and amplification gain. As computed in Eq. 4.11, the amplification gain is a function of D which corroborates with the findings in the graphs.

4.4.3 Transmit Signal Optical Power

By adjusting P_{Tx} between 1 and 10 mW while keeping D at 50%, Fig. 4.12 captures the received and transmitted optical power along with the input electrical power. This information is then utilized to graph efficiency and optical gain in relation to D, highlighting the simulated impact of P_{Tx} on both efficiency and total gain with D held constant. Notably, as the signal power increases from 1mW to 10mW, the efficacy and amplification gain of the repeater remain relatively constant. This constancy stems from the amplitude of the optical signal being significantly lower than the LED's DC current. Consequently, it has minimal impact on the LED's DC operating point and the conversion ratio, thus preserving the gain and efficacy. It is important to note that this holds true so long as the received optical power remains below the nominal ratings of the photodiode; exceeding these ratings leads to saturation of the photodiode, precipitating a decline in gain.

4.4.4 Communication Results

In this section, simulations were conducted to assess the repeater's performance in terms of the BER [191] for a signal transmitted from T_x, amplified by the repeater, and subsequently received at R_x. The distance between the transmitter and the repeater and also between the repeater and receiver is set at 1 m and the converter is switching at 5 kHz with $D = 50\%$. The BER is depicted in Fig. 4.13, where the mean value of the optical signal transmitted by the receiver varies. As expected, augmenting μ enhances the SNR and subsequently reduces the BER. However, excessive increases in μ lead to photodiode saturation within the repeater, resulting in

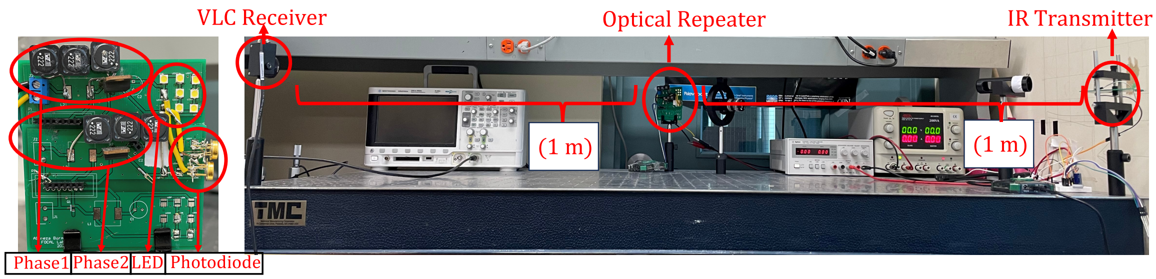

Figure 4.14: a) Repeater printed board b)Experimental setup with the transmitter (T_x) on the right, repeater in the middle, and the receiver (R_x) on the left

a deterioration of the BER. Moreover, the assumption of the optical signal's amplitude being negligible in comparison to the DC current of the LEDs becomes invalid in such scenarios. Consequently, the efficacy of the LEDs declines, along with the overall gain. Consequently, the SNR experiences a decline as well.

4.5 Experimental Setup

Fig. 4.14 illustrates the experimental configuration employed for validating the analyses detailed in the simulation section. It is important to mention that the components utilized for the experiments are identical to those modeled for simulation. Additionally, similar to the simulations, the configurations and angles in the setup are set to create a linear arrangement. Initially, optical and electrical measurements were conducted to examine the impact of D and P_{Tx} on the amplification gain and efficiency of the repeater. To generate a 256-subcarrier OFDM signal with 64 QAM modulation, we utilized an Analog Discovery 2 from DIGILENT [178]. The electrical signal was converted to optical domain using 4 IR LEDs and transmitted toward the repeater. Each phase of the repeater was equipped with two MT03-004 photodiodes,

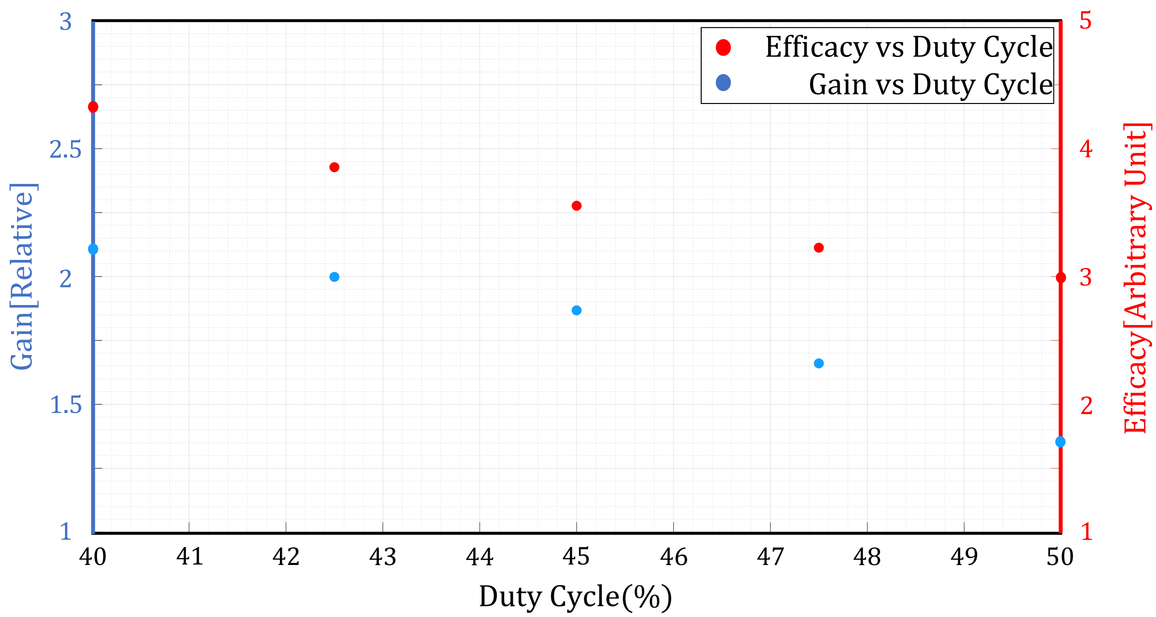

Figure 4.15: The impact of the duty cycle on the experimental amplification gain and efficacy when the average optical power (P_{Tx}) is 10 mW. The 2-phase boost converter is switching at $F_{sw} = 5$ kHz with $D \in [40\%, 50\%]$. The specifications of the simulation are detailed in Table. 4.2.

responsible for receiving the IR signal and converting it to an electrical signal. The electrical signal passing through the repeater was then converted to a visible optical signal by seven 3535L Lumiled LEDs [179] positioned at the repeater output. On the receiving end, a PDA36A(-EC) optical receiver from Thorlabs collected the emitted visible, which was then captured by an oscilloscope [213] connected to the receiver. Subsequently, the captured signal underwent decoding in Matlab [216]. Additionally, an integrating sphere, positioned to capture all emitted light from the LEDs, was used to measure efficacy. Notably, the uplink and downlink channel distances in all the experiments were set to 1 m, as the experiments were conducted in a constrained lab environment. Additionally, the optical measurements conducted were relative values, as the optical receiver was uncalibrated.

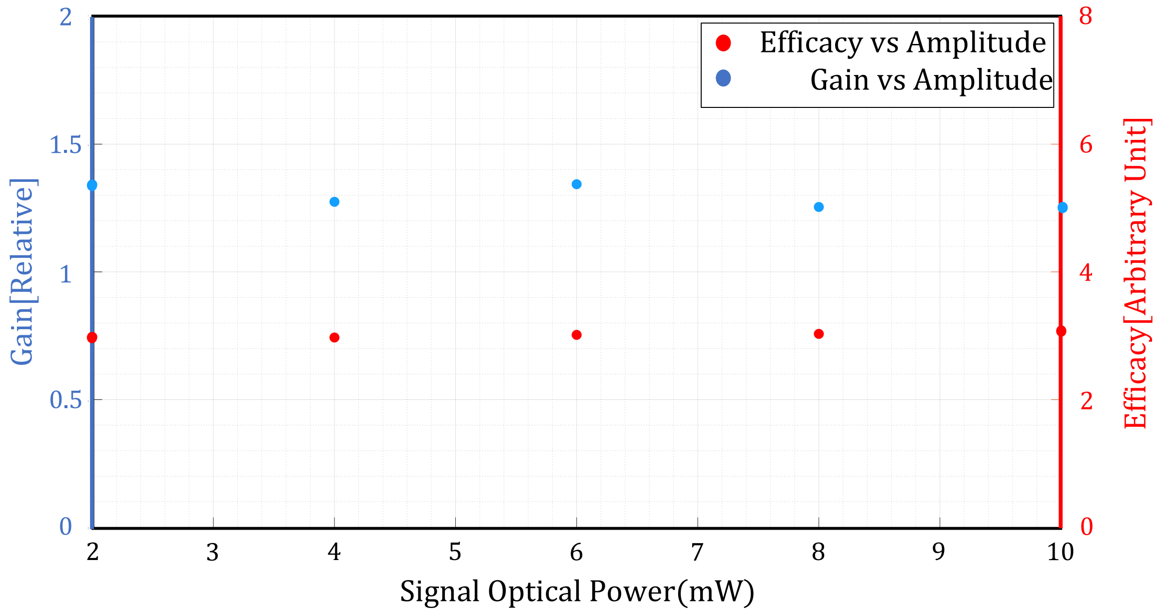

Figure 4.16: Experimentally measured end-to-end gain (G_{e2e}) and efficacy vs the optical power of the signal(P_{Tx}) when $D = 50\%$ and the P_{Tx} changes from 2 mW to 10 mW. The 2-phase boost converter is switching at $F_{sw} = 5$ kHz with $D \in [40\%, 50\%]$. The specifications of the simulation are detailed in Table. 4.2.

4.5.1 Gain and Efficacy Results

Duty Cycle

Initially, the impact of the duty cycle on both amplification gain and efficacy was studied. To assess amplification gain, the optical receiver detected the incoming optical signal at the receiver terminal, which was then decoded in Matlab. Subsequently, the DC component was eliminated and the amplitude of the received optical signal at R_x was compared with the signal transmitted from the IR LEDs at T_x to gauge the gain. Given the lack of calibration, it was unsuitable for measuring the emitted IR signal to verify its desired amplitude. Nonetheless, using the available datasheet of the IR LEDs and its associated current-optical power relationship, adjustments to

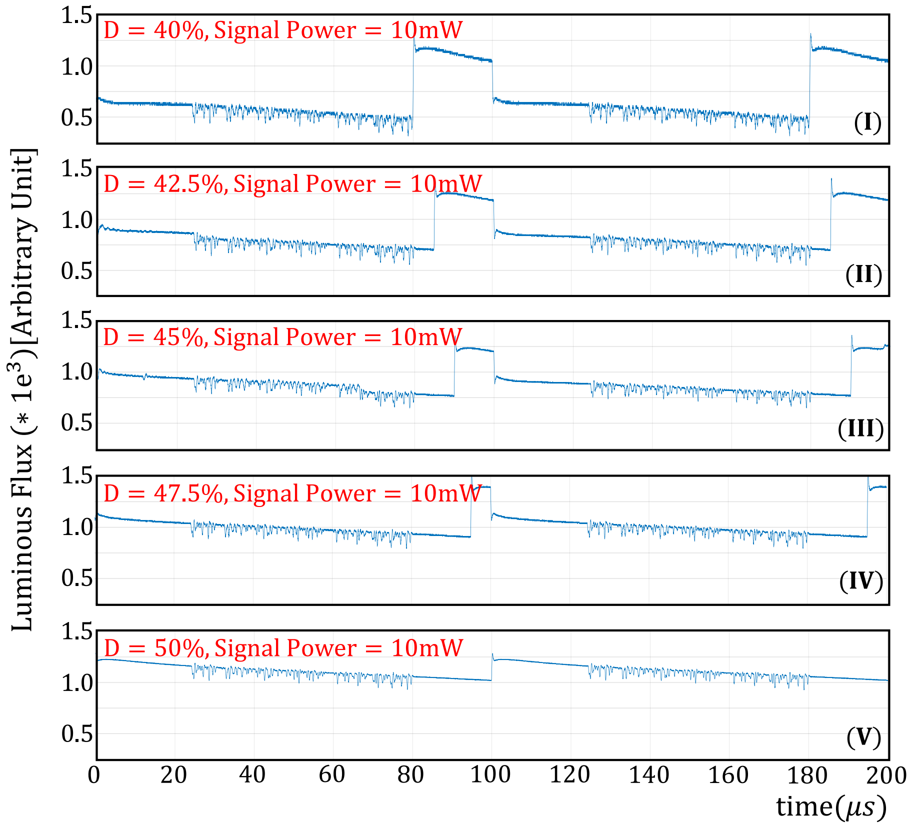

(a)

Figure 4.17: Experimental measurements of the received signal in switching cycle when the mean value of the signal is fixed and duty cycle varies

the electrical signal were made to achieve the desired optical power level. The value of the signal mean was set to $\mu_{ACO} = 10$ mW and the duty cycle was changed from 40 to 50% in 2.5% increments. It can be observed from Fig. 4.15 that the gain reduces as the duty cycle increases and at a duty cycle of 50%, the gain decreases by approximately 35% compared to that at 40%. Simulation outcomes in Fig.4.11 corroborate this trend, exhibiting a decline in gain from 9.75 to 6.75, marking a 31% reduction over the same range. To evaluate the efficacy, precise alignment ensured all emitted light entered the integrating sphere for total lumen flux measurement while recording

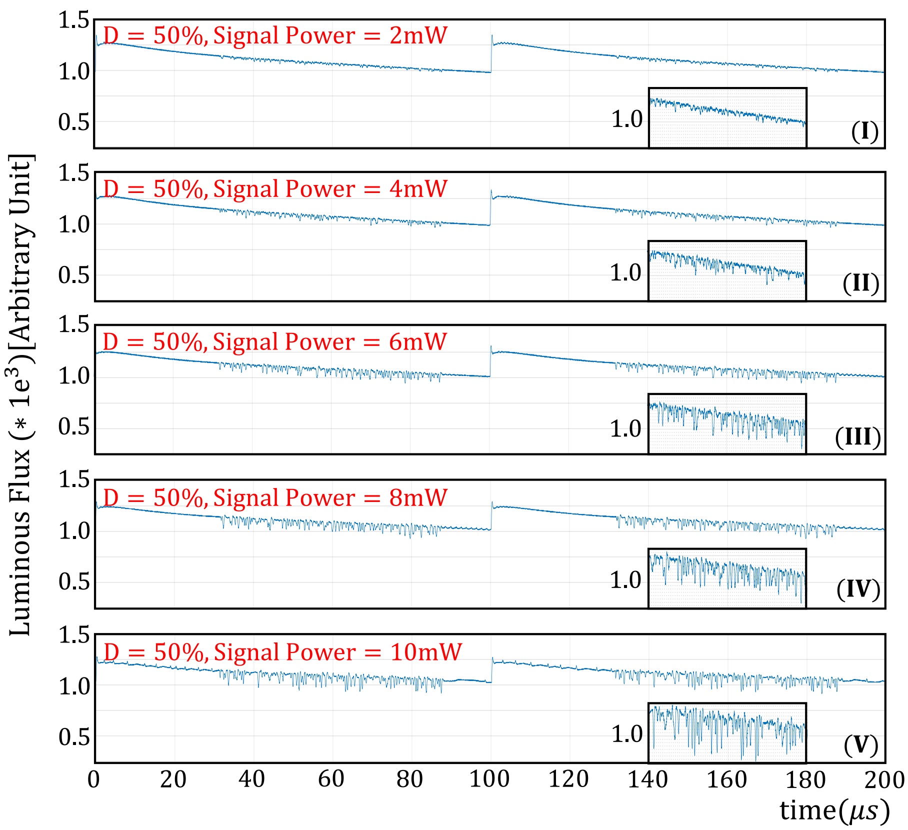

(b)

Figure 4.18: Experimental measurements of the received signal in switching cycle when the duty cycle is fixed and the mean value of the signal varies

the electrical power supplied to the repeater from the supply source for all instances. Fig. 4.11 depicts a 32% decrease in efficacy at a duty cycle of 50% compared to 40%, which simulation results in Fig.4.11 also confirm. This is a drop in efficacy from 125 to 88 lm/W over the same duty cycle range, representing an approximate 30% reduction. The underlying reasons behind the observed loss in gain and efficacy are elucidated comprehensively in Section 4.4.2. Figure. 4.17 which is captured in one switching cycle, clearly demonstrates how increasing the duty cycle slightly from 40% to 50% decreases the power of the signal at R_x while it increases the length of the

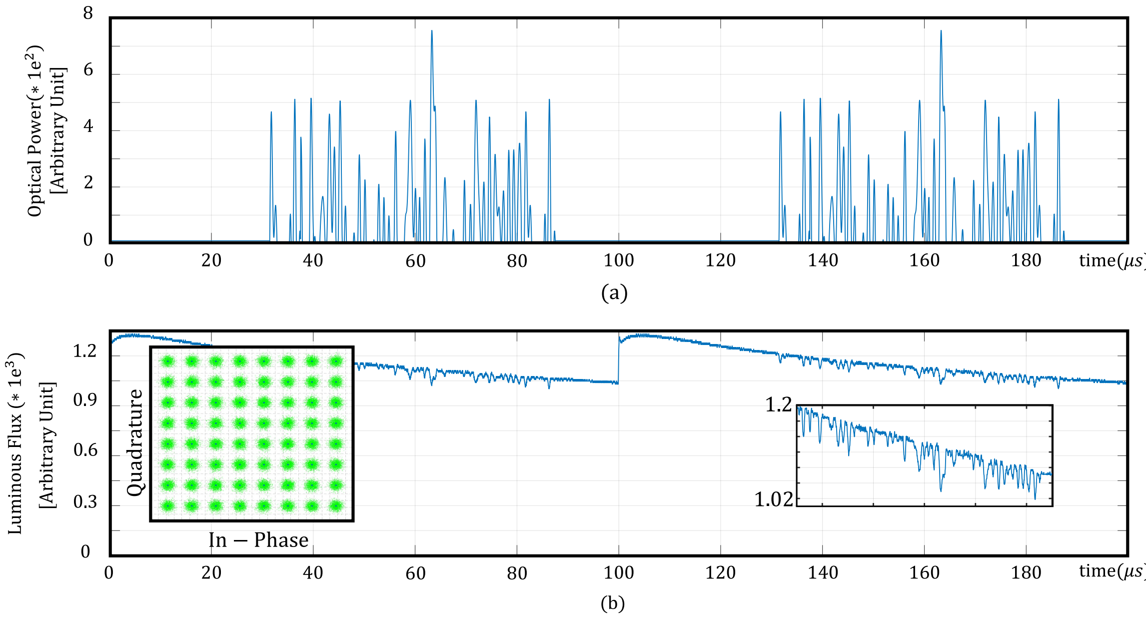

Figure 4.19: 64 QAM ACO OFDM signal with 128 subcarriers and $\Delta f_{sub} = 20kHz$. The 2-phase boost converter is supplied with a 12 V DC source and is switching with $D = 50\%$ at a rate of $5kHz$. The luminaire contains 7 LEDs at the output and there is 1 PDs in each phase of the converter. a) Measured Transmitted Signal at T_x b) Measured Received signal at the receiver R_x.

detection window.

Transmit Signal Optical Power

In a separate experiment, the duty cycle was fixed at 50%, while the value of the signal mean, μ_{ACO}, was varied from 2 to 10 mW in increments of 2 mW to explore its impact on efficacy and amplification gain. The findings, as illustrated in Fig.4.16, indicate a consistent pattern: both efficacy and gain remain relatively stable across adjustments in the value of signal mean, aligning with the simulation outcomes demonstrated in Fig.4.12. Figure. 4.18 illustrates the impact of the signal power on the received signal within a single switching cycle.

4.5.2 Communication Results

In order to acquire communication outcomes, BER measurements were conducted for one instance. The value of the optical power of the signal (P_{Tx}) and the duty cycle was set to $\mu_{ACO} = 10$ mW and $D = 50\%$ respectively. The transmitted and received optical signals were captured by the optical detector and imported to Matlab for BER analysis. The experiments successfully demonstrate a data rate of 15.36 Mbps and a total of 2000 symbols were transmitted through the channel, yielding over 3 million bits, and the BER was found to be $BER = 2.75 \times 10^{-5}$. This result demonstrates a close correlation with the simulation results in Fig. 4.13 where the BER at $P_{Tx} = 10$ mW is approximately 2×10^{-5}. An illustration of the transmitted and received frame is presented in Fig. 4.19 where a 128 subcarriers 64 QAM ACO OFDM signal was transmitted in the channel. As labeled on the figure, in the first half of the switching cycle phase 1 is detecting the received IR signal, and the second half reception is conducted by phase 2 of the repeater. Note that the received optical modulated signal displays an inverted polarity in contrast to the modulated signal. This inversion arises from the opposite direction of the photo-generated current, i_{sig}, of the photodiode in relation to the DC current direction in the photodiode, i_{PD}, as depicted in Fig. 4.4.

4.6 Conclusion

This study demonstrated the feasibility of integrating a VLC repeater into a luminaire for uplink channels in VLC systems. By using a multiphase boost converter and replacing Schottky diodes with photodiodes, a receiver and transmitter were incorporated into the luminaire to relay signals via various emitters like visible light or infrared, with minimal modification to an LED driver for seamless integration.

This topology not only extended the capabilities of VLC but also presented a potential solution for direct communication in constrained environments, effectively tackling issues such as field of view constraints. Additionally, it introduced possibilities for indoor system applications, such as positioning.

Additionally, given that the entire system was housed within a luminaire, it was well-suited to serve both as fronthauling and backhauling solutions using IR LEDs within the luminaire, without requiring modifications to the building's wiring infrastructure.

This method allowed for the reception, amplification, and transmission of infrared signals, regardless of modulation, with an optical gain of up to 7 in the examined prototype. As shown throughout the sections, the repeater demonstrated consistent stability in characteristics like gain and efficiency across different signal amplitudes, as long as the photodiodes were not overdriven.

Future investigations will explore different combinations of emitters at the output, such as incorporating visible and infrared LEDs. Additionally, avalanche photodiodes (APD) can be considered to increase the gain. However, APDs require substantial reverse bias to deliver high gain and in turn can generate significant shot noise [243]. While briefly mentioned, another avenue for research involves optimizing the number of LEDs, photodiodes, and phases of the multiphase boost converter. Such optimization efforts hold the potential to yield enhanced design guidelines for future implementations.

Moreover, similar to Chapter 3 and unlike Chapter 2, the bandwidth is limited by the optoelectronic elements, including the LEDs and photodiodes, rather than by the switching device in the topology. Dissimilar to Chapters 2 and 3 where only the LECD was modulated, in this topology the illumination string is modulated. This can result in a lower life span of illumination LEDs, possible color shift, and possibility of flicker. As discussed in the chapter, these issues can be dealt with through the careful consideration of the number of phases and selection of the duty cycle.

Chapter 5

Conclusions

5.1 Conclusions

Despite the numerous advantages of visible light communication (VLC), the integration of VLC into lighting fixtures remains a challenging research area. This is largely due to difficulties in maintaining both the efficacy and quality of illumination, as well as implementing an exclusively optical communication system. Specific challenges include issues related to backhauling, fronthauling, and the uplink channel. This thesis presented a novel concept called LECD, along with the combined use of switching MOSFETs as amplifiers, to tackle the challenges of illumination and communication in VLC transmitter integration into luminaires. Furthermore, it proposed an optical repeater architecture to integrate into SMPS to address the issues related to uplink and the connectivity between access points and the backbone network.

By substituting Schottky diodes in the LED driver with LEDs, a light-emitting commutating diode (LECD) was introduced to integrate a VLC transmitter into LED drivers. **Chapter 2** presented an approach that separates the illumination and communication LED strings, thereby enhancing illumination quality by preventing color shifts and extending the lifespan of the LEDs. Additionally, the power dissipated in the diodes was utilized by the LECDs, improving the overall efficacy of the luminaire up to 15%. This topology also preserved the simplicity characteristic of LED luminaires, further facilitating the integration of VLC into lighting systems. Communication was carried out using straightforward modulation methods such as PPM or OPPM.

Chapter 3 explored the use of the MOSFET's off state in an LED driver to amplify the transmission signal, thereby eliminating the need for a linear amplifier and a Bias-T. As a result the efficacy of the luminaire was enhanced, up to 6.25%, and the component count was reduced by 30%, as compared to the traditional bias-T method by removing the inductor and capacitor for Bias-T and the linear amplifier. This approach supported advanced modulation schemes such as OFDM while maintaining high illumination quality and cost-effectiveness, aligning with the latest standards in optical wireless communications. Additionally, the control scheme was simpler than other existing methods in the literature. This chapter also provided a comprehensive design guideline, followed by experimental results that serve as proof of concept.

While the earlier chapters addressed the challenges of the downlink channel, **chapter 4** focused on providing solutions for the uplink channel of a VLC system. By replacing the Schottky diodes in a multiphase boost converter with photodiodes, an optical repeater was integrated into luminaires. This repeater receives relatively weak IR signals from handheld devices, amplifies them, and broadcasts them within the environment. The amplification level achieved was 7, while it can be adjusted by modifying the ratio of LEDs to photodiodes. This topology also offered a fully optical solution for fronthauling and backhauling in VLC systems by incorporating a string of IR LEDs in series with the illumination string, enabling the transmission of received signals at different wavelengths. The chapter included a comprehensive design guideline and presented an experimental setup that has been built and tested as proof of concept. To the knowledge of the author, this was the first such integrated optical repeater design and demonstration for indoor OWC.

The data rate in the method outlined in Chapter 2 was constrained by the MOSFET's switching frequency (400 kHz), which is in the range of a few hundred kHz. However, in Chapters 3 and 4, the bandwidth is restricted by optoelectronic components such as the LECD, LEDs, and photodiodes. Consequently, the switching frequency in these chapters is reduced to minimize the MOSFET switching losses. In Chapter 3, the switching frequency was set at 10 kHz to be compatible with the laboratory equipment and to accommodate the transmission of the symbol length specified by the standards. In Chapter 4, the switching frequency was decreased by half because the configuration is a 2-phase boost converter, where the effective switching frequency is double that of each MOSFET's switching frequency.

The method introduced in Chapter 2 replaces Schottky diodes with LEDs (LECDs), which raises concerns about reverse biasing LEDs. Although Chapter 2 demonstrated the viability of this approach by testing 40 commercial visible LEDs, the feasibility of utilizing higher reverse bias voltages or the impact of reverse biasing on the lifespan and longevity of LEDs remains uncertain. Furthermore, in Chapter 3, a switching MOSFET was employed as both a switching device and an amplifying device. While this dual functionality proved to be possible, the conduction losses in the saturation region and the resultant heat generated from these losses pose concerns regarding long-term effects. Similarly, continuing the trend of substituting optoelectronic devices for Schottky diodes, Chapter 4 replaced the Schottky diode with a photodiode. The forward current through the photodiode is a concern since photodiodes are not designed to be forward biased. Although the photodiodes used were tested for forward currents up to 500 mA, their performance under higher forward currents is not guaranteed. In general, each chapter introduces a new application for an element that was not intended by its original design during manufacturing, leading to concerns as outlined above.

This thesis began by describing the present obstacles in the deployment of VLC, concentrating specifically on the downlink and uplink channels within indoor scenarios with short link distances [41]. Consequently, all experiments maintained link distances within 1 m, simplifying experimentation in a laboratory setting. The proposed designs were all developed with the primary function of the luminaire—providing illumination—at the forefront. Consequently, the main focus of the designs introduced in the chapters of this thesis was to preserve illumination efficacy while harnessing existing losses in an LED driver toward performing optical communication. This approach ensured that the integration of VLC technology did not compromise the primary lighting function of the luminaires. Needless to say, in all the scenarios and topologies, the communication link will be disrupted in the absence of illumination. However, the approaches presented in this thesis can be generalized using IR components (e.g., the visible LECD in Chapter 2 could be replaced with and infrared LED). An interesting approach to investigate is the use of "lights off VLC" [237] where optical communications are possible from a visible source which has the brightness of the luminare set to imperceptible levels.

5.2 Future Work

This thesis addresses the integration of VLC equipment into LED drivers to simplify implementation and maintain the efficacy of the luminaires. Based on the findings and the overarching vision of this work, several future research directions and extensions are suggested.

5.2.1 Utilizing High Frequency Switching Devices

The topology presented in Chapter 2 employs the relatively slow PPM/OPPM modulation scheme, resulting in a lower data rate. Increasing the switching frequency of the converter can enhance the data rate; however, the switching frequency of MOSFETs is typically capped at less than 1 MHz [108, 238]. Exceeding this limit increases switching losses, thereby reducing efficacy. By incorporating high-frequency GaN [239] switches into the topology, the switching frequency can be further increased up to the bandwidth limit of the LEDs, thereby improving the data rate.

5.2.2 Optimizing the Ratio of LEDs to LECDs

The topology discussed in Chapters 2 and 3 separates the illumination and communication LED strings. Increasing the number of LECDs enhances the signal-to-noise ratio (SNR), thereby improving the bit error rate (BER). However, this increase also limits the dimming range of the device, as the forward voltage drops of the LECDs accumulate. Additionally, the signal amplitude is constrained by the current passing through the LEDs. These constraints necessitate the optimization of the ratio between LEDs and LECDs to meet the specific requirements of each application. To perform this optimization, an objective function can be defined that takes into account factors such as the bit error rate (BER), dimming range, and signal amplitude. This function can then be minimized using optimization methods to achieve the optimal ratio of LEDs to LECDs based on the specific requirements of the application.

5.2.3 Implementing Hybrid Modulation Schemes

The method described in Chapter 3 supports advanced modulation schemes, including OFDM. By integrating the power efficient PPM/OPPM modulation schemes with spectrally efficient OFDM, a hybrid modulation scheme can be achieved [241, 242], significantly enhancing the data rate and spectral efficiency of the transmitter. While information is encoded and transmitted during each conduction interval of the LECDs, the hybrid modulation allows for additional information to be encoded based on the position of the conduction interval within each switching cycle of the converter.

5.2.4 Integration of VLC Transceiver into LED Driver

The topology described in Chapter 4 integrates reception capability within an LED driver. With the removal of the capacitor, the output LEDs are modulated to transmit the amplified received signal. Utilizing the MOSFET modulation technique introduced in Chapter 3, this topology can be used to inject and amplify signals for transmission in the off-state of the MOSFET, while it receives IR signals, amplifies, and transmits them during the MOSFET's on-state. This results in a transceiver that receives signals during the MOSFET's on-state and transmits signals during its off-state.

5.2.5 Exploring Other DC/DC Converters

This thesis focuses on integrating communication capabilities into buck and boost converters, as they are the most widely used converters in illumination applications. However, the core concept of this work—replacing the diode in a topology with optoelectronic components to facilitate signal transmission and reception—opens the door for further research into alternative topologies. Topologies like full-bridge [240] and other multi-diode configurations, which inherently include multiple diodes, could be explored. Such configurations have the potential to achieve higher SNRs or extended transmission windows, thereby enhancing communication performance.

5.2.6 Optoelectronic Devices for Commutation and Amplification

Section 5.1 highlighted that the optoelectronic devices were utilized in contexts beyond their original design intentions. In particular, LEDs were reverse biased and photodiodes were forward- biased when used as communicating devices. Future work includes a systematic investigation of the impact of this anomalous operating modes on the lifetime and performance of the optoelectronic devices. If required, another interesting avenue to pursue is the design of tailor-made optoelectronic components with this dual functionality in mind.

Appendix A

Theoretical Calculations Regarding the Noise Figure

This section provides additional details on deriving the noise figure discussed in Chapter 4 of the thesis. The noise figure for an N-phase boost converter will be calculated, with simplifications provided for the special case of a 2-phase converter. It is assumed that the duty cycle is maintained such that at any given time, only one phase is in detection mode while the others are in conduction. In other words, at any arbitrary moment, only one phase's MOSFET will be turned on and conducting.

Figure. A.1.a illustrates the repeater integrated into a n-phase boost converter and Fig. A.1.b demonstrates the noise equivalent model of the converter where phase 1 is in detection mode (MOSFET on and photodiode reverse-biased) and other phases are in conduction mode (MOSFET off and photodiode forward-biased). In this circuit, the DC voltage source and output LEDs are modeled with small signal resistance R_s and R_o respectively. The photodiodes, either reverse or forward-biased, mainly exhibit shot noise while the dominant noise in a MOSFET in triode is thermal noise. The spectral density of the noise in the forward-biased photodiodes is modeled with $V_{n1}^2(f)$ connected in series with R_p and the noise source in the reverse-biased photodiode is modeled with $I_n^2(f)$. Since I_n depends on the power of the received optical signal, P_{Ri} is considered an input noise rather than a noise the repeater adds. Finally, the noise in the MOSFET in the triode region is modeled with $V_{n2}^2(f)$ connected in series with R_m which represents the channel resistance.

$$\begin{aligned} V_{n1}^2(f) =& 2KTR_{pd} \quad V/Hz \\ V_{n2}^2(f) =& 4KTR_m \quad V/Hz \\ I_n^2(f) =& 2qP_{in}\alpha\eta \quad A/Hz \end{aligned} \tag{A.1}$$

The noise figure is defined as:

$$\frac{SNR_i}{SNR_o} = \frac{\frac{P_{Ri}}{N_i}}{\frac{P_{Ro}}{N_o}} = \frac{P_{Ri}G(N_i + N_A)}{N_i P_{Ri} G} = 1 + \frac{N_A}{N_i} \tag{A.2}$$

In this expression, N_A is the noise added by the repeater, V_{n1} and V_{n2}, while N_i is the input noise that is added by I_n. By finding the output referred noises, the noise figure can be calculated according to :

$$\begin{aligned} N_A =& \int_0^{BW} V_{out-Vn1}^2(f)df + \int_0^{BW} V_{out-Vn2}^2(f)df \\ N_i =& \int_0^{BW} V_{out-In}^2(f)df \end{aligned} \tag{A.3}$$

where $V_{out-Vn1}$, $V_{out-Vn2}$, and V_{out-In} are output referred noises of V_{n1}, V_{n2}, and I_n respectively.

(a)

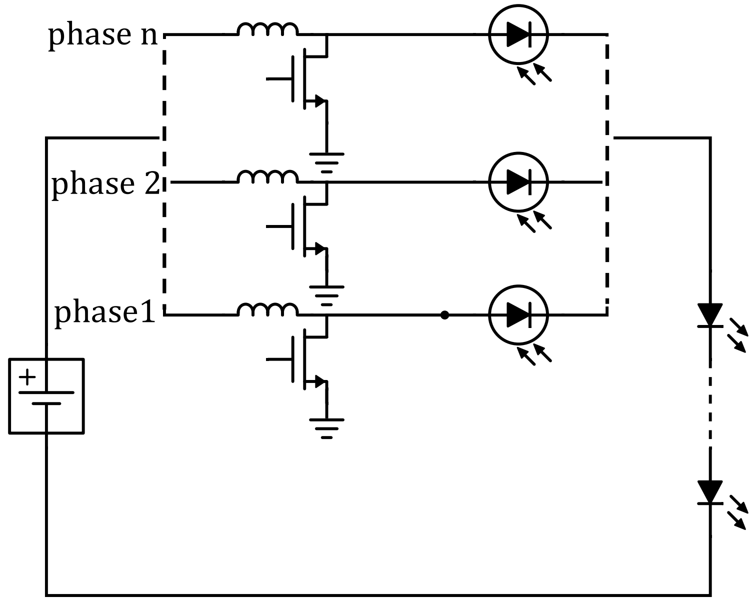

(b)

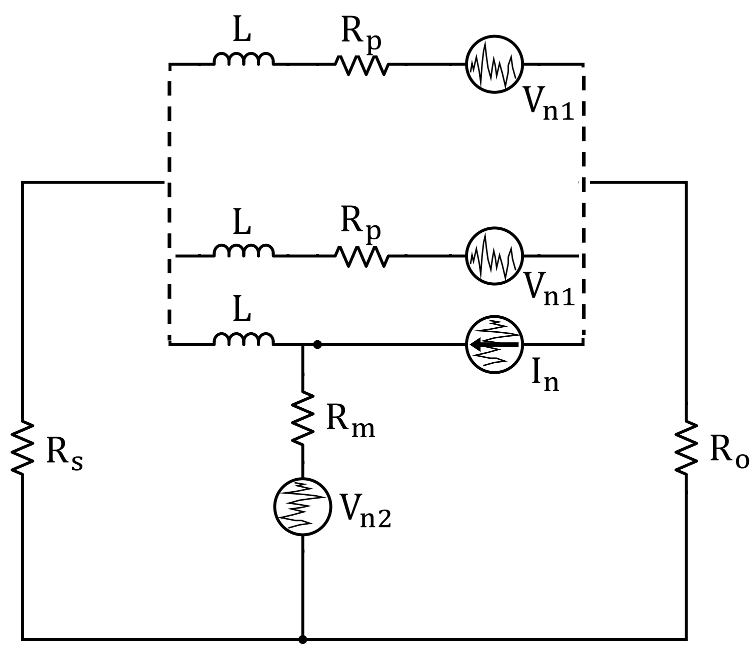

Figure A.1: a) Repeater integrated boost converter. b) equivalent noise model.

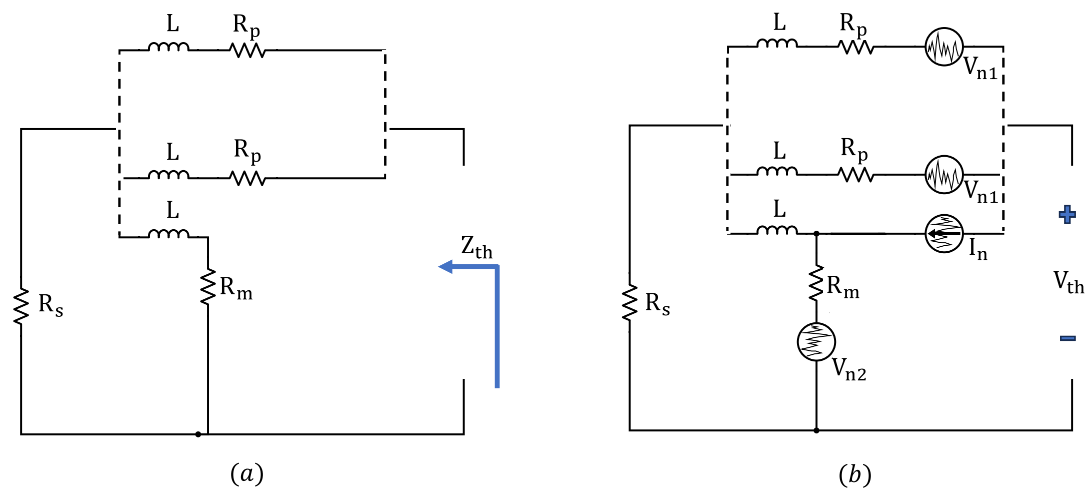

Figure A.2: a) Repeater integrated boost converter. b) equivalent noise model.

A.1 Thevenin Equivalent Circuit

Thevenin equivalent voltage and impedance of the circuit, seen from the output, can be found in order to find the output referred voltages. In this regard, the Thevenin impedance (Z_{th}) is calculated and Thevenin voltage (V_{th}) for each source will be found. Finally, superposition is used to add all the sources and find the final Thevenin equivalent.

$$V_{out} = \frac{R_o}{R_o + Z_{th}} \times V_{th} \tag{A.4}$$

In order to find the Thevenin impedance of the circuit, all the voltage/current sources are replaced by short/open circuits, see Fig. A.2, and the impedance, seen from the output, is calculated:

$$Z_{th} = [R_s||(Ls+R_m)]+[(Ls+R_p)||(Ls+R_p)||...] = [R_s||(Ls+R_m)]+\frac{Ls+R_p}{n-1} \tag{A.5}$$

To find the Thevenin voltage for each noise source, the other sources will be disregarded (open-circuit or short-circuit) and V_{th} is found according to Fig. A.2.b.

- V_{th} according to V_{n1}:

$$V_{th-Vn1} = V_{n1} \times \frac{\frac{Ls+R_p}{n-1}}{\frac{Ls+R_p}{n-1} + (Ls + R_p)} \tag{A.6}$$

- V_{th} according to V_{n2}:

$$V_{th-Vn2} = V_{n2} \times \frac{R_s}{Ls + R_m + R_s} \tag{A.7}$$

- V_{th} according to I_n:

$$V_{th-In} = I_n \times \left[\left(\frac{Ls + R_p}{n - 1}\right) + \frac{Ls}{Ls + R_s + R_m} R_s \right] \tag{A.8}$$

These expressions are for the general form and according to the number of phases and values of the components one can find the noise figure of the repeater.

A.2 2-Phase Boost Converter

In this section values from the 2-phase boost designed in Chapter 4 will be used in the expressions to find the noise figure:

$$\begin{aligned}
Z_{th} &= \frac{L^2s^2 + Ls(2R_s + R_m + R_p) + (R_sR_m + R_pR_m)}{Ls + (R_s + R_m)} \\
V_{out-Vn1} &= V_{n1} \times \frac{1}{2} \times \frac{R_o}{R_o + Z_{th}} \\
V_{out-Vn2} &= V_{n2} \times \frac{R_s}{Ls + R_m + R_s} \times \frac{R_o}{R_o + Z_{th}} \\
V_{out-In} &= I_n \times \big[(\frac{Ls + R_p}{n-1}) + \frac{Ls}{Ls + R_s + R_m}R_s\big]..... \\
&.... \times \frac{R_o}{R_o + Z_{th}}
\end{aligned} \tag{A.9}$$

The noise sources in the circuit are as follows:

- V_{n1}:

  The shot noise model for the photodiode in forward bias carrying the load current of 400 mA.

$$\begin{aligned}
R_{pd} &= \frac{KT}{qI_D} = \frac{1.38 \times 10^{-23} \times 300}{1.6 \times 10^{-19} \times 0.4} = 646.875 \times 10^{-4}\Omega \\
V_{n1}^2(f) &= 2KTR_p = 2 \times 1.38 \times 10^{-23} \times 300 \times 0.065 \\
V_{n1}^2(f) &= (23 \text{ pV}/\sqrt{\text{Hz}})^2 \qquad R_p = 0.065\Omega
\end{aligned} \tag{A.10}$$

- V_{n2}:

  The Thermal noise model for the MOSFET in triode region with a channel resistance of $R_m = 700$ mΩ.

$$
\begin{aligned}
&R_m = 700\ \text{m}\Omega \\
&V_{n2}^2(f) = 4KTR_m = 4 \times 1.38 \times 10^{-23} \times 300 \times 0.7 \qquad \text{(A.11)} \\
&V_{n2}^2(f) = (108\ \text{pV}/\sqrt{\text{Hz}})^2 \qquad R_m = 0.7\Omega
\end{aligned}
$$

- I_n:

  The shot noise model for the photodetector while reverse biased and detecting an IR signal with an average optical power of $P_{Ri} = 10$ mW with a responsivity of $R_1(950\ \text{nm}) = 0.6$ A/W.

$$
\begin{aligned}
&I_n^2(f) = 2qP_{Ri}R_1(\lambda) = 2 \times 1.6 \times 10^{-19} \times 10^{-2} \times 0.6 \\
&I_{n1}^2(f) = (44\ \text{pA}/\sqrt{\text{Hz}})^2
\end{aligned} \qquad \text{(A.12)}
$$

Additionally, 7 LEDs at the output will be modeled with their small signal resistance equivalent:

$$
R_{out} = 7 \times \frac{KT}{qI_D} = 7 \times 0.065 = 0.455\ \Omega \qquad \text{(A.13)}
$$

The small signal resistance of the DC voltage source, R_s, is considered 0.02 Ω as it is typical in a good voltage supply. Finally, the inductors in the experiment have identical values of $L = 10$ mH.

In order to find the total noise power attributed to each noise source, the following integrals, over the bandwidth of the repeater, have been calculated in MATLAB. In other words, the area under the magnitude of the transfer function over the bandwidth has been calculated:

$$\begin{aligned}
&|V_{out-n1}(f)| = \frac{23 \text{ pV}/\sqrt{\text{Hz}} \times 0.455}{|0.52 + (0.02||(0.01s + 0.7)) + 0.01s|} \\
&= 10.465 \text{ pV}/\sqrt{\text{Hz}} \times |\frac{1}{0.01s + 0.52 + \frac{2\times10^{-4}s+0.014}{0.01s+0.72}}| \\
&\longrightarrow \int_0^{BW} V_{out-n1}^2(f)df = (179 \text{ pV})^2 \\
&|V_{out-n2}(f)| = 108 \text{ pV}/\sqrt{\text{Hz}} \times |\frac{0.455 \times 0.02}{10^{-4}s^2 + \frac{1.26}{100}s + 0.3416}| \\
&= 1 \text{ pV}/\sqrt{\text{Hz}} \times |\frac{1}{10^{-4}s^2 + 0.0126s + 0.3416}| \\
&\longrightarrow \int_0^{BW} V_{out-n2}^2(f)df = (19.1 \text{ pV})^2 \\
&|V_{out-In}(f)| = 44 \text{ pV}/\sqrt{\text{Hz}} \times |\frac{0.455}{0.01s + 0.52 + \frac{2\times10^{-4}s+0.014}{0.01s+0.72}}| \\
&\times |[\frac{0.01s + 0.065}{1} + \frac{0.0002s}{0.01s + 0.02 + 0.7}]| \\
&\longrightarrow \int_0^{BW} V_{out-In}^2(f)df = (159 \text{ nV})^2
\end{aligned} \tag{A.14}$$

According to Eq. SA.2:

$$\begin{aligned}
&NF = 1 + \frac{N_A}{N_i} = 1 + \frac{(179 \text{ pV})^2 + (19.1 \text{ pV})^2}{(159 \text{ nV})^2} \\
&NF \approx 1 + 0 = 1 \\
&10\log(1) = 0 \text{ dB}
\end{aligned} \tag{A.15}$$

which indicates that the signal is a shot-noise limited signal, where the noise added to the signal from the repeater is negligible compared to the shot noise in the signal. This conclusion could have been made earlier according to Fig. A.2.b where it is observed that except for the noise source I_n which is directly connected to output, the noise from V_{n1} and V_{n2} are both filtered by the inductors in their paths.

Appendix B

Design Consideration for Chapter 3 for OFDM LECD Transmitter

This chapter provides additional details on the boost converter design of Chapter 3. The following steps were taken, following common power converter design practics as outlined in [181], to design the converter and select the components of the circuit illustrated in Fig. B.1.

B.1 OFDM Enabled Boost Converter

Step 1: Necessary Information

Input Voltage

The input voltage is considered to be 12 V, consistent with the typical DC output voltage of commercially available photovoltaic (PV) panels. In selecting the components and nominal values of the circuit elements, derating is taken into account to

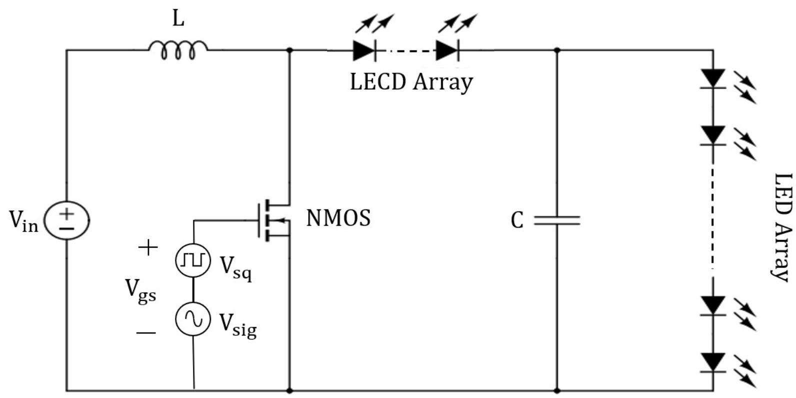

Figure B.1: OFDM VLC enabled topology (reproduced from Fig. 3.2).

prevent failure and increase longevity and reliability.

Output Current and Voltage

- **Maximum Output Current**: The maximum output current is set to the nominal current of commercially available high-brightness LEDs, which is 400 mA.

- **Output Voltage Range**: The output voltage range is determined based on the nominal brightness level and the desired dimming capability. The design aims for a brightness of 1200 lumens with 50% dimming capability.

Illumination Considerations

For design purposes, it is assumed that the desired illumination level is entirely achieved by the illumination strings, not the LECD. Note, however that the presence of the LECD contributes to the overall illumination. Consequently, the entire circuit will operate under lower current levels, which reduces the stress on the components.

LED Selection

One of the typical commercial LEDs is Lumiled 3535L and given that each LED can produce up to 200 lumens at 400 mA, six LEDs are theoretically sufficient to achieve 1200 lumens. However, following the derating to avoid operating LEDs close to their nominal values, seven LEDs are selected. This choice ensures reliability and extends the lifespan of the illumination LEDs.

Voltage and Duty Cycle Calculations

- **Maximum Output Voltage**: Based on the $I-V$ and $\phi-I$ characteristics of the LEDs, the maximum output voltage ($V_{\text{out, max}}$) is calculated to be 27 V.

- **Duty Cycle**: Using the relation for the output voltage of a boost converter with an LECD:

$$V_o = \frac{V_{\text{in}}}{1-D} - V_{LECD}$$

The maximum duty cycle (D) is calculated using the input and output voltage values.

$$V_{o,max} = \frac{V_{\text{in}}}{1-D_{max}} - V_{LECD} \Rightarrow 27 = \frac{12}{1-D_{max}} - 3 \rightarrow D_{max} = 1 - \frac{12}{30} = 60\%$$

The maximum duty cycle is far from the two extremes to prevent elevated conduction loss or discontinuous conduction mode (DCM) operation mode. Otherwise, the type and number of the LEDs should have been revised to ensure operation under the desired duty cycle.

Step 2: Switching Frequency

Design Considerations

Several factors influence the selection of the switching frequency:

1. **Inductor Size**: Higher switching frequencies result in smaller inductor sizes due to the relationship between current ripple, frequency, and inductor size

$$\Delta I_L = \frac{V_{\text{in}} \cdot D}{f_{\text{sw}} \cdot L}$$

   where the terms in the above are defined in Chapter 3.

2. **Switching Losses**: Higher switching frequencies increase the switching losses in the MOSFET, which decreases efficiency.

3. **Transmission Bandwidth**: For this design, the switching frequency does not limit the transmission bandwidth. However, the decreasing operating current slope of LECD is directly related to the switching frequency, favoring lower frequencies to simplify filtering and remove the slope.

4. **Transmission Window**: Lowering the frequency increases the length of the transmission window, enabling the transfer of a full OFDM symbol with sub-carrier spacing chosen from applicable standards.

5. **Laboratory Equipment**: The available equipment in the lab could reliably sink and source sufficient current to switch the MOSFET on and off efficiently at these frequencies.

Chosen Frequency

While the chosen MOSFET could support a switching frequency of up to 100 kHz, a lower frequency of 10 kHz was selected to be compatible with the laboratory equipment [178] and to accommodate the transmission symbols whose length has been selected according to communication standards [87]. The size of the inductor was instead increased to maintain the current ripple within the desired level [181]. The switching frequency is not further decreased as it causes slow responses to adjusted dimming levels.

Step 3: Inductor Selection

Calculation Process

To select the appropriate inductor, the following equation is used. When the MOSFET is on, the voltage across the inductor is V_{in}

$$L\frac{di}{dt} = V_L$$

The MOSFET is on for a duration of $D \cdot T_{\text{sw}}$, leading to

$$L \cdot \frac{\Delta I}{\Delta t} = V_L \rightarrow L \cdot \frac{\Delta I}{D \cdot T_{\text{sw}}} = V_{\text{in}}$$

In a boost converter

$$V_{\text{out}} = \frac{V_{\text{in}}}{1 - D} \quad \Rightarrow \quad D = \frac{V_{\text{out}} - V_{\text{in}}}{V_{\text{out}}}$$

Rearranging gives the inductor value

$$L = \frac{V_{\text{in}} \cdot D \cdot T_{\text{sw}}}{\Delta I_L} = \frac{V_{\text{in}} \cdot (V_{\text{out}} - V_{\text{in}})}{\Delta I \cdot f_{\text{sw}} \cdot V_{\text{out}}}$$

This shows that the inductor size depends on the allowed ripple current (ΔI).

Ripple Current Considerations

It is common practice to allow a ripple current of 20% to 40% of the output current. However, to minimize the capacitor size and avoid significant changes or flicker in the LED light, a ripple of 10% is chosen

$$\Delta I_L = 0.1 \cdot I_{\text{out, max}} \cdot \frac{V_{\text{out}}}{V_{\text{in}}}.$$

Inductor Value Calculation

The maximum output current is 400 mA, occurring at an output voltage of 27 V. Considering a 10% ripple

$$\Delta I = 0.1 \cdot 0.4 \cdot \frac{27}{12} = 90 \text{ mA}.$$

Plugging this into the equation for L

$$L = \frac{12 \cdot (27 - 12)}{0.09 \cdot 10000 \cdot 27} \approx 7.5 \text{ mH}.$$

Final Selection

The smallest commercially available inductor value meeting this requirement is a 10 mH inductor, which is selected for this design.

Step 4: MOSFET Selection

Current Calculation

To select the MOSFET, the maximum current flowing through it must be calculated. The current through the MOSFET consists of the inductor average current plus half the ripple current. Since the inductor current equals the input current, it can be calculated based on the output current.

The maximum output current is 400 mA, occurring at a maximum output voltage of 27 V. Therefore, the input current is:

$$I_{\text{in}} = 400 \cdot \frac{27}{12} = 900 \text{ mA}.$$

The maximum current through the MOSFET is

$$I_{\text{sw, max}} = 400 \cdot \frac{27}{12} + \frac{1}{2} \cdot 90 = 945 \text{ mA}$$

This value represents the maximum current the MOSFET must handle.

Selection Criteria

Based on the calculated $I_{\text{sw, max}}$ and the switching frequency f_{sw}, a suitable MOSFET is selected to ensure reliable performance.

Step 5: MOSFET Driver

Compared to a buck converter, the boost converter has a simpler MOSFET driving process because its MOSFET is positioned on the low side of the circuit (between the inductor and ground). This configuration allows the gate drive to reference the same ground as the circuit, eliminating the need for a complex high-side driver which are often required in buck converters to drive the high-side MOSFET. This simplicity makes the boost converter more compatible with direct control using basic waveform generation tools [244]. Given the relatively low switching frequency of 10 kHz and the straightforward driving process of the MOSFET in a boost converter, the waveform generator of the Analogue Discovery 2 device was used to control the MOSFET switching.

Appendix C

Design Considerations for Chapter 4 Optical Repeater Multiphase Boost Converter

Figure. C.1 illustrates the two-phase boost converter employed in Chapter 4. While the design process remains identical to that of the single-phase boost converter, several key differences and considerations are highlighted below.

Effective Switching Frequency

The effective switching frequency of a two-phase boost converter is *twice* the switching frequency of each phase, i.e.,

$$f_{sw,\text{eff}} = 2 \cdot f_{sw,\text{phase}}.$$

For this design, the switching frequency of each phase is set to $f_{sw,\text{phase}} = 5\,\text{kHz}$,

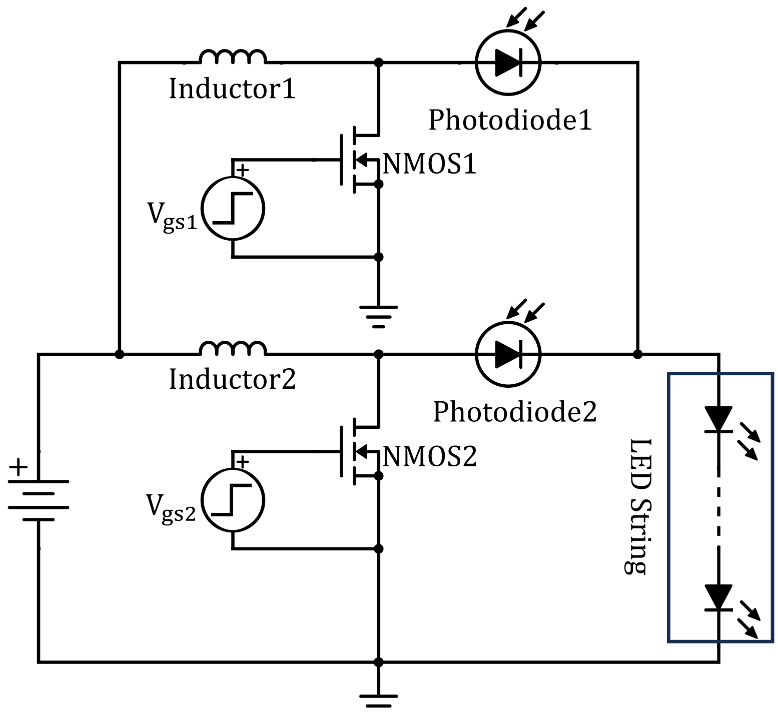

Figure C.1: Optical repeater integrated into a 2-phase boost converter presented in Chapter 4.

resulting in an effective switching frequency of:

$$f_{sw,\text{eff}} = 2 \cdot 5\,\text{kHz} = 10\,\text{kHz}$$

This choice ensures the same effective frequency as the single-phase design.

Duty Cycle

Due to system restrictions discussed extensively in Chapter 5, the duty cycle is limited to a maximum of **50%**. This restriction impacts the output voltage and brightness as follows.

- **Maximum Output Voltage**: The duty cycle constraint reduces the achievable output voltage.
- **Nominal Brightness**: The maximum brightness is reduced to 1000 lm, a reduction compared to the single-phase converter.

Component Selection

The components selected for the single-phase boost converter were overdesigned by **20%** to account for tolerances and safety margins. Given that the duty cycle constraint reduces the nominal brightness and therefore the current requirements by approximately **16.6%**, the same components can be reused without modification. Specifically:

- **Inductor**: The previously chosen inductor remains valid due to the reduced current ripple and overall load.
- **MOSFET**: The selected MOSFET can handle the reduced maximum current while maintaining efficient switching.

MOSFET Driver

Similar to the single-phase boost converter, the MOSFETs in both phases of the two-phase boost converter are also positioned on the low side [244] and operate at an even lower switching frequency of 5 kHz. Consequently, the Analogue Discovery 2 is capable of driving the MOSFET switching.

Conclusion

By leveraging the design margins of the single-phase boost converter, the same components are reused for the two-phase boost converter. This approach simplifies the design process while ensuring reliable operation under the specified conditions.

Bibliography

[1] L. E. M. Matheus, A. B. Vieira, L. F. M. Vieira, M. A. M. Vieira, and O. Gnawali, "Visible light communication: Concepts, applications and challenges" in *IEEE Communications Surveys & Tutorials*, vol. 21, no. 4, pp. 3204-3237, 2019, doi: 10.1109/COMST.2019.2913348.

[2] O. Alamu, T. O. Olwal, K. Djouani, "Cooperative visible light communications: An overview and outlook." in *Optical Switching and Networking*, vol. 52-53, 2024, doi: 10.1016/j.osn.2024.100772.

[3] K. Kadam and M. R. Dhage, "Visible light communication for IoT," in *Proc. 2nd International Conference on Applied and Theoretical Computing and Communication Technology (iCATccT)*, pp. 275-278, 2016, doi: 10.1109/ICATCCT.2016.7912007.

[4] A. M. Kurien, K. Djouani and S. S. Oyewobi, "Visible light communications for internet of things: Prospects and approaches, challenges, solutions and future directions," in *Technologies*, vol. 10, no. 1, Art. no. 28, 2022, doi: 10.3390/technologies10010028.

[5] J. Lian, Z. Vatansever, M. Noshad, and M. Brandt-Pearce, "Indoor visible

light communications, networking, and applications," in *Journal of Physics: Photonics*, vol. 1, no. 1, Art. no. 012001, 2019, doi: 10.1088/2515-7647/aaf74a.

[6] H. Abuella, M. Elamassie, M. Uysal, Z. Xu, E. Serpedin, K. A. Qaraqe, and S. Ekin, "Hybrid RF/VLC systems: A comprehensive survey on network topologies, performance analyses, applications, and future directions," in *IEEE Access*, vol. 9, pp. 160402–160436, 2021, doi: 10.1109/ACCESS.2021.3129154.

[7] S. U. Rehman, S. Ullah, P. H. J Chong, S. Yongchareon, and D. Komosny, "Visible light communication: A system perspective—overview and challenges" in *Sensors*, vol. 19, no. 5, Art. no. 1153, 2019, doi: 10.3390/s19051153.

[8] P. H. Pathak, X. Feng, P. Hu and P. Mohapatra, "Visible light communication, networking, and sensing: A survey, potential and challenges" in *IEEE Communications Surveys & Tutorials*, vol. 17, no. 4, pp. 2047–2077, 2015, doi: 10.1109/COMST.2015.2476474.

[9] C. Elliott, *et al.* "Energy savings forecast of solid-state lighting in general illumination applications,", Navigant Consulting, Inc., Washington, DC (United States), 2019, doi: 10.2172/1607661.

[10] M. Kashef, M. Abdallah, N. Al-Dhahir, and K. Qaraqe, "On the Impact of PLC backhauling in multi-user hybrid VLC/RF communication systems," in *Proc. IEEE Global Communications Conference (GLOBECOM)*, pp. 1–6, 2016, doi: 10.1109/GLOCOM.2016.7842055.

[11] H. Marshoud, P. C. Sofotasios, S. Muhaidat, and G. K. Karagiannidis, "Multiuser techniques in visible light communications: A survey," in *Proc.*

International Conference on Advanced Communication Systems and Information Security (ACOSIS), pp. 1–6, 2016, doi: 10.1109/ACOSIS.2016.7843945.

[12] H. Mazar, "Radio spectrum Management: Policies, regulations and techniques," *John Wiley & Sons*, 2016.

[13] HR. Ji, S. Wang, Q. Liu, and W. Lu, "High-speed visible light communications: Enabling technologies and state of the art," in *Applied Sciences*, vol. 8, no. 4, Art. no. 589, 2018, doi: 10.3390/app8040589.

[14] J. Grubor, S. Randel, K. -D. Langer and J. W. Walewski, "Broadband Information Broadcasting Using LED-Based Interior Lighting," in *Journal of Lightwave Technology*, vol. 26, no. 24, pp. 3883–3892, 2008.

[15] C. Rohner, S. Raza, D. Puccinelli, and T. Voigt, "Security in visible light communication: Novel challenges and opportunities," in *Sensors Transducers* vol. 192, no. 9, pp. 9–15, 2015.

[16] D. Karunatilaka, F. Zafar, V. Kalavally, and R. Parthiban, "LED based indoor visible light communications: State of the art," *IEEE Commun. Surv. Tut.*, vol. 17, no. 3, pp. 1649–1678, 2015, doi: 10.1109/COMST.2015.2417576.

[17] K. Rose, S. Eldridge, and L. Chapin, "The internet of things: An overview," in *The Internet Society (ISOC)*, vol. 80, no. 15, pp. 1–53, 2015.

[18] S. Li, L. D. Xu, and S. Zhao, "The internet of things: a survey," in *Information Systems Frontiers*, vol. 17, pp. 243–259, 2015, doi: 10.1007/s10796-014-9492-7.

[19] Y. K. Chen, "Challenges and opportunities of internet of things," in *17th*

Asia and South Pacific Design Automation Conference, pp. 383–388, 2012, doi: 10.1007/s10796-014-9492-7.

[20] L. C. D. Silva, C. Morikawa, C. and I. M. Petra, “State of the art of smart homes,” in *Engineering Applications of Artificial Intelligence*, vol. 25, no. 7, pp. 1313–1321, 2012, doi: 10.1016/j.engappai.2012.05.002.

[21] M. R. Alam, M. B. I. Reaz, and M. A. M. Ali, “A review of smart homes—Past, present, and future,” in *IEEE Transactions on Systems, Man, and Cybernetics, Part C*, vol. 42, no. 6, pp. 1190–1203, 2012, doi: 10.1109/TSMCC.2012.2189204.

[22] M. Chan, D. Estève, C. Escriba, and E. Campo, “A review of smart homes—Present state and future challenges,” in *Computer Methods and Programs in Biomedicine*, Vol. 91, no. 1, pp. 55–81, 2008, doi: 10.1016/j.cmpb.2008.02.001.

[23] F. Miramirkhani, M. Karbalayghareh, E. Zeydan, R. Mitra, “Enabling 5G indoor services for residential environment using VLC technology,” in *Physical Communication*, vol. 53, Art. no. 101679, 2022, doi: 10.1016/j.phycom.2022.101679.

[24] H. Yang, A. Alphones, W. -D. Zhong, C. Chen, and X. Xie, “Learning-based energy-efficient resource management by heterogeneous RF/VLC for ultra-reliable low-latency industrial IoT networks,” in *IEEE Transactions on Industrial Informatics*, vol. 16, no. 8, pp. 5565–5576, 2020, doi: 10.1109/TII.2019.2933867.

[25] S. K. Sharma and X. Wang, “Towards massive machine type communications in ultra-dense cellular IoT networks: Current issues and machine learning assisted

solutions," in *IEEE Commun. Surveys & Tuts.*, vol. 22, no. 1, pp. 426-471, 2020, doi: 10.1109/COMST.2019.2916177.

[26] L. Feng, R. Q. Hu, J. Wang, P. Xu, and Y. Qian, "Applying VLC in 5G Networks: Architectures and Key Technologies," in *IEEE Network*, vol. 30, no. 6, pp. 77-83, 2016, doi: 10.1109/MNET.2016.1500236RP.

[27] A. Sarkar, A. Shalabh, and N. Asoke, "Li-Fi technology: Data transmission through visible light." in *International Journal of Advance Research in Computer Science and Management Studies* vol. 3, no. 6, pp. 1–10, 2015.

[28] G. A. Mapunda, R. Ramogomana, L. Marata, B. Basutli, A. S. Khan, and J. M. Chuma, "Indoor visible light communication: A tutorial and survey," in *Wireless Communications and Mobile Computing*, Art. no. 8881305, 2020, doi: 10.1155/2020/8881305.

[29] D. O'Brien, H. Minh, L. Zeng, G. Faulkner, K. Lee, D. Jung, Y. Oh, and E. T. Won, "Indoor visible light communications: challenges and prospects," in *Proc. Free-Space Laser Communications VIII*, vol. 7091, pp. 60–68, 2008, doi: 10.1117/12.799503.

[30] SH. Lin, C. Liu, X. Bao, et al., "Indoor visible light communications: performance evaluation and optimization," in *J. Wireless Com. Network*, pp. 1–12, 2018, doi: 10.1186/s13638-018-1243-x.

[31] S. Yuhan, L. Yuchen, L. Sicong, L. Minghui, L. Xinqin, and W. Tingzhu "Coexistence of Hybrid VLC-RF and Wi-Fi for Indoor Wireless Communication

Systems: An Intelligent Approach," in *IEEE Transactions on Network and Service Management*, Early Access, 2024.

[32] S. Refas, *et al.*, "Performance analysis of bidirectional multi-hop vehicle-to-vehicle visible light communication," in *IEEE Access*, vol. 11, pp. 129436–129448, 2023, doi: 10.1109/ACCESS.2023.3333046.

[33] M. Uysal, Z. Ghassemlooy, A. Bekkali, A. Kadri and H. Menouar, "Visible light communication for vehicular networking: Performance study of a V2V system using a measured headlamp beam pattern model," in *IEEE Vehicular Technology Magazine*, vol. 10, no. 4, pp. 45–53, Dec. 2010, doi: 10.1109/MVT.2015.2481561.

[34] A, Memedi and D. Falko, "Vehicular visible light communications: A survey," in *IEEE Communications Surveys & Tutorials*, vol. 23, no. 1, pp. 161–181, 2020.

[35] M. Akanegawa, Y. Tanaka, and M. Nakagawa, "Basic study on traffic information system using LED traffic lights," in *IEEE Transactions on Intelligent Transportation Systems*, vol. 2, no. 4, pp. 197-203, Dec. 2001, doi: 10.1109/6979.969365.

[36] W. Yang, H. Liu, and G. Cheng, "Modeling and Performance Study of Vehicle-to-Infrastructure Visible Light Communication System for Mountain Roads," in *Sensors*, vol. 24, no. 17, Art. no. 5541, 2024.

[37] "Frequency of target crashes for intellidrive safety systems" *U.S. Dept. Transp. Res. Innov. Technol. Admin., John A. Volpe Nat. Transp. Syst. Center,*, Cambridge, MA, USA, Tech. Rep. DOT HS 811 381, Oct. 2010, [Online]. Available: https://rosap.ntl.bts.gov/view/dot/12066/dot_12066_DS1.pdf.

[38] A. Gil-de-Castro, A. Moreno-Munoz, A. Larsson, J. de la Rosa, M. Bollen, "LED street lighting: A power quality comparison among street light technologies," in *Lighting Research & Technology*, vol. 45, no. 6, pp. 710–728, 2013, doi: 10.1177/1477153512450866.

[39] X. Long, J. He, J. Zhou, L. Fang, X. Zhou, F. Ren, T. Xu, "A review on light-emitting diode based automotive headlamps," in *Renewable and Sustainable Energy Reviews*, vol. 41, pp. 29-41, 2015, doi: 10.1016/j.rser.2014.08.028.

[40] G. Pang, T. Kwan, Chi-Ho Chan, and Hugh Liu, "LED traffic light as a communications device," in *Proc. 199 IEEE/IEEJ/JSAI International Conference on Intelligent Transportation Systems*, vol. 2, no. 4, pp. 788–793, 1999, doi: 10.1109/ITSC.1999.821161.

[41] Miramirkhani, Farshad, et al. "IEEE 802.11 BB reference channel models for light communications," in *IEEE Communications Standards Magazine*, vol. 7, no. 4, pp. 84–89, 2023.

[42] A. M. Căilean, and M. Dimian, "Current challenges for visible light communications usage in vehicle applications: A Survey," in *IEEE Communications Surveys & Tutorials*, vol. 19, no. 4 pp. 129436–129448, 2017, doi: 10.1109/COMST.2017.2706940.

[43] A.-M. Cailean, B. Cagneau, L. Chassagne, V. Popa, and M. Dimian, "A survey on the usage of DSRC and VLC in communication-based vehicle safety applications," in *Proc. IEEE 21st Symp. Commun. Veh. Technol. Benelux (SCVT)*, pp. 69–74, 2014, doi: 10.1109/SCVT.2014.7046710.

[44] J. M. Kahn and J. R. Barry, "Wireless infrared communications" in *Proceedings of the IEEE*, vol. 85, no. 2, pp. 265-298, Feb. 1997, doi: 10.1109/5.554222.

[45] D.-R. Kim, S.-H. Yang, H.-S. Kim, Y.-H. Son, and S.-K. Han, "Outdoor visible light communication for inter-vehicle communication using controller area network," in *Proc. 4th Int. Conf. Commun. Electron. (ICCE)*, pp. 31—34, 2012, doi: 10.1109/CCE.2012.6315865.

[46] U. Kurokawa, B. I. Choi, and C.-C. Chang, "Filter-based miniature spectrometers: Spectrum reconstruction using adaptive regularization," in *IEEE Sensors J.*, vol. 11, no. 7, pp. 1556—1563, 2011, doi: 10.1109/JSEN.2010.2103054.

[47] A. Cailean et al., "Visible light communications: Application to cooperation between vehicles and road infrastructures," in *Proc. IEEE Intell. Veh. Symp. (IV)*, pp. 1055—1059, 2012, doi: 10.1109/IVS.2012.6232225.

[48] K. Cui, G. Chen, Z. Xu, and R. D. Roberts, "Experimental characterization of traffic light to vehicle VLC link performance," in *Proc. IEEE GLOBECOM Wkshps (GC Wkshps)*, pp. 808—812, 2011, 2012, doi: 10.1109/GLOCOMW.2011.6162566.

[49] J. M. Kahn, W. J. Krause, and J. B. Carruthers, "Experimental characterization of non-directed indoor infrared channels," in *IEEE Trans. Commun.,* vol. 43, no. 234, pp. 1613–1623, 1995.

[50] A. J. C. Moreira, R. T. Valadas, and A. M. de Oliveira Duarte, "Characterisation and modeling of artificial light interference in optical wireless communication

systems," in *Proc. 6th IEEE Int. Symp. Wireless Merging Inf. Superhighway Pers. Indoor Mobile Radio Commun. (PIMRC),*, pp. 326–331, 1995, doi: 10.1109/PIMRC.1995.476907.

[51] R. Corsini et al., "Free space optical communication in the visible bandwidth for V2V safety critical protocols," in *Proc. 8th Int. Conf. Wireless Commu. Mobile Comput. (IWCMC)*, pp. 1097—1102, 2012, doi: 10.1109/IWCMC.2012.6314359.

[52] I. Takai et al., "LED and CMOS image sensor based optical wireless communication system for automotive applications," in *IEEE Photon. J.*, vol. 5, no. 5, Art. no. 6801418, Oct. 2013, doi: 10.1109/JPHOT.2013.2277881.

[53] F. Furfari, et al., "Discovering location based services: A unified approach for heterogeneous indoor localization systems," in *Internet of Things*, vol. 13, Art. no. 100334, 2021, doi: 10.1016/j.iot.2020.100334.

[54] S. He and S.-H. G. Chan, "Wi-Fi fingerprint-based indoor positioning: Recent advances and comparisons," in *IEEE Commun. Surveys Tuts.*, vol. 18, no. 1, pp. 466–490, 2016, doi: 10.1109/COMST.2015.2464084.

[55] A. Hameed and H. A. Ahmed, "Survey on indoor positioning applications based on different technologies," in *12th International Conference on Mathematics, Actuarial Science, Computer Science and Statistics (MACS)*, pp. 1–5, 2018, doi: 10.1109/MACS.2018.8628462.

[56] L. Mainetti, L. Patrono and I. Sergi, "A survey on indoor positioning systems", in *22nd International Conference on Software, Telecommunications*

and Computer Networks (SoftCOM), pp. 111–120, 2014, doi: 10.1109/SOFTCOM.2014.7039067.

[57] Y. Gu, A. Lo and I. Niemegeers, "A survey of indoor positioning systems for wireless personal networks," in *IEEE Communications Surveys & Tutorials*, vol. 11, no. 1, pp. 13–32, 2009, doi: 10.1109/SURV.2009.090103.

[58] Hofmann-Wellenhof, Bernhard, Herbert Lichtenegger, and James Collins, "Global positioning system: theory and practice," *Springer Science & Business Media*, 2012.

[59] Z. Jiao, B. Zhang, M. Liu, and C. Li, "Visible light communication based indoor positioning techniques," in *IEEE Netw.*, vol. 31, no. 5, pp. 12–18, 2017, doi: 10.1109/MNET.2017.1600264.

[60] Y. Yang, Z. Zeng, J. Cheng, C. Guo, and C. Feng, "A relay-assisted OFDM system for VLC uplink transmission," in *IEEE Trans. Commun.*, vol. 67, no. 9, pp. 6268–6281, 2019, doi: 10.1109/TCOMM.2019.2923237.

[61] L. He, L. Shi, X. Li, and M. Sun, "Supermarket commodity guide system based on indoor visible light positioning," in *2022 5th World Symposium on Communication Engineering (WSCE)*, Nagoya, Japan, pp. 33–37, 2022.

[62] A. Madahian, P. A. Ardakani, J. Abouei, A. Mirvakili, A. Mohammadi, and V. Koomson, "A hybrid VLC/RF parking automation system," in *IEEE Access*, vol. 11, pp. 66960–66978, 2023.

[63] M. Pang, G. Shen, X. Yang, K. Zhang, P. Chen, and G. Wang, "Achieving

reliable underground positioning with visible light," in *IEEE Transactions on Instrumentation and Measurement*, vol. 71, pp. 1 –15,2022

[64] J. Luo, L. Fan, and H. Li, "Indoor positioning systems based on visible light communication: State of the art," in *IEEE Communications Surveys & Tutorials*, vol. 19, no. 4, pp. 2871–2893, 2017, doi: 10.1109/COMST.2017.2743228.

[65] Z. Zhu, C. Guo, R. Bao, M. Chen, W. Saad, and Y. Yang,"Positioning using visible light communications: A perspective arcs approach," in *IEEE Transactions on Wireless Communications*, vol. 22, no. 10, pp. 6962–6977, 2023, doi: 10.1109/TWC.2023.3247458.

[66] T.-H. Do and M. Yoo, "An in-depth survey of visible light communication based positioning systems," in *Sensors*, vol. 16, no. 5, Art. no. 678, 2016, doi: 10.3390/s16050678.

[67] Y. Zhuang, L. Hua, L. Qi, J. Yang, P. Cao, Y. Cao, Y. Wu, J. Thompson, and H. Haas, "A survey of positioning systems using visible LED lights," in *IEEE Commun. Surv. Tutorials*, vol. 20, no. 3, pp. 1963–1988, 2018, doi: 10.1109/COMST.2018.2806558.

[68] K. Majeed and S. Hranilovic, "Passive Indoor Localization for Visible Light Communication Systems," in *IEEE Global Communications Conference (GLOBECOM)*, pp. 1–6, 2018, doi: 10.1109/GLOCOM.2018.8647875.

[69] K. Majeed and S. Hranilovic, "Performance bounds on passive indoor positioning using visible light," in *Journal of Lightwave Technology*, vol. 38, no. 8, pp. 2190–2200, 2020.

[70] N. Farr, A. Bowen, J. Ware, C. Pontbriand, and M. Tivey, “An integrated, underwater optical/acoustic communications system,” in *Proc. OCEANS’10 IEEE SYDNEY*, pp. 1–6, 2010,doi: 10.1109/OCEANSSYD.2010.5603510.

[71] M. F. Ali, D. N. K. Jayakody and Y. Li, “Recent trends in underwater visible light communication (UVLC) systems,” in *IEEE Access*, vol. 10, pp. 22169–22225, 2022, doi: 10.1109/ACCESS.2022.3150093.

[72] J. Wang, C. Chen, B. Deng, Z. Wang, M. Liu, and H. Fu, “Enhancing underwater VLC with spatial division transmission and pairwise coding,” in *Optics Express*, vol. 31, no. 10, pp. 16812–16832, 2023.

[73] Z. Lu, C. Shen, J. Shi, and N. Chi, “Security enhanced underwater visible light communication system based on chaotic phase scrambling and conjugate frequency hopping,” in *Chinese Optics Letters*, vol. 21, no. 6, Art. no. 060602, 2023.

[74] Y. Wang, N. Chi, Y. Wang, L. Tao, and J. Shi, “Network architecture of a high-speed visible light communication local area network,” in *IEEE Photonics Technology Letters*, vol. 27, no. 2, pp. 197–200, 2014, doi: 10.1109/LPT.2014.2364955.

[75] X. Li, B. Hussain, J. Kang, H. S. Kwok and C. P. Yue, “Smart LED display-VLC system with a PD-based/camera-based receiver for NFC applications,” in *IEEE Photonics Journal*, Vol. 11, no. 1, pp. 1–8, 2019.

[76] J. -S. Park and B. -J. Jang, “Electronic shelf label system employing a visible

light identification link," in *IEEE Radio and Wireless Symposium (RWS)*, pp. 219–222, 2016.

[77] H. Burchardt, N. Serafimovski, D. Tsonev, S. Videv and H. Haas, "VLC: Beyond point-to-point communication," in *IEEE Communications Magazine*, Vol. 52, no. 7, pp. 98–105, 2014.

[78] F. Wang, F. Yang, C. Pan, J. Song, and Z. Han, "Joint illumination and communication optimization in indoor VLC for IoT applications," in *IEEE Internet of Things Journal*, vol. 9, no. 21, pp. 20788–20800, 2022.

[79] H. Zhou, M. Zhang, and X. Ren, "Design and implementation of wireless optical access system for VLC-IoT networks," in *Journal of Lightwave Technology*, vol. 41, no. 8 pp. 2369–2380, 2023.

[80] D. J. Love, R. W. Heath, V. K. N. Lau, D. Gesbert, B. D. Rao and M. Andrews, "An overview of limited feedback in wireless communication systems," in *IEEE Journal on Selected Areas in Communications*, vol. 26, no. 8, pp. 1341–1365, October 2008.

[81] S. Bi, Y. Zeng and R. Zhang, "Wireless powered communication networks: an overview," in *IEEE Wireless Communications*, vol. 23, no. 2, pp. 10–18, April 2016.

[82] Du, Ke-Lin, and Madisetti NS Swamy, "Wireless communication systems: from RF subsystems to 4G enabling technologies," in *Cambridge University Press*, 2010.

[83] R. W. Erickson, "DC–DC power converters," in *Wiley Encyclopedia of Electrical and Electronics Engineering*, 2001.

[84] B. Razavi, "The transimpedance amplifier [a circuit for all seasons]," in *IEEE Solid-State Circuits Magazine*, vol. 11, no. 1, pp. 10–97, 2019.

[85] International Telecommunication Union, "High-speed indoor visible light communication transceiver–system architecture, physical layer and data link layer specification," in *ITU-TG*, vol. 9991, 2019, [Online]. Available: https://www.itu.int/rec/T-REC-G.9991/en.

[86] K. L. Bober, E. Ackermann, R. Freund, V. Jungnickel, T. Baykas and S. -K. Lim, "The IEEE 802.15.13 standard for optical wireless communications in industry 4.0," in *IECON - 48th Annual Conference of the IEEE Industrial Electronics Society*, Brussels, Belgium, pp. 1–6, 2022.

[87] IEEE Standards Association, "IEEE standard for multi-gigabit per second optical wireless communications (OWC), with ranges up to 200 m, for both stationary and mobile devices," in *IEEE std 802.15.13-2023*, pp. 1–158, 2023, doi: 10.1109/IEEESTD.2023.10205961.

[88] L. Teixeira, F. Loose, C. H. Barriquello, and M. A. Dalla Costa, "On the LED efficacy and modulation design space for visible light communication," in *Proc. IEEE Ind. Appl. Soc. Annu. Meeting(IAS)*, Portland, OR, USA, pp. 1–6, 2018. doi: 10.1109/IAS.2018.8544602.

[89] A. Khreishah, S. Shao, A. Gharaibeh, M. Ayyash, H. Elgala and N. Ansari, "A hybrid RF-VLC system for energy efficient wireless access," in *IEEE*

Transactions on Green Communications and Networking, vol. 2, no. 4, pp. 932–944, Dec. 2018.

[90] L. Teixeira, F. Loose, C. H. Barriquello, V. A. Reguera, M. A. Dalla Costa, & J. M. Alonso, "On energy efficiency of visible light communication systems," in *IEEE Journal of Emerging and Selected Topics in Power Electronics*, vol. 9, no. 5, pp. 6396–6407, 2021.

[91] F. Zafar, D. Karunatilaka and R. Parthiban, "Dimming schemes for visible light communication: the state of research," in *IEEE Wireless Communications*, vol. 22, no. 2, pp. 29–35, April 2015.

[92] I. Stefan, H. Elgala and H. Haas, "Study of dimming and LED nonlinearity for ACO-OFDM based VLC systems," in *IEEE Wireless Communications and Networking Conference (WCNC)*, pp. 990–994, Paris, France, 2012.

[93] M. Oh, "A flicker mitigation modulation scheme for visible light communications," in *Proc. 15th International Conference on Advanced Communications Technology (ICACT)*, vol. 9, no. 21 pp. 933–936, 2013.

[94] S. He, G. Ren, L. Wu, Z. Sun, and Y. Zhao, "Flicker mitigation and dimming control analyze of duty cycle fixed-MVPM for indoor VLC system," in *Proc. Int. Conf. Comput., Netw. Commun. (ICNC)*, Big Island, HI, USA, pp. 6–9, 2020, doi: 10.1109/ICNC47757.2020.9049813.

[95] B. Lehman and A. J. Wilkins, "Designing to mitigate effects of flicker in LED lighting: Reducing risks to health and safety," in *IEEE Power Electronics Magazine*, vol. 1, no. 3, pp. 18–26, Sept. 2014.

[96] C. Qian, F. Cheng, J. Fan, X. Fan, and G. Zhang, "Prediction of lumen depreciation and color shift for phosphor-converted white light-emitting diodes based on a spectral power distribution analysis method," in *IEEE Access*, vol. 5, pp. 24054–24061, 2017.

[97] L. Liu, X. Zhang, L. Li, D. Teng, and G. Wang, "In-situ monitoring the degradation of LEDs en route the visible light communication system," in *IEEE Transactions on Device and Materials Reliability*, vol. 17, no. 4, pp. 722–726, 2017, doi: 10.1109/TDMR.2017.2756627.

[98] J. Sebastián, D. G. Lamar, D. G. Aller, J. Rodriguez, and P. F. Miaja, "On the role of power electronics in visible light communication," in *IEEE Journal of Emerging and Selected Topics in Power Electronics*, vol. 6, no. 3, pp. 1210–1223, 2018, doi: 10.1109/JESTPE.2018.2830878.

[99] J. Vučič, C. Kottke, S. Nerreter, K.-D. Langer, and J. W. Walewski, "513 Mbit/s visible light communications link based on DMT-modulation of a white LED," in *Journal of Lightwave Technology*, vol. 28, no. 24, pp. 3512–3518, 2010, doi: 10.1109/JLT.2010.2089602.

[100] H. Chun *et al.*, "LED based wavelength division multiplexed 10 Gb/s visible light communications," in *Journal of Lightwave Technology*, vol. 34, no. 13, pp. 3047—3052, 2016.

[101] D. G. Aller et al., "Adapting techniques to improve efficiency in Radio frequency power amplifiers for visible light communications," in *Electronics*, vol. 9, no. 1, Art. no. 131, 2020.

[102] X. Deng, Y. Wu, K. Arulandu, G. Zhou, and J.-P. M. G. Linnartz, "Performance comparison for illumination and visible light communication system using buck converters," in *Proc. IEEE Globecom Workshops (GC Wkshps)*, pp. 547–552, 2014, doi: 10.1109/GLOCOMW.2014.7063489.

[103] J. Rodríguez, D. G. Lamar, P. F. Miaja, and J. Sebastian, "Reproducing single-carrier digital modulation schemes for VLC by controlling the first switching harmonic of the DC-DC power converter output voltage ripple," in *IEEE Transactions on Power Electronics*, vol. 33, no. 9, pp. 7994–8010, 2018, doi: 10.1109/TPEL.2017.2774178.

[104] J. Rodríguez, J. R. García-Meré, D. G. Lamar, and J. Sebastián, "A novel version of the ripple-modulation technique for enabling the use of single-phase buck converters in VLC applications," in *IEEE Journal of Emerging and Selected Topics in Power Electronics*, vol. 11, no. 2, pp. 1966–1978, 2023, doi: 10.1109/JESTPE.2022.3225874.

[105] D. G. Aller, D. G. Lamar, P. F. Miaja, J. Rodríguez, and J. Sebastián, "Taking advantage of the sum of the light in outphasing technique for visible light communication transmitter," *IEEE Journal of Emerging and Selected Topics in Power Electronics*, vol. 9, no. 1, pp. 138–145, 2021, doi: 10.1109/JESTPE.2020.2965774.

[106] J. Du, W. Xu, H. Zhang, and C. Zhao, "Visible light communications using spatial summing PAM with LED array," in *Proc. IEEE Wireless Commun. Netw. Conf. (WCNC)*, pp. 1–6, 2017, doi: 10.1109/WCNC.2017.7925910.

[107] J. Rodriguez, D. G. Lamar, J. Sebastian, and P. F. Miaja, "Taking advantage

of the output voltage ripple of a two-phase buck converter to perform quadrature amplitude modulation for visible light communication," in *Proc. IEEE Appl. Power Electron. Conf. Expo. (APEC)*, pp. 2116–2123, 2017, doi: 10.1109/APEC.2017.7930991.

[108] Y.-C. Lee, J.-L. Lai, C.-H. Yu, and C.-S. A. Gong, "The high-efficiency LED driver for visible light communication applications," in *Proc. Inc. Conf. Ubiquitous Future Netw.(ICUFN)*, pp. 56–58, 2016, doi: 10.1109/ICUFN.2016.7536979.

[109] T. Kishi, H. Tanaka, Y. Umeda, and O. Takyu, "A high-speed LED driver that sweeps out the remaining carriers for visible light communications," in *Journal of Lightwave Technology*, vol. 32, no. 2, pp. 239–249, 2013, doi: 10.1109/JLT.2013.2292896.

[110] X. Deng, K. Arulandu, Y. Wu, G. Zhou, and J.-P. M. G. Linnartz, "Performance analysis for joint illumination and visible light communication using buck driver," in *IEEE Transactions on Communications*, vol. 66, no. 5, pp. 2065–2078, 2018, doi: 10.1109/TCOMM.2018.2792018.

[111] Rodriguez Mendez, D. G. Lamar, D. G. Aller, P. F. Miaja and J. Sebastian, "Reproducing multicarrier modulation schemes for visible light communication with the ripple modulation technique," in *IEEE Transactions on Industrial Electronics*, vol. 67, no. 2, pp. 1532–1543, Feb. 2020.

[112] M. Obeed, A. M. Salhab, M. -S. Alouini and S. A. Zummo, "On optimizing VLC networks for downlink multi-user transmission: A survey," in *IEEE Communications Surveys & Tutorials*, vol. 21, no. 3, pp. 2947–2976, 2019.

[113] S. Aboagye, T. M. N. Ngatched and O. A. Dobre, "Subchannel and power allocation in downlink VLC under different system configurations," in *IEEE Transactions on Wireless Communications*, vol. 21, no. 5, pp. 3179–3191, 2022.

[114] A. M. Abdelhady, O. Amin, A. Chaaban, B. Shihada and M. -S. Alouini, "Downlink Resource Allocation for Dynamic TDMA-Based VLC Systems," in *IEEE Transactions on Wireless Communications*, vol. 18, no. 1, pp. 108–120, 2019.

[115] H. Tabassum and E. Hossain, "Coverage and rate analysis for co-existing RF/VLC downlink cellular networks," *IEEE Transactions on Wireless Communications*, vol. 17, no. 4, pp. 2588–2601, 2018.

[116] O. R. B. Sayco and A. C. Gordillo, "Development of an IR system as an alternative for VLC uplink," in *Proc. 2019 IEEE Colombian Conf. Commun. Comput. (COLCOM)*, Barranquilla, Colombia, pp. 1–5, 2019, doi: 10.1109/ColComCon.2019.8809131.

[117] M. T. Alresheedi, A. T. Hussein, and J. M. Elmirghani, "Uplink design in VLC systems with IR sources and beam steering," *IET Commun.*, vol. 11, no. 3, pp. 311–317, Feb. 2017, doi: 10.1049/iet-com.2016.0495.

[118] P. Pérez-Nicoli, F. Silveira, X. Zhang, and A. Amara, "Uplink wireless transmission overview in bi-directional VLC systems," in *Proc. IEEE Int. Conf. Electron. Circuit Syst. (ICECS)*, Monte Carlo, Monaco, pp. 588–591, 2016, doi: 10.1109/ICECS.2016.7841270.

[119] W. Yuanquan and C. Nan, "A high-speed bi-directional visible light

communication system based on RGB-LED," *China Commun.*, vol. 11, no. 3, pp. 40–44, 2014, doi: 10.1109/CC.2014.6825257.

[120] O. Z. Aletri, M. T. Alresheedi, and J. M. Elmirghani, "Infrared uplink design for visible light communication (VLC) systems with beam steering," in *Proc. 2019 IEEE Int. Conf. Comput. Sci. Eng. (CSE) IEEE Int. Conf. Embedded Ubiquitous Comput. (EUC)*, pp. 57–60, 2019, doi: 10.1109/CSE/EUC.2019.00020.

[121] S. Shao et al., "An indoor hybrid WiFi-VLC internet access system," in *Proc. IEEE 11th International Conference on Mobile Ad Hoc and Sensor Systems*, pp. 569–574, 2014.

[122] H. Kazemi, M. Safari and H. Haas, "A wireless optical backhaul solution for optical attocell networks," *IEEE Trans. Wireless Commun.*, vol. 18, no. 2, pp. 807–823, Feb. 2019, doi: 10.1109/TWC.2018.2883465.

[123] T. Komine and M. Nakagawa, "Integrated system of white LED visible-light communication and power-line communication," *IEEE Trans. Consum. Electron.*, vol. 49, no. 1, pp. 71–79, 2003, doi: 10.1109/TCE.2003.1205458.

[124] J. Song, W. Ding, F. Yang, H. Yang, B. Yu, and H. Zhang, "An indoor broadband broadcasting system based on PLC and VLC," *IEEE Trans. Broadcast.*, vol. 61, no. 2, pp. 299–308, 2015, doi: 10.1109/TBC.2015.2400825.

[125] X. Ma, J. Gao, F. Yang, W. Ding, H. Yang, and J. Song, "Integrated power line and visible light communication system compatible with multi-service transmission," *IET Commun.*, vol. 11, no. 1, pp. 104–111, 2017,doi: 10.1049/iet-com.2015.1002.

[126] P. Mark, "Ethernet over light," Ph.D. dissertation, University of British Columbia, 2014, doi: 10.14288/1.0167659.

[127] Z. Huang, Z. Wang, M. Huang, W. Li, T. Lin, P. He, and Y. Ji, "Hybrid optical wireless network for future SAGO-integrated communication based on FSO/VLC heterogeneous interconnection," *IEEE Photon. J.*, vol. 9, no. 2, pp. 1–10, 2017, doi: 10.1109/JPHOT.2017.2655004.

[128] A. Gupta, N. Sharma, P. Garg, and M.-S. Alouini, "Cascaded FSO-VLC communication system," *IEEE Wireless Commun. Lett.*, vol. 6, no. 6, pp. 810–813, 2017, doi: 10.1109/LWC.2017.2745561.

[129] L. Feng, R. Q. Hu, J. Wang, P. Xu, and Y. Qian, "Applying VLC in 5G networks: Architectures and key technologies," *IEEE Netw.*, vol. 30, no. 6, pp. 77–83, 2016, doi: 10.1109/MNET.2016.1500236RP.

[130] Y. Wu, M. Pickavet, and D. Colle, "Analysis of interference on mirror-aided non-LOS backhaul data transmission in VLC attocell networks," *Photon. Netw. Commun.*, vol. 41, pp. 189–201, 2021, doi: 10.1007/s11107-021-00928-w.

[131] S. Haruyama, "Japan's visible light communications consortium and its standardization activities," 2020, [Online]. Available: https://mentor.ieee.org/802.15/dcn/08/15-08-0061-00-0vlc-japan-svisible-%20light-communications-consortium-and-its.pdf.

[132] "IEEE standard for local and metropolitan area networks–part 15.7: Short-range wireless optical communication using visible light," in *IEEE Std 802.15.7-2011*, pp. 1–309, 2011, doi: 10.1109/IEEESTD.2011.6016195.

[133] H. Haass, L. Yin, Y. Wang, and C. Chen, "What is LiFi," in *Journal of lightwave technology*, vol. 34, no. 6, pp. 1533–1544, 2015.

[134] M. Uysal, F. Miramirkhani, T. Baykas, and K. Qaraqe, "IEEE 802.11 bb reference channel models for indoor environments," Technical report, 2018, [Online]. Available: https://mentor.ieee.org/802.11/dcn/18/11-18-1236-01-00bb-ieee-802-11bb-reference-channel-models-for-indoor-environments.pdf.

[135] H. Zhu, M. Li, I. Chlamtac, and B. Prabhakaran, "A survey of quality of service in IEEE 802.11 networks," in *IEEE Wireless Communications*, vol. 11, no. 4, pp. 6–14, 2004, doi: 10.1109/MWC.2004.1325887.

[136] IEEE Standards Association, "IEEE 802.15 WPAN Task Group 13 (TG13) Multi-Gigabit/s Optical Wireless Communications," 2020, [Online]. Available: https://www.ieee802.org/15/pub/TG13.html.

[137] L. J. Cimini, Jr., "Analysis and simulation of a digital mobile channel using orthogonal frequency division multiplexing," *IEEE Trans. Commun.*, vol. CM-33, no. 3, pp. 665–675, 1985.

[138] R. Lassalle and M. Alard, "Principles of modulation and channel coding for digital broadcasting for mobile receivers," *EBU Tech. Rev.*, pp. 168–190, 1987.

[139] J. S. Chow, J. C. Tu, and J. M. Cioffi, "A discrete multitone transceiver system for HDSL applications," *IEEE J. Sel. Areas Commun.*, vol. 9, pp. 895–908, 1991.

[140] I. Koffman and V. Roman, “Broadband wireless access solutions based on OFDM access in IEEE 802.16,” *IEEE Commun. Mag.*, vol. 40, pp. 96–103, 2002.

[141] U. Reimers, “Digital video broadcasting,” *IEEE Commun. Mag.*, vol. 36, pp. 104–110, 1998.

[142] J. Armstrong, “From copper and wireless to optical,” *Optical Fiber Communication/National Fiber Optic Engineers Conference*, OSA Technical Digest (CD) (Optica Publishing Group, 2008), paper OMM1, 2008.

[143] J. Armstrong, “OFDM for optical communications,” *Journal of Lightwave Technology*, vol. 27, no. 3, pp. 189–204, 2009, doi: 10.1109/JLT.2008.2010061.

[144] S. D. Dissanayake and J. Armstrong, “Comparison of ACO-OFDM, DCO-OFDM and ADO-OFDM in IM/DD systems,” *Journal of Lightwave Technology*, vol. 31, no. 7, pp. 1063–1072, 2013, doi: 10.1109/JLT.2013.2241731.

[145] X. Zhang, Q. Wang, R. Zhang, S. Chen and L. Hanzo, “Performance Analysis of Layered ACO-OFDM,” in *Opt. Express*, vol. 29, pp. 10613–10630, 2021.

[146] R. Bai and S. Hranilovic, “Layered antisymmetry-constructed clipped optical OFDM for low-complexity VLC systems,” in *IEEE Access*, vol. 5, pp. 18366–18381, 2017.

[147] H. S. Kim, D. R. Kim, S. H. Yang, Y. H. Son and S. K. Han, “Mitigation of Inter-Cell Interference Utilizing Carrier Allocation in Visible Light Communication System,” in *IEEE Communications Letters*, vol. 16, no. 4, pp. 526–529, 2012.

[148] S. Y. Jung, D. H. Kwon, S. H. Yang and S. K. Han,“Inter-cell interference mitigation in multi-cellular visible light communications,” *Optics Express*, vol. 24, no. 8, pp. 8512–8526, 2016.

[149] X. Li, B. Hussain, L. Wang, J. Jiang and C. P. Yue,“Design of a 2.2-mW 24-Mb/s CMOS VLC Receiver SoC With Ambient Light Rejection and Post-Equalization for Li-Fi Applications,” in *Journal of Lightwave Technology*, vol. 36, no. 12, pp. 2366–2375, 2018.

[150] P. Nabavi and M. Yuksel,“Comprehensive Design and Prototype of VLC Receivers With Large Detection Areas,” in *Journal of Lightwave Technology*, vol. 38, no. 16, pp. 4187–4204, 2020.

[151] D. Terra, N. Kumar, N. Lourenço, L. N. Alves, and R. L. Aguiar,“Design, development and performance analysis of DSSS-based transceiver for VLC,” in *IEEE EUROCON-International Conference on Computer as a Tool*, pp. 1–4, 2011.

[152] N. Huang, X. Wang and M. Chen,“Transceiver Design for MIMO VLC Systems With Integer-Forcing Receivers,” in *IEEE Journal on Selected Areas in Communications*, vol. 36, no. 1, pp. 66–77, 2018.

[153] “Guide for the Preparation of Master’s and Doctoral Theses,” *McMaster University*, 2019, [Online]. Available: https://gs.mcmaster.ca/app/uploads/2019/10/Prep_Guide_Masters_and_Doctoral_Theses_August-2021.pdf

[154] W. Pawlikowski, A. Barmaki, M. Narimani, and S. Hranilovic, “Light-emitting commutating diodes for optical wireless communications within LED

drivers," *IEEE Photonics Journal*, vol. 12, no. 5, pp. 1–11, 2020, doi: 10.1109/JPHOT.2020.3020749.

[155] A. Barmaki, M. Narimani, and S. Hranilovic, "Integrating OFDM into switching power supplies for visible light communications," *IEEE Transactions on Circtuis and Systems I: Regular Papers*, vol. 71, no. 6, pp. 2925–2937, Jun 2024, doi: 10.1109/TCSI.2024.3386365.

[156] Cisco Systems, "Cisco visual networking index: Forecast and trends, 2017–2022 white paper," 2019. [Online]. Available: https://cloud.report/Resources/Whitepapers.pdf.

[157] "IEEE standard for information technology– local and metropolitan area networks– specific requirements–Part 3: CSMA/CD access method and physical layer specifications amendment 3: Data terminal equipment (DTE) power via the media dependent interface (MDI) enhancements," *IEEE Std 802.3at-2009 (Amendment to IEEE Std 802.3-2008)*, pp. 1–137, Oct 2009.

[158] M. Halper, "Cisco stokes PoE lighting push with dedicated Ethernet switch, signs up Marriott," *LEDs Magazine*, Feb. 2017.

[159] Maxim Integrated, "The bright new outlook for LEDs: New drivers, new possibilities," 2015. [Online]. Available: https://www.maximintegrated.com/content/dam/files/design/technical-documents/white-papers/led-white-paper.pdf

[160] A. Rammohan and C. RameshKumar, "Investigation on light intensity and temperature distribution of automotive's halogen and LED headlight," in *2017*

International Conference on Microelectronic Devices, Circuits and Systems (ICMDCS), pp. 1–6, Aug 2017.

[161] B. Fleming, "Solid state headlights [automotive electronics]," in *IEEE Vehicular Technology Magazine*, vol. 3, no. 3, pp. 12–15, 2008.

[162] T. Stratil, P. Koudelka, J. Jankovych, V. Vasinek, R. Martinek, and T. Pavelek, "Broadband over visible light: High power wideband bias-T solution," in *2016 10th International Symposium on Communication Systems, Networks and Digital Signal Processing (CSNDSP)*, pp. 1–5, July 2016.

[163] E. Monteiro and S. Hranilovic, "Design and implementation of color-shift keying for visible light communications," *Journal of Lightwave Technology*, vol. 32, no. 10, pp. 2053–2060, May 2014.

[164] I. Castro, S. Lopez, K. Martin, M. Arias, D. G. Lamar, and J. Sebastian, "High frequency DC-DC AC-LED driver based on ZCS-QRCs", in *Proc. IEEE Energy Convers. Congr. Expos.*, Cincinnati, OH, USA, pp. 3688–3695, 2017.

[165] I. Castro, A. Vazquez, D. G. Aller, M. Arias, D. G. Lamar, and J. Sebastian, "On supplying LEDs from very low DC voltages with high-frequency AC-LED drivers," in *IEEE Transactions on Power Electronics*, vol. 34, no. 6, pp. 5711-5719, June 2019.

[166] I. Castro, D. G. Lamar, S. Lopez, K. Martin, M. Arias and J. Sebastian, "A Family of High Frequency AC-LED Drivers Based on ZCS-QRCs," in *IEEE Transactions on Power Electronics*, vol. 33, no. 10, pp. 8728-8740, Oct. 2018.

[167] K. Modepalli and L. Parsa, "Dual-purpose offline LED driver for illumination and visible light communication," in *IEEE Transactions on Industry Applications*, vol. 51, no. 1, pp. 406–419, Jan 2015.

[168] X. Deng, Y. Wu, K. Arulandu, G. Zhou, and J. P. M. G. Linnartz, "Performance comparison for illumination and visible light communication system using buck converters," in *2014 IEEE Globecom Workshops (GC Wkshps)*, pp. 547–552, 2014.

[169] X. Deng, K. Arulandu, Y. Wu, G. Zhou, and J. M. G. Linnartz, "Performance analysis for joint illumination and visible light communication using buck driver," in *IEEE Transactions on Communications*, vol. 66, no. 5, pp. 2065–2078, May 2018.

[170] C. Qian, J. Fan, X. Fan, and G. Zhang, "Prediction of lumen depreciation and color shift for phosphor-converted white light-emitting diodes based on a spectral power distribution analysis method," *IEEE Access*, vol. 5, pp. 24 054–24 061, 2017.

[171] W. Pawlikowski, M. Narimani, and S. Hranilovic, "A novel method of integrating visible light communications within LED drivers," in *IEEE Globecom Workshops (GC Wkshps)*, pp. 1–6, 2017.

[172] C. Deekshitha and K. L. Shenoy, "Design and simulation of synchronous buck converter for LED application," in *2nd IEEE International Conference on Recent Trends in Electronics, Information Communication Technology (RTEICT)*, pp. 142–146, May 2017.

[173] Philips Lumileds, "Luxeon Rebel Line," 2016. [Online]. Available: http://www.lumileds.com/uploads/28/DS64-pdf.

[174] Infineon, "MOSFET Power Losses Calculation Using the Data- Sheet Parameters," 2006. [Online]. Available: http://application-notes.digchip.com/070/70-41484.pdf

[175] Infineon, "Power Loss and Optimised MOSFET Selection in BLDC Motor Inverter Designs Understanding MOSFET power losses in block (trapezoidal) commutation," 2016. [Online]. Available: https://www.infineon.com/dgdl/Infineon-WhitePaper_PowerLoss_and_Optimized_MOSFET_Selection_in_BLDC_Motor_Inverter_Designs-WP-v01_00-EN.pdf

[176] Texas Instruments, "Basic calculation of a buck converter's power stage," 2011. [Online]. Available: http://www.ti.com/lit/an/slva477b/slva477b.pdf

[177] Texas Instruments, "TPS92550 450mA 14W Constant Current Buck LED Driver Micro-Module," 2012. [Online]. Available: http://www.ti.com/lit/ds/symlink/tps92550.pdf

[178] DIGILENT. *Analog Discovery 2*,[Online]. Available: https://digilent.com/reference/test-and-measurement/analog-discovery-2/reference-manual, Accessed 12 July 2024.

[179] P. Lumileds. *LUXEON 3535L Line*, 2016. [Online]. Available: https://lumileds.com/wp-content/uploads/files/DS203-L.pdf.

[180] M. Meneghini, A. Tazzoli, E. Ranzato, N. Trivellin, G. Meneghesso, E. Zanoni, M. Pavesi, M. Manfredi, R. Butendeich, U. Zehnder, and B. Hahn, "A study of

the failure of GaN-based LEDs submitted to reverse-bias stress and ESD events," in *2010 IEEE International Reliability Physics Symposium*, pp. 522–527, May 2010.

[181] B. Meneghini, "Basic calculation of a boost converter's power stage," in *Texas Instruments, Application Report*, pp. 1–9, 2009.

[182] terasIC Altera, "DE0-Nano User Manual," 2015. [Online]. Available: https://www.ti.com/lit/ug/tidu737/tidu737.pdf

[183] A. Jovicic, J. Li, and T. Richardson, "Visible light communication: opportunities, challenges and the path to market," in *IEEE Communications Magazine*, vol. 51, no. 12, pp. 26–32, 2013, doi: 10.1109/MCOM.2013.6685754.

[184] H. Elgala, R. Mesleh, and H. Haas, "Indoor optical wireless communication: potential and state-of-the-art," in *IEEE Communications Magazine*, vol. 49, no. 9, pp. 56–62, 2011, doi: 10.1109/MCOM.2011.6011734.

[185] C. Medina, M. Zambrano, and K. Navarro, "LED based visible light communication: Technology, applications and challenges-a survey," in *International Journal of Advances in Engineering & Technology*, vol. 8, no. 4, Art. no. 482, 2015.

[186] B. Lin, Q. Guo, Z. Ghassemlooy, X. Tang, C. Lin, and Z. Zhou, "Experimental demonstration of a non-orthogonal multiple access scheme for visible light communications with SCFDM transmission," in *Physical Communication*, vol. 31, pp. 181–186, 2018.

[187] F. Wu, C. Lin, C. Wei, C. Chen, Z. Chen, and H. Huang, "3.22-Gb/s WDM

visible light communication of a single RGB LED employing carrier-less amplitude and phase modulation," in *Proc. Opt. Fiber Commun. Conf. Expo., Nat. Fiber Opt. Eng. Conf. (OFC/NFOEC)*, Anaheim, CA, USA, 2013, pp. 1—3.

[188] M. K. Kazimierczuk, *Pulse-width modulated DC-DC power converters*. Hoboken, NJ, USA: John Wiley, 2008.

[189] Z. Wang, T. Mao, and Q. Wang, "Optical OFDM for visible light communications," in *Proc. 13th Int. Wireless Commun. Mobile Comput. Conf. (IWCMC)*, pp. 1190–1194, 2017, doi: 10.1109/IWCMC.2017.7986454.

[190] R. Mesleh, H. Elgala, and H. Haas, "On the performance of different OFDM based optical wireless communication systems," *Journal of Optical Communications and Networking*, vol. 3, no. 8, pp. 620–628, 2011, doi: 10.1364/JOCN.3.000620

[191] J. G. Proakis and M. Salehi, *Digital communications*. 5th ed. New York, NY, USA: McGraw-Hill, 2007.

[192] X. Li, R. Mardling, and J. Armstrong, "Channel capacity of IM/DD optical communication systems and of ACO-OFDM," in *Proc. Int. Conf. Commun. (ICC)*, pp. 2128–2133, 2007, doi: 10.1109/ICC.2007.358.

[193] S. Liu, X. Xie, X. Zhang, and W. Zhu, "Analysis of thermal instability in power MOSFET," in *Proc. 3rd Int. Conf. Electron. Inf. Technol. Comput. Eng. (EITCE)*, pp. 541–545, 2019, doi: 10.1109/EITCE47263.2019.9095159.

[194] P. Spirito, G. Breglio, V. d'Alessandro, and N. Rinaldi, "Analytical model for thermal instability of low voltage power MOS and SOA in pulse operation,"

in *Proc. IEEE Int. Symp. Power Semiconductor Devices and ICs (ISPSD)*, pp. 269–272, 2002, doi: 10.1109/ISPSD.2002.1016223.

[195] D. Dibra, M. Stecher, S. Decker, A. Lindemann, J. Lutz, and C. Kadow, "On the origin of thermal runaway in a trench power MOSFET," *IEEE Transactions on Electron Devices*, vol. 58, no. 10, pp. 3477–3484, 2011, doi: 10.1109/TED.2011.2160867.

[196] A. Sedra and K. Smith, *Microelectronic circuits.* 8th ed. London, U.K.: Oxford Univ. Press, 2020.

[197] N. Pal *et al.*, "A 91% efficient 30V hybrid boost-SC converter based backlight LED driver in 180nm CMOS," in *Proc. IEEE Custom Integr. Circuits Conf. (CICC)*, pp. 1–4, 2020, doi: 10.1109/CICC48029.2020.9075886.

[198] P. Sathya and R. Natarajan, "Design and implementation of 12V/24V closed loop boost converter for solar powered LED lighting system," *International Journal of Engineering and Technology (IJET)*, vol. 5, no. 1, pp. 254–264, 2013.

[199] B. A. Soltani, M. Sabahi, E. Babaei, and J. Pouladi, "Two-input boost converter for street-lighting applications," *Computers & Electrical Engineering*, vol. 92, Art. no. 107126, 2021.

[200] M. W. Umar, N. B. Yahaya, and Z. B. Baharuddin, "Design and simulation of DC-DC converter for automobile LED front lighting applications," in *Proc 6th Int. Conf. Intel. Adv. Sys. (ICIAS)*, pp. 1–4, 2016, doi: 10.1109/ICIAS.2016.7824062.

[201] J.-H. Yoo, J.-S. Jang, J. Kwon, H.-C. Kim, D.-W. Song, and S.-Y. Jung, “Demonstration of vehicular visible light communication based on LED headlamp,” *International Journal of Automotive Technology*, vol. 17, pp. 347–352, 2016.

[202] B. Hauke, “Basic calculation of a boost converter’s power stage,” Texas Instrum., Dallas, TX, USA, Appl. Rep. SLVA372C, 2009, [Online]. Available: https://www.ti.com/lit/pdf/slva372.

[203] B. Hauke, “White LED power supply design techniques,” Texas Instrum., Dallas, TX, USA, Appl. Rep. SLVA130, 2003, [Online]. Available: https://www.ti.com/lit/pdf/slva130, Accessed 2 Jul 2024.

[204] P. A. A. Honadia, F. I. Barro, and M. Sané, “Performance analysis of a boost converter with components losses,” *Energy and Power Engineering*, vol. 10, no. 09, pp. 399–413, 2018.

[205] A. M. Rahimi and A. Emadi, “Discontinuous-conduction mode DC/DC converters feeding constant-power loads,” *IEEE Transactions on Industrial Electronics*, vol. 57, no. 4, pp. 1318–1329, 2010, doi: 10.1109/TIE.2009.2029514.

[206] E.-S. Kim, K.-Y. Joe, M.-H. Kye, Y.-H. Kim, and B.-D. Yoon, “An improved soft-switching PWM FB DC/DC converter for reducing conduction losses,” *IEEE Transactions on Power Electronics*, vol. 14, no. 2, pp. 258–264, 1999, doi: 10.1109/63.750178.

[207] R. W. Erickson and D. Maksimovic, *Fundamentals of power electronics*. Springer Science & Business Media, 2007.

[208] Alpha & Omega Semiconductor (AOSMD). *AO3442 100V N-Channel MOSFET*, 2012. [Online]. Available: https://aosmd.com/sites/default/files/res/datasheets/AO3442.pdf

[209] THORLABS. *PDA36A(-EC) Si Switchable Gain Detector*, 2017. [Online]. Available: https://www.thorlabs.com/_sd.cfm?fileName=13053-D04.pdf&partNumber=PDA36A-EC

[210] W. Hassan, R. Hasan, D. D.-C. Lu, and W. Xiao, "Design and development of high step-up DC-DC converter to realize high efficiency and reduced voltage stress," in *Proc. IEEE Appl. Power Electron. Conf. Expo. (APEC)*, pp. 2098–2103, 2020, doi: 10.1109/APEC39645.2020.9124411.

[211] TEKTRONIX. *AWG2021*,[Online]. Available: https://download.tek.com/manual/070909750web.pdf

[212] Mini Circuits, *Coaxial Bias-T ZFBT-4R2GW-FT+*, [Online]. Available: https://www.minicircuits.com/pdfs/ZFBT-4R2GW-FT+.pdf

[213] Keysight Technologies. *DSO-X 2002A*, 2019 – 2022. [Online]. Available: https://www.keysight.com/us/en/assets/7018-02733/data-sheets/5990-6618.pdf..

[214] L. Yu, L. Wang, Z. Hao, Y. Luo, C. Sun, B. Xiong, Y. Han, J. Wang, and H. Li,"High-speed micro-LEDs for visible light communication: Challenges and progresses," *Semiconductor Science and Technology*, vol. 37, no. 2, Art. no. 023001, 2021.

[215] Y. Wang, Y. Wang, N. Chi, J. Yu, and H. Shang, "Demonstration of 575-Mb/s

downlink and 225-Mb/s uplink bi-directional SCM-WDM visible light communication using RGB LED and phosphor-based LED," *Optics Express*, vol. 21, no. 1, pp. 1203–1208, 2013.

[216] T. M. Inc., *Matlab version: 9.13.0 (r2022b)*, Natick, Massachusetts, United States, 2022. [Online]. Available: https://www.mathworks.com

[217] M. Sandell, J. van de Beek, and P. O. Börjesson, "Timing and frequency synchronization in OFDM systems using the cyclic prefix," in *Proc. IEEE Int. Symp. Synchronization*, pp. 16–19, 1995.

[218] S. Aboagye, T. M. N. Ngatched, O. A. Dobre and H. V. Poor, "Energy-efficient resource allocation for aggregated RF/VLC systems," *IEEE Trans. Wireless Commun.*, vol. 22, no. 10, pp. 6624–6640, Oct 2023, doi: 10.1109/TWC.2023.3244871.

[219] M. B. Rahaim, A. M. Vegni, and T. D. Little, "A hybrid radio frequency and broadcast visible light communication system," in *IEEE GLOBECOM Workshops (GC Wkshps)*, pp. 792–796, 2011.

[220] H. Kazemi, M. Safari, and H. Haas, "A wireless backhaul solution using visible light communication for indoor Li-Fi attocell networks," in *Proc. 2017 IEEE Int. Conf. Commun. (ICC)*, Paris, France, pp. 1–7, 2017, doi: 10.1109/ICC.2017.7996637.

[221] M. S. A. Mossaad, S. Hranilovic and L. Lampe, "Visible Light Communications Using OFDM and Multiple LEDs," *IEEE Trans. Commun.*, vol. 63, pp. 4304–4313, Nov 2015, doi: 10.1109/TCOMM.2015.2469285.

[222] E. F. Schubert, *Light-emitting Diodes*. E. Fred Schubert: New York,2018.

[223] *Eye Safety Risk Assessment of Infrared Emitting Diodes According IEC 62471 (based on CIE S009)*, VISHAY. [Online]. Available: https://www.vishay.com/docs/81935/eyesafe.pdf.

[224] H. van der Broeck, G. Sauerlander, and M. Wendt, "Power driver topologies and control schemes for LEDs," in *Proc. 22nd Annu. IEEE Appl. Power Electron. Conf. Expo. (APEC)*, Anaheim, CA, USA, pp. 1319-1325, 2007, doi: 10.1109/TCOMM.2012.020612.090300.

[225] R. R. Duarte, G. G. Pereira, M. A. Dalla Costal, C. H. Barriquello and J. M. Alonso, "Off-grid commercial LED driver optimization using GaN transistors," in *Proc. 2018 IEEE Ind. Appl. Soc. Annu. Meeting (IAS)*, Portland, OR, USA, pp. 1–7, 2017, doi: 10.1109/IAS.2018.8544686.

[226] Occupational Safety and Health Administration (OSHA). "1915.82 - Lighting." U.S. Department of Labor, Occupational Safety and Health Administration, [Online]. Available: https://www.osha.gov/laws-regs/regulations/standardnumber/1915/1915.82.

[227] R. Lenk and C. Lenk, *Practical lighting design with LEDs*. John Wiley & Sons, 2017.

[228] X. Li, J. Vucic, V. Jungnickel, and J. Armstrong, "On the capacity of intensity-modulated direct-detection systems and the information rate of ACO-OFDM for indoor optical wireless applications," *IEEE Transactions on Communications*, vol. 60, no. 3, pp. 799–809, 2012, doi: 10.1109/TCOMM.2012.020612.090300.

[229] G. Lakkas,"MOSFET power losses and how they affect power-supply efficiency," *Analog Appl. J.*, vol. 10, pp. 22–26, 2016.

[230] Osram Opto Semiconductors GmbH, *SFH 4727AS IR Emitter*, USA INC, 2021. [Online]. Available: https://mm.digikey.com/Volume0/opasdata/d220001/medias/docus/2599/SFH%204727AS.pdf.

[231] Marktech Optoelectronics, *MT03-004 Photodiode*, 2018. [Online]. Available: https://www.marktechopto.com/pdf/products/datasheet/MT03-004.pdf.

[232] T. Wu, T. S. Rappaport, and C. M. Collins, "Safe for generations to come: Considerations of safety for millimeter waves in wireless communications," *IEEE Microw. Mag.*, vol. 16, no. 2, pp. 65–84, 2015, doi: 10.1109/MMM.2014.2377587.

[233] S. Okhonin, et al, "A dynamic operation of a PIN photodiode.," in *Appl. Phys. Lett.* 106.3, (2015).

[234] A. O. Goushcha and B. Tabbert, "On response time of semiconductor photodiodes," *Optical Engineering*, vol. 56, no. 9, pp. 097101–097101, 2017.

[235] X. Li, J. Vucic, V. Jungnickel, and J. Armstrong, "On the capacity of intensity-modulated direct-detection systems and the information rate of ACO-OFDM for indoor optical wireless applications," *IEEE Transactions on Communications*, vol. 60, no. 3, pp. 799–809, 2012, doi: 10.1109/TCOMM.2012.020612.090300.

[236] H. Abuella, M. Elamassie, M. Uysal, Z. Xu, E. Serpedin, K.A. Qaraqe, and S. Ekin, "Hybrid RF/VLC systems: A comprehensive survey on network topologies, performance analyses, applications, and future directions," *IEEE Access*, vol. 9, pp. 160402–160436, 2021, doi: 10.1109/ACCESS.2021.3129154.

[237] T. Borogovac, M.B. Rahaim, M. Tuganbayeva , and T.D. Little, "Lights-off" visible light communications," in *IEEE GLOBECOM Workshops (GC Wkshps)*, pp. 797–801, 2011.

[238] J. Wang, H. S. -h. Chung and R. T. -h. Li, "Characterization and experimental assessment of the effects of parasitic elements on the MOSFET switching performance," *IEEE Transactions on Power Electronics*, vol. 28, no. 1, pp. 573–590, 2013, doi: 10.1109/TPEL.2012.2195332.

[239] D. K. Saini, A. Ayachit, M. K. Kazimierczuk and T. Suetsugu, "High switching frequency performance of E-GaN FETs and silicon MOSFETs," *IEEE Industry Applications Society Annual Meeting*, Cincinnati, OH, USA, pp. 1–6, 2017, doi: 10.1109/IAS.2017.8101846.

[240] Texas Instrument, "Phase-shifted full bridge dc/dc power converter design guide," May 2014.

[241] H. S. Khallaf, H. M. H. Shalaby and Z. Kawasaki, "Proposal of a hybrid OFDM-PPM technique for free space optical communications systems," *IEEE Photonics Conference*, Bellevue, WA, USA, pp. 287–288, 2013, doi: 10.1109/IPCon.2013.6656549.

[242] H. S. Khallaf, A. E. Morra, A. E. Elfiqi, H. M. H. Shalaby, and S. Hranilovic, "Hybrid two-level MPPM–MDPSK modulation for high-speed optical communication networks," *Appl. Opt.*, vol. 58, pp. 9757–9767, 2019.

[243] B. Fahs, M. Romanowicz, and M. M. Hella, "A Gbps building-to-building VLC

link using standard CMOS avalanche photodiodes," *IEEE Photonics Journal*, vol. 9, no. 6, pp. 1–9, 2017.

[244] L. Balogh, "Fundamentals of MOSFET and IGBT gate driver circuits" *Texas Instruments–Application report*, pp. 28-33, 2017, [Online]. Available: https://www.ti.com/lit/pdf/slua618.